

# NAVAL POSTGRADUATE SCHOOL MONTEREY, CALIFORNIA



## THESIS

### THE DYNAMICS OF TELECONNECTIONS INDUCED BY SHORT TERM TROPICAL FORCING

by

Mark D. Malsick

September, 1995

Thesis Advisor:

Tom Murphree

Approved for public release; distribution is unlimited.

19960401 011

DTIC QUALITY INSPECTED 1

REPORT DOCUMENTATION PAGE			Form Approved OMB No. 0704-0188	
Public reporting burden for this collection of information is estimated to average 1 hour per response, including the time for reviewing instruction, searching existing data sources, gathering and maintaining the data needed, and completing and reviewing the collection of information. Send comments regarding this burden estimate or any other aspect of this collection of information, including suggestions for reducing this burden, to Washington Headquarters Services, Directorate for Information Operations and Reports, 1215 Jefferson Davis Highway, Suite 1204, Arlington, VA 22202-4302, and to the Office of Management and Budget, Paperwork Reduction Project (0704-0188) Washington DC 20503.				
1. AGENCY USE ONLY (Leave blank)		2. REPORT DATE SEPTEMBER 1995		3. REPORT TYPE AND DATES COVERED Master's Thesis
4. TITLE AND SUBTITLE THE DYNAMICS OF TELECONNECTIONS INDUCED BY SHORT TERM TROPICAL FORCING			5. FUNDING NUMBERS	
6. AUTHOR(S) MARK D. MALSICK				
7. PERFORMING ORGANIZATION NAME(S) AND ADDRESS(ES) Naval Postgraduate School Monterey CA 93943-5000			8. PERFORMING ORGANIZATION REPORT NUMBER	
9. SPONSORING/MONITORING AGENCY NAME(S) AND ADDRESS(ES)			10. SPONSORING/MONITORING AGENCY REPORT NUMBER	
11. SUPPLEMENTARY NOTES The views expressed in this thesis are those of the author and do not reflect the official policy or position of the Department of Defense or the U.S. Government.				
12a. DISTRIBUTION/AVAILABILITY STATEMENT Approved for public release; distribution is unlimited.			12b. DISTRIBUTION CODE	
13. ABSTRACT (maximum 200 words) Recent observational and modeling studies have suggested that transient tropical perturbations may induce significant intraseasonal teleconnections between the tropics and midlatitudes. We have investigated the mechanisms for such teleconnections using a nonlinear global shallow water model with a realistically wavy basic state. The model perturbations were designed to simulate tropical cyclones with prescribed growth, decay, and propagation. The model responses to the tropical perturbations showed distinct midlatitude wavetrain responses to the perturbation. The typical response became large within a few days and remained as a coherent pattern for two to three weeks after the demise of the tropical perturbation. The response was particularly strong if the perturbation propagated close to an extratropical jet. This propagation allowed Rossby wave induction as divergent outflow from the perturbation crossed the jet's region of high ambient vorticity gradient. This initial wave response was then guided by the jet and amplified in barotropically unstable regions on the jet flanks. This produced a persistent response downstream of the jet exit (e.g., over the northeast Pacific and North America). The response showed a marked variation with the season and with the tropical ocean basin in which the perturbation occurred, apparently because of temporal and spatial changes in the basic state conditions. The responses closely resemble observed anomaly patterns associated with transient tropical perturbations, and are dynamically consistent with the responses to more persistent tropical perturbations (e.g., ENSO events).				
14. SUBJECT TERMS Teleconnections; Tropical Forcing; Tropical Cyclones; Rossby Waves; Barotropic Instability; Extended Range Forecasting; Numerical Modeling			15. NUMBER OF PAGES 139	
			16. PRICE CODE	
17. SECURITY CLASSIFICATION OF REPORT Unclassified	18. SECURITY CLASSIFICATION OF THIS PAGE Unclassified	19. SECURITY CLASSIFICATION OF ABSTRACT Unclassified	20. LIMITATION OF ABSTRACT UL	

NSN 7540-01-280-5500

Standard Form 298 (Rev. 2-89)  
Prescribed by ANSI Std. Z39-18 298-102



Approved for public release; distribution is unlimited.

**THE DYNAMICS OF TELECONNECTIONS INDUCED BY  
SHORT TERM TROPICAL FORCING**

Mark D. Malsick  
Lieutenant Commander, United States Navy  
B.S., University of Connecticut, 1984

Submitted in partial fulfillment  
of the requirements for the degree of

**MASTER OF SCIENCE IN METEOROLOGY AND PHYSICAL  
OCEANOGRAPHY**

from the

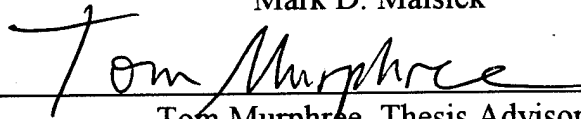
**NAVAL POSTGRADUATE SCHOOL  
September 1995**

Author:

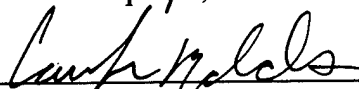


Mark D. Malsick

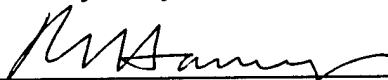
Approved by:



Tom Murphree, Thesis Advisor



Carolyn Reynolds, Second Reader



Robert L. Haney, Chairman  
Department of Meteorology



## ABSTRACT

Recent observational and modeling studies have suggested that transient tropical perturbations may induce significant intraseasonal teleconnections between the tropics and midlatitudes. We have investigated the mechanisms for such teleconnections using a nonlinear global shallow water model with a realistically wavy basic state. The model perturbations were designed to simulate tropical cyclones with prescribed growth, decay, and propagation.

The model responses to the tropical perturbations showed distinct midlatitude wavetrain responses to the perturbation. The typical response became large within a few days and remained as a coherent pattern for two to three weeks after the demise of the tropical perturbation. The response was particularly strong if the perturbation propagated close to an extratropical jet. This propagation allowed Rossby wave induction as divergent outflow from the perturbation crossed the jet's region of high ambient vorticity gradient. This initial wave response was then guided by the jet and amplified in barotropically unstable regions on the jet flanks. This produced a persistent response downstream of the jet exit (e.g., over the northeast Pacific and North America).

The response showed a marked variation with the season and with the tropical ocean basin in which the perturbation occurred, apparently because of temporal and spatial changes in the basic state conditions. The responses closely resemble observed anomaly patterns associated with transient tropical perturbations, and are dynamically consistent with the responses to more persistent tropical perturbations (e.g., ENSO events).

# TABLE OF CONTENTS

I. INTRODUCTION .....	1
A. BACKGROUND .....	1
B. GLOBAL SCALE ATMOSPHERIC INTERACTIONS .....	1
C. INTERANNUAL TELECONNECTIONS .....	2
D. INTRASEASONAL TELECONNECTIONS .....	4
E. TELECONNECTION MODELING .....	5
F. DESIGN OF THIS STUDY .....	7
II. METHODS .....	9
A. MODEL DESCRIPTION .....	9
B. MODEL EQUATIONS .....	9
1. Basic State Forcing .....	13
2. Perturbation Forcing .....	14
C. MODEL OUTPUT FIELDS .....	15
1. Geopotential Height .....	15
2. Stream Function .....	16
3. Velocity Potential .....	16
D. MODEL RUNS .....	16
1. Basic Runs .....	17
2. Tropical Basin Runs .....	17
3. Tropical Cyclone Runs .....	18
E. ANALYSIS METHODS .....	18
1. Quasi-Geostrophic Wave Activity Flux Vectors .....	18
2. Barotropic Instability (BTI) .....	19
3. Stationary Wave Number .....	20
4. Rossby Wave Source Calculation .....	21



III. RESULTS .....	23
A. INTRODUCTION TO MODEL RUNS .....	23
B. WESTERN NORTH PACIFIC RUN DESCRIPTIONS .....	24
1. January Fixed Forcing Runs. ....	24
a. Rossby Wave Source Analyses .....	25
b. Wave Energy Analyses .....	26
2. January Fixed Location-Variable Strength Runs .....	27
3. January Variable Location-Fixed Strength Runs .....	28
4. January Recurving Cyclone Run .....	28
5. January Straight Running Cyclone Run .....	29
6. July Fixed Forcing Runs .....	29
a. Rossby Wave Source Analyses .....	30
b. Wave Energy Analyses .....	31
7. July Fixed Location-Variable Strength Runs .....	32
8. July Variable Location-Fixed Strength Runs .....	32
9. July Recurving Cyclone Run .....	33
10. July Straight Running Cyclone Run .....	33
C. BAY OF BENGAL RUN DESCRIPTIONS .....	33
1. January Fixed Forcing Runs. ....	34
a. Rossby Wave Source Analyses .....	35
b. Wave Energy Analyses .....	35
2. January Recurving Cyclone Run .....	36
3. July Recurving Cyclone Run .....	37
D. NORTH ATLANTIC RUN DESCRIPTIONS .....	37
1. January Fixed Forcing Runs. ....	38
a. Rossby Wave Source Analyses .....	39
b. Wave Energy Analyses .....	40
2. January Recurving Cyclone Run .....	41
3. July Recurving Cyclone Run .....	42
a. Rossby Wave Source Analyses .....	42
b. Wave Energy Analyses .....	42
E. SUMMARY .....	43
1. Height Responses .....	43
2. Teleconnection Dynamics .....	45

a. Rossby Wave Source Analyses .....	45
b. Wave Energy Analyses .....	46
IV. CONCLUSIONS .....	47
A. SUMMARY .....	47
B. IMPLICATIONS FOR EXTENDED-RANGE FORECASTING .....	48
C. RECOMMENDATIONS FOR FUTURE RESEARCH .....	49
APPENDIX A. FIGURES .....	55
LIST OF REFERENCES .....	119
DISTRIBUTION LIST .....	123



## LIST OF ACRONYMS AND SYMBOLS

ADVDIV	advection of absolute vorticity by the divergent part of the wind
ADVROT	advection of absolute vorticity by the rotational part of the wind
$\beta$	total derivative of the Coriolis parameter,
BTI	barotropic instability
$\chi$	velocity potential
$D$	divergence
ECMWF	European Center for Medium-range Weather Forecasting
ENSO	El Niño-Southern Oscillation
$f$	Coriolis parameter
$\vec{F}_s$	Quasi-geostrophic wave activity flux vector
GCM	general circulation model
GSWM	global shallow water model
gpm	geopotential meter
$k_s$	zonal wavenumber
K	degrees Kelvin
$\lambda$	longitude
m	meter
mb	millibar

NOGAPS	Navy Operational Global Atmospheric Prediction System
$\phi$	latitude
PNA	Pacific-North America
$\Psi$	streamfunction
Q	atmospheric heating
QG	quasi-geostrophic
S	Rossby wave source
s	second
SO	Southern Oscillation
SLP	sea level pressure
u	zonal component of the wind
$u_x$	zonal component of the divergent wind
$u_\Psi$	zonal component of the rotational wind
v	meridional component of the total wind
$\vec{V}$	horizontal wind vector
$\vec{V}_x$	divergent horizontal wind vector
$\vec{V}_\Psi$	rotational horizontal wind vector
$v_x$	meridional component of the divergent wind
$v_\Psi$	meridional component of the rotational wind
$\zeta$	relative vorticity

## ACKNOWLEDGMENT

I am deeply grateful for Dr. Tom Murphree's energetic guidance and instruction during the course of this project. His boundless patience and teaching abilities were invaluable at every stage of this study. I also gratefully acknowledge the contributions of Dr. Carolyn Reynolds, of the Naval Research Laboratory in Monterey, who provided valuable guidance and constructive suggestions.

## **I. INTRODUCTION**

### **A. BACKGROUND**

Understanding climate has been an object of study throughout history due to climate's large impacts on human endeavors. Early observers realized the importance of the net effects of the atmosphere on a continental or even a global scale. Drought, floods, and famine have occurred throughout history in an unpredictable manner. Yet many aspects of climate (the large scale, low frequency state of the atmosphere) showed distinct spatial and temporal patterns. These patterns have long motivated researchers to explore the underlying processes. These climate studies continue today, with the objective of making long range atmospheric predictions that would provide adequate warning of adverse environmental conditions.

### **B. GLOBAL SCALE ATMOSPHERIC INTERACTIONS**

Walker (1924) and Walker and Bliss (1932) conducted seminal climate research on global patterns of atmospheric pressure, temperature and precipitation anomalies associated with monsoonal circulations in the Indian Ocean and the western Pacific. Walker and Bliss (1932) identified a major periodic atmospheric mass transfer between the eastern and western tropical Pacific which has come to be known as the Southern Oscillation. Walker and Bliss (1932) detailed long range statistical correlations between

the Southern Oscillation and:

- Hawaiian Island precipitation,
- western Canadian surface temperatures,
- sea level pressure over the southeastern United States.

By correlating periodic variations in various atmospheric fields at distant locations, Walker and Bliss (1932) produced the first study of atmospheric teleconnections (Horel and Wallace 1981, Wallace and Gutzler 1981). Bjerknes (1966, 1969, 1971) furthered teleconnection research by suggesting that large scale circulation anomalies were driven by anomalous tropical air-sea interactions that produced anomalous energy and mass transports between the tropics and the mid-latitudes. Bjerknes (1969) furthered Sir Gilbert Walker's Southern Oscillation research by linking the oscillation of sea level pressure anomalies to low frequency fluctuations in sea surface temperature.

### **C. INTERANNUAL TELECONNECTIONS**

The bulk of atmospheric teleconnection research has been focused on the interannual teleconnections that arise due to the phenomena called El Niño and its symbiotic relationship with the Southern Oscillation. Bjerknes (1966) first used the term El Niño to describe a large scale anomalous warming of the eastern equatorial Pacific from the South American west coast to the international dateline. During El Niño, coastal upwelling along the western coast of South America weakens, easterly trade



winds weaken, and the sea surface temperature (SST) gradient diminishes between the western and eastern regions of the equatorial Pacific. El Niño events generally occur every 2-7 years (Rasmusson and Carpenter 1982). Contrasting events, sometimes called La Niña events also occur. In these events, the anomalies seen during El Niño events occur in reverse (Bradley et al. 1987).

Bjerknes (1966,1969,1972) was the first to recognize the link between El Niño events and large scale extratropical atmospheric circulation anomalies. He related these circulation anomalies to changes in the strength of the Hadley and Walker circulations. Horel and Wallace (1981) described the teleconnections associated with El Niño, La Niña, and the Southern Oscillation, emphasizing the vertical structure of the atmosphere and interactions between the tropics and the middle latitudes. They studied the Northern Hemisphere winters between 1951 and 1971 during which several El Niño and La Niña events occurred and obtained significant correlations between the interannual variability of mean tropospheric temperature, 200 mb heights, SST, and many other variables. In particular, the correlations of tropical Pacific SST with Northern Hemisphere geopotential heights exhibited well defined teleconnections in the Northern Hemisphere. The anomaly patterns reported by Horel and Wallace (1981) are consistent with the northern winter teleconnection patterns discussed by Walker and Bliss (1932) and Bjerknes (1966, 1969).

Wallace and Gutzler (1981) also studied Northern Hemisphere winter teleconnections using sea level pressure and 500 mb geopotential height analyses for a 15 year period and found distinct teleconnection patterns not only in the Pacific but in the Atlantic as well. They described:

- a North Atlantic oscillation,
- a North Pacific oscillation,
- a Pacific/North American (PNA) pattern.

The PNA pattern is an arc-like arrangement of four tropospheric circulation anomaly cells: an anticyclonic cell near Hawaii, a cyclonic cell over the North Pacific, an anticyclonic cell over western North America, and a cyclonic cell over the western North Atlantic. This pattern is very similar to one found by Horel and Wallace (1981) (Figure 1). Wallace and Gutzler (1981), Hoskins and Karoly (1981), and others suggested that these teleconnection patterns represent standing oscillations in the tropospheric geopotential height field. These oscillations strongly resemble the standing wave pattern found in many atmospheric models forced by tropical disturbances (e.g., Hoskins and Karoly 1981).

#### **D. INTRASEASONAL TELECONNECTIONS**

Teleconnections may occur on intraseasonal time scales, apparently due to anomalous forcing occurring on intraseasonal scales. Nitta (1987) correlated tropical western Pacific SST anomalies and convection anomalies with anomalies in mid-latitude

tropospheric winds. He found that the intraseasonal response to anomalously warm sea surface temperatures was more than twice the interannual response. Chang and Lum (1985) studied the relationships between the northern hemisphere winter east Asian - North Pacific jet and nearby tropical convection. They found a strong positive correlation between convection anomalies and jet strength anomalies with no apparent time lag. However, they suggested that the tropical convection forced the strengthening of the jet via a process in which increased upper tropospheric divergent flow from the convective region experienced Coriolis turning and intensified the jet flow. This extratropical jet response to increased tropical convection has also been seen in the southern hemisphere (Hurrell and Vincent 1991).

Harr and Elsberry (1995) conducted an observational study which showed that western Pacific tropical cyclones, especially those that recurve, were associated with large scale mid-latitude tropospheric flow anomalies.

## **E. TELECONNECTION MODELING**

The anomalies identified by Horel and Wallace (1981), Wallace and Gutzler (1981), and others have many similarities with the response to tropical forcing found in teleconnection modeling studies (e.g, Matsuno 1966, Egger 1977, Opsteegh and van den Dool 1980, Hoskins and Karoly 1981, Webster 1981). In particular, Hoskins and Karoly (1981) suggested that the arcing pattern of Rossby wave energy propagation from

the tropics into the mid-latitudes found in many modeling studies might explain arcing patterns such as the PNA pattern.

Simmons et al. (1983) found that a variety of localized forcings in the northern hemisphere tropics and subtropics tended to produce teleconnection patterns similar to the empirical patterns found by Wallace and Gutzler (1981). Simmons et al. (1983) attributed the model teleconnection patterns to the most rapidly growing mode associated with the barotropic instability of a zonally variable basic state. In effect, the model response to the localized forcing grew via the extraction of kinetic energy, particularly in the vicinity of strong jets. Branstator (1983) and Lau and Lim (1985) suggested that westerly jets may act as a barrier to and guide for propagating upper tropospheric waves.

Short term teleconnection studies using tropical cyclones as the tropical forcing were conducted by Woll (1993), Springer (1994), and Jakus (1995). These three studies used an operational global data assimilation system with tropical cyclone bogusing and a numerical weather prediction model. They found that tropical cyclones may produce a strong response over the North Pacific - North American (NPNA) region which persists well after the tropical cyclone dissipated. These studies also demonstrated that:

- Tropical cyclones can induce teleconnections,
- Teleconnections are strongly affected by wave guiding and amplification associated with the east Asian - North Pacific jet,

- The absolute vorticity flux associated with the divergent outflow from the tropical cyclone crossing the jet may initiate the wave response to the storm.

## **F. DESIGN OF THIS STUDY**

This study builds upon the previous work of Woll (1993), Springer (1994), and Jakus (1995) to examine the response of a global atmosphere to individual tropical cyclones with varying tracks and intensities. This study differs from these three previous studies in that it uses a simplified general circulation model. The usefulness of such a model for this kind of teleconnection study was determined in part by comparison to the results of Woll (1993), Springer (1994), and Jakus (1995).

Our intent was to develop a model that is inexpensive to run and easy to modify, so that numerous case studies could be conducted.

The major hypotheses tested in this study were based on the results and speculations produced in the three case studies conducted by Woll (1993), Springer (1994), and Jakus (1995). These hypotheses are given below.

- Tropical cyclones can produce strong teleconnections.
- The development of teleconnections is strongly influenced by wave guiding and amplification effects associated with the mid-latitude westerly jet.

- The absolute vorticity flux associated with the divergent outflow from the tropical cyclone crossing the jet may initiate the wave response to the storm.
- Barotropic instability (BTI) processes play a major role in the amplification process.
- The basic teleconnection process varies with season and the forcing location due to temporal and spatial variations in the ambient flow, especially the westerly jets.
- The results of the simplified general circulation model and the results of the NWP model are qualitatively similar because: (1) the ambient upper tropospheric flow plays a dominant role in the development of the teleconnection response; and (2) the ambient flow is similar in the two models.

The modeling and analysis methods used in this study are described in Chapter II. The model results are documented in Chapter III. Conclusions and recommendations for further study are presented in Chapter IV.

## II. METHODS

### A. MODEL DESCRIPTION

The atmospheric model used in this study is a nonlinear spectral shallow water equation model (GSWM) on a global spherical domain. The model has basic state forcings that maintain a realistic basic state circulation. A perturbation forcing is used in the model to represent a tropical cyclone for which the amplitude and location may vary both temporally and spatially.

### B. MODEL EQUATIONS

The derivation of the basic set of shallow water equations and the spectral formulations is described by Bourke (1972) and Haltiner and Williams (1980). The derivation for the equations used in this study is similar but includes dissipation, basic state forcing, and perturbation forcing terms. The basic governing equations of the model are the equation of motion and the continuity equation:

$$\frac{d\vec{V}}{dt} = -f(\hat{k} \times \vec{V}) - \nabla \Phi + Q_{bm} - \Delta_m \quad (1)$$

$$\frac{d\Phi}{dt} = -\Phi_t \nabla \cdot \vec{V} + Q_{bg} - \Delta_g + Q_p \quad (2)$$

$\vec{V}$  is the total horizontal wind vector,  $\Phi_t = \Phi_e + \Phi$  with  $\Phi_e = gh_e$  being a constant global mean geopotential with a fixed equivalent depth  $h_e$ , and  $\Phi$  being the deviation from  $\Phi_e$ . The  $Q_b$  forcing terms maintain zonal and meridional variations in the basic state during the model run.  $Q_p$  represents the perturbation forcing. The  $\Delta$  terms are the model's dissipation terms.

An expression for vorticity is found by taking the curl of (1). Divergence is found by taking the divergence of (2). Applying the Helmholtz theorem, the model atmosphere circulation can be represented in terms of stream function,  $\Psi$ , and the velocity potential,  $\chi$ , with the expressions:

$$\zeta = \nabla^2 \Psi \quad (3)$$

$$D = \nabla^2 \chi \quad (4)$$

It is more convenient to replace the equation of motion with vorticity and divergence equations in spectral models because their relation is simplified when spherical functions are used as basis functions. An additional benefit of using  $\Psi$  and  $\chi$  is that the equations contain only scalar terms (Haltiner and Williams 1980).

Equations (3) and (4) are substituted into (1) and (2). The resulting equations are then converted into spherical coordinates. The dissipation terms in (1) and (2) are expanded into damping and diffusion terms. The damping relaxes the perturbation state



back to the basic state on a time scale of 15 days. The diffusion terms transfer vorticity, divergence, or potential energy from small to large length scales with diffusivity coefficients:  $K_v$ ,  $K_d$ , and  $K_g$ . Each diffusivity coefficient has a value equal to  $10^{17} \text{ m}^4/\text{s}$ .

To solve the spherical coordinate forms of the basic shallow water equations, they were spectrally formulated with a rhomboidal 25 (R25) truncation that corresponds to a spherical Gaussian grid resolution of  $2.8^\circ$  latitude by  $4.7^\circ$  longitude. The resulting model equations are:

$$\begin{aligned} \frac{\partial \nabla^2 \Psi}{\partial t} = & -1 / (a \cos^2 \varphi) \left[ \frac{\partial}{\partial \lambda} (U_r \nabla^2 \Psi) + \cos \varphi \frac{\partial}{\partial \varphi} (V_r \Psi) \right] \\ & - 2 \Omega (\sin \varphi \nabla^2 \chi + V_r / a) \\ & + Q_{bv} - F_v (\nabla^2 \Psi_i) - K_v \nabla^4 (\nabla^2 \Psi) \end{aligned} \quad (5)$$

$$\begin{aligned} \frac{\partial \nabla^2 \chi}{\partial t} = & -1 / (a \cos^2 \varphi) \left[ \frac{\partial}{\partial \lambda} (V_r \nabla^2 \Psi) + \cos \varphi \frac{\partial}{\partial \varphi} (U_r \Psi) \right] \\ & - 2 \Omega (\sin \varphi \nabla^2 \Psi - U_r / a) - \nabla^2 [(U^2_r + V^2_r) / 2 \cos^2 \varphi + \Phi] \\ & + Q_{bd} - F_d (\nabla^2 \chi - \nabla^2 \chi_i) - K_d \nabla^4 (\nabla^2 \chi) \end{aligned} \quad (6)$$

$$\begin{aligned} \partial \Phi / \partial t = & -1 / (a \cos^2 \varphi) \left[ \frac{\partial}{\partial \lambda} (U_r \Phi) + \cos \varphi \frac{\partial}{\partial \varphi} (V_r \Phi) \right] - \Phi_e \nabla^2 \chi \\ & + Q_{bg} - F_g (\Phi - \Phi_i) - K_g \nabla^4 \Phi + Q_p \end{aligned} \quad (7)$$

The horizontal wind components are represented by:

$$u = U_r / \cos \varphi = \left| -(\cos \varphi) \frac{\partial \Psi}{\partial \varphi} + \frac{\partial \chi}{\partial \lambda} \right| / (a \cos \varphi) \quad (8)$$

$$v = V_r / \cos \varphi = \left| \frac{\partial \Psi}{\partial \lambda} + (\cos \varphi) \frac{\partial \chi}{\partial \varphi} \right| / (a \cos \varphi) \quad (9)$$

$\lambda$  and  $\varphi$  longitude and latitude coordinates.  $\Omega$  is Earth's angular velocity and  $a$  is Earth's radius. These equations are solved via semi-implicit differencing and the transform method (Haltiner and Williams 1980). Implicit and explicit leapfrog steps were used with 0.5 hour time steps for all model runs. The model fields,  $\Psi$ ,  $\chi$ , and  $\Phi$ , were initialized with the basic state fields used for each particular model run.

The model equations describe the horizontal circulation and height fields of the model atmosphere for a single vertical mode. The equivalent depth,  $h_e$ , determines the vertical mode. For this study, an equivalent depth of  $h_e = 2000$  m was used for all model runs. This depth was chosen to represent the observed low frequency global mean tropospheric structure, accounting for both the first internal baroclinic mode of the tropical troposphere (Gill 1980) and the external equivalent barotropic mode of the extratropics (Sawyer 1970, Wallace 1987).

## 1. Basic State Forcing

$Q_b$  terms were calculated for each basic state and then held constant through the model runs. These terms are the negatives of the residuals of the steady state forms of the expanded spherical forms of the vorticity and divergence equations in the absence of perturbation forcing. The basic state forcing terms are used to maintain a zonally and meridionally varying ambient atmospheric. These terms give a rough approximation of orographic effects, land-sea contrast effects, radiation, and other processes not explicitly contained in the model.

The basic state fields used in this study were the European Center for Medium-range Forecasting (ECMWF) analyses of global long term monthly mean values of 200 mb stream function, velocity potential, and geopotential height. For most of the runs in this study, the January and July fields were used. These two months showed the best contrast of summer and winter tropospheric conditions.

Figure 2 shows the January basic state fields. A prominent feature is the strong east Asian - North Pacific jet with a jet maximum southeast of Japan (Figure 2a). Other features of the January basic state include a region of diffluence over the western coast of North America and a weak North American subtropical jet over the southeastern U.S. coast (Figure 2a). The southern hemisphere 200 mb basic state is much more zonal in nature.

In the July basic state (Figure 3), the east Asian - North Pacific jet and the North American jet are weaker and have shifted poleward, and there is a wide band of tropical easterlies encircling the globe in the northern tropics. The southern hemisphere exhibits a very zonal structure with a strong jet over Australia and the southwest Pacific. Additional features of the January and July basic states are discussed in the Analysis Methods section of this chapter.

## 2. Perturbation Forcing

The equation for the spatial variation of the perturbation forcing,  $Q_p$ , is:

$$Q_p(\lambda, \varphi) = Q_{po} \exp[-(a/2s)(\cos^{-1}(\cos(\lambda - \lambda_0)\pi/M_R \times \cos(\varphi - \varphi_0)\pi/N_R))^2] \quad (10)$$

The term  $s$  is the perturbation forcing scale length in meters.  $\lambda_0$  and  $\varphi_0$  are the central longitude and latitude of the perturbation forcing.  $M_R$  and  $N_R$  are the total number of model gridpoints in the longitudinal and latitudinal directions, respectively.

$Q_{po}$  is the amplitude factor for the perturbation forcing. This term defines the central and maximum magnitude of the perturbation forcing. This value, with units of  $m^2 s^{-3}$ , may be converted via the hypsometric equation to an equivalent heating rate. In this study, the maximum perturbation forcing used was equivalent to a heating rate of 20K/day or less.

The perturbation forcing is intended to represent a strong and relatively long-lasting tropical cyclone. Thus, the parameters in (5) were selected to produce a forcing

for which the region with equivalent heating of 1K/day or more has a spatial scale of about 2000 km or less. The forcing is allowed to vary in its amplitude and location, with the amplitude variations being linear functions of time. The amplitude and spatial scale of the forcing are representative of observed and theoretical tropical cyclones of typhoon strength (Elsberry 1985). The location variations simulate the tracks of recurving and straight running tropical cyclones, with the recurving forcing extending into the tropics and the straight running forcing staying within 28° of the equator. For most of the runs in this study, the duration of the forcing is the first 11.5 days of the run. Some basic features of the perturbation forcing are shown in Figure 4.

### **C. MODEL OUTPUT FIELDS**

The model output fields used in this study have a spatial resolution of 2.8 degrees latitude by 4.7 degrees longitude and a temporal resolution of 12 hours. The following fields were examined. Because the basic state fields are based on analyses at 200 mb, the model output fields, and the fields derived from them (e.g., wave activity flux) are representations of the atmosphere at 200 mb.

#### **1. Geopotential Height**

The geopotential field is especially effective in showing the model's response to tropical forcing and in identifying teleconnection mechanisms.

## **2. Stream Function**

The model's stream function was used to calculate the rotational component of the horizontal wind. This field and the model's velocity potential field were used to calculate the model's total wind field.

## **3. Velocity Potential**

The model's velocity potential was used to calculate the divergent component of the horizontal wind. The divergent winds are capable of advecting absolute vorticity and are key component of Rossby wave source calculations (Sardeshmukh and Hoskins 1988).

## **D. MODEL RUNS**

The standard model runs simulate a 24-day period with constant basic state forcing throughout the run and perturbation forcing only during the first 11.5 days. We conducted several model runs, outlined in Table 1, to study the response of the model atmosphere to short term localized forcing. The primary model parameters that we varied for the different runs were the perturbation forcing's amplitude,  $Q_{po}$ , and location. We used different basic states for the runs but focused on the January and July basic states. The model's equivalent depth, perturbation forcing scale length, dissipation terms, and other parameters were not varied for this study. Only one perturbation forcing was used for each run. We conducted three categories of model runs which are described below.

## **1. Basic Runs**

The basic runs were the simplest runs used in this study. These runs were conducted for both January and July basic states and with the perturbation forcing being located in the tropical western North Pacific. These runs were conducted to establish the baseline responses to tropical forcing.

In the first set of these runs, the perturbation forcing was held at a constant amplitude and location for the first 11.5 days of the model run then turned off for the last 12.5 days of the model run. The fixed amplitude and location were the averages of those used in the recurving and straight running cases described earlier.

In the second set of basic runs, the location of the perturbation forcing was fixed as in the first set of basic runs. But the forcing amplitude was linearly increased during the first six days and linearly decreased during the next six days to simulate the strengthening and weakening of a tropical cyclone.

In the third set of basic runs, the perturbation forcing location was varied while its amplitude was held constant as in the first set of basic runs. The location variations simulated recurving and straight running cases.

## **2. Tropical Basin Runs**

The tropical basin runs reproduced the first set of the basic runs, with fixed perturbation forcing amplitude and location but with the forcing located in three tropical ocean basins: Bay of Bengal, the western North Pacific, and the western North Atlantic.

These runs were done to establish the basic sensitivity of the response to the tropical basin on which the forcing was located.

### **3. Tropical Cyclone Runs**

The tropical cyclone runs give the most realistic simulation of tropical cyclone forcing. In these runs, the full variability of the perturbation forcing is used. Thus this forcing had variable amplitude, recurving and straight running tracks, and was located in all three basins. For the runs using different basins, the amplitudes and tracks of the perturbation forcing were the same. These runs were done to test the sensitivity to a combination of forcing changes.

## **E. ANALYSIS METHODS**

The **model response** to the perturbation forcing is defined for this study as the difference between a model run with perturbation forcing and a comparable run without perturbation forcing, the difference being the former minus the latter. This response was analyzed using several diagnostic tools. The basic response patterns were identified using the geopotential height fields.

### **1. Quasi-Geostrophic Wave Activity Flux Vectors**

Plumb (1985) developed a method of tracking quasi-geostrophic (QG) wave activity fluxes based on conservation relations and the phase independent nature of QG wave activity. The flux vectors he developed are parallel to the path of wave energy propagation while the vector magnitude are proportional to the strength of the



propagation. Divergent flux vectors are indicative of a source of QG wave energy, while convergent flux vectors indicate a wave energy sink. Plumb flux vectors and flux divergence were not calculated within  $10^\circ$  of the equator due to the inherent weakness of the QG approximation in the tropics.

## 2. Barotropic Instability (BTI)

As discussed in Chapter I, barotropic instability processes may be involved in the development of teleconnection responses. In this case, energy from the background flow is directed into the response to produce an amplified response. Areas of potential BTI are strongly associated with the flanks of the extratropical jets. Areas of potential BTI were calculated using the Rayleigh-Kuo instability criterion (Kuo 1949):

$$\beta - \frac{\partial^2 u}{\partial y^2} = 0 \quad (11)$$

$\beta$  is the total derivative of the Coriolis parameter. The Rayleigh-Kuo criterion is a necessary, but not sufficient condition for the existence of barotropic instability.

Therefore, the Rayleigh-Kuo criterion only indicates areas where BTI might be involved in the teleconnection process. The model's zonal wind fields,  $u_{200}$ , and  $\beta$  were used to calculate regions where (11) was satisfied. Figures 2e and 3e show the areas of potential BTI for the January and July basic states. Note in particular the large regions along the jets (see Figures 2a and 3a) where (11) is satisfied.

### 3. Stationary Wave Number

To estimate the impacts of the basic state flow on the meridional propagation of low frequency QG wave energy, the stationary wave number (Karoly 1978) was calculated for the January and July basic states. This quantity gives an estimate of the largest zonal wave number for which meridional propagation is possible, and is inversely proportional to the zonal wind:

$$K_s^2 = \frac{\beta}{u} - K_R^2 \quad (12)$$

Here,  $K_s$  is the stationary wave number,  $K_R$  is the internal Rossby radius of deformation =  $(f^2/gh_e)^{1/2}$ , and  $u$  is the zonal flow. This relation shows that strong zonal flows limit meridional propagation, with the limitation being greater for waves with smaller zonal scales. Figures 2f and 3f show  $K_s \leq 8$  for the January and July basic states. In these figures, each contour indicates the limit of meridional propagation for waves with zonal wave numbers less than or equal to that designated by the contour. Note that the  $K_s = 5$  contour tends to coincide with the equatorward flanks of the extratropical jets (see Figures 2a and 3a). This indicates that the jets may be a significant wave guide for waves with zonal wave numbers  $\leq 5$ .

#### 4. Rossby Wave Source Calculation

Sardeshmukh and Hoskins (1988) suggested that the advection of absolute vorticity by the horizontal component of the divergent wind could be a significant process for generating Rossby waves. Previous teleconnection modeling studies ignored the divergent portion of the horizontal wind and focused solely on the rotational component of the horizontal wind, due to its greater magnitude on the large scales associated with teleconnections. Sardeshmukh and Hoskins (1988) concluded that a tropical forcing may not directly generate an extratropical Rossby wave trains, but rather do so by producing strong divergent winds that cross regions of large absolute vorticity gradients along the jets. This in turn would lead to a large wave generation term in the absolute vorticity equation.

The isobaric coordinate form of the absolute vorticity equation contains the Rossby wave source term,  $S$ :

$$\left( \frac{\partial}{\partial t} + \vec{V}_\Psi \cdot \nabla \right) (\zeta + f) = S \quad (13)$$

Where  $(\zeta + f)$  is the absolute vorticity term.

The Rossby source term,  $S$ , is defined as:

$$S = -\nabla \cdot [\vec{V}_x(\zeta + f)] \quad (14)$$

Expansion of (14) yields:

$$S = - \left[ u_x \frac{\partial \zeta}{\partial x} + v_x \frac{\partial \zeta}{\partial y} + v_x \beta + (\zeta + f) \left( \frac{\partial u_x}{\partial x} + \frac{\partial v_x}{\partial y} \right) \right] \quad (15)$$

The first three terms on the right-hand side of (15) represent advection of absolute vorticity by the divergent wind (ADV DIV). The other source term in (15) is the vortex stretching or divergence term.

The terms in (15) were calculated for various times in the model runs using finite difference approximations of the derivatives. The differences between these source terms and those in the initial fields represent the Rossby wave source response to the perturbation forcing.

### III. RESULTS

#### A. INTRODUCTION TO MODEL RUNS

To test the model's response to short term forcing, a series of model runs was developed and executed. These model runs began with basic forcing scenarios and progressed to model runs that simulated the more complex forcing behavior associated with tropical cyclones (Table 1).

Before conducting the model experiments, we performed a series of model tests to determine the basic characteristics and range of responses to different basic state conditions and perturbation forcing values. These tests showed that the results from runs with the January (July) basic state conditions were very representative of the results from runs with other northern winter (summer) basic state conditions. In addition, these tests showed that the results obtained when using a January basic state or a July basic state were markedly different from each other. Thus, we selected as our primary basic state conditions those from January and July in order to highlight the effects of seasonal variations in the basic state using a minimum of runs.

Our tests of the model's sensitivity to the forcing amplitude showed qualitatively similar responses for all reasonable values of the amplitude. Thus, we used forcing amplitudes that were  $\leq 20$  K/day, with the amplitude being constant for some runs and varying with time for other runs (see Table 1).

Recurving and straight running forcing paths were developed for the variable forcing location runs. These paths were based upon the characteristic tracks of actual tropical cyclones. The recurving path (Figure 4a) allowed the perturbation forcing to penetrate the mid-latitudes, while the straight running path remained entirely in the tropics below 28° N (Figure 4b).

In the following sections of this chapter, we review the major results from the runs conducted for this study and summarized in Table 1. Our focus in this review is on the northern hemisphere responses to the tropical perturbation forcing. This is because: (1) our forcing experiments all used northern hemisphere perturbation forcing and gave responses that were relatively large in the northern hemisphere; and (2) we wanted to compare our results to those from the studies of Woll (1993), Springer (1994), and Jakus (1995) which focused on responses in the North Pacific - North American region.

## **B. WESTERN NORTH PACIFIC RUN DESCRIPTIONS**

### **1. January Fixed Forcing Runs**

Figure 5 shows the fixed forcing and height response for the most basic January western North Pacific (run PJ1, Table 1). The response after 12 hours (Figure 5a) was a positive height response over southern Japan north-northwest of the perturbation forcing location. A wave pattern developed rapidly across the North Pacific to the east of this early response. This wave pattern had a very slow westward drift during the first few days.

However, by day four of the model run, the initial positive response became fixed over the west coast of China (Figure 5b).

This fixed pattern continued to amplify eastward from the east Asian region along approximately  $35^{\circ}$  N. The pattern encircled the northern hemisphere by day eight with a clear zonal wavenumber four component (Figure 5c). During most of the run, the amplitude in the initial response region decreased as the amplitude increased progressively further to the east. This suggests an eastward group velocity for the wave response. The response persisted well after the perturbation forcing ceased (Figure 5b-g). Throughout most of the run, the high and low height responses over the northeast Pacific had a pronounced northwest-southeast tilt and roughly resembled the negative of the PNA pattern.

#### *a. Rossby Wave Source Analyses*

Figure 6 shows the early responses for some of the terms in the Rossby wave source equation, (15). The divergent wind response (Figure 6a) showed a distinct radial outflow from the perturbation forcing region, with strong flow crossing the jet over east Asia (Figure 2a). The ADVDIV component of the Rossby wave source response (Figure 6b) had a distinct negative feature just south of Japan that coincided with the position of the initial positive height response (Figure 5a). This ADVDIV response persisted throughout the first 12 days of the run (not shown). The stretching component of the Rossby wave source response (Figure 6c) had a negative feature over the

perturbation forcing region which persisted throughout the forcing period (the first 11.5 days)(not shown). There were also distinct positive and negative features over northern Japan and northeastern Asia. These features were associated with weak height responses (e.g., the positive height response southeast of Lake Baikal, Figure 5a). Throughout the first 12 days, these stretching responses varied considerably and were associated with relatively weak and transient height responses (not shown).

Throughout the first 12 days of the model run, the ADVDIV and stretching responses had the same magnitude, but only the negative ADVDIV response was associated with the positive height response over east Asia. The negative source response is consistent with the positive height response, since both are associated with the generation of negative relative vorticity. Thus, it appears that the ADVDIV response may have helped initiate the height response.

#### ***b. Wave Energy Analyses***

The QG wave activity flux vectors corresponding to the height responses in Figure 5 are shown in Figure 7. There was a weak energy propagation away from the forcing region at 12 hours (Figure 7a). The region of strongest propagation shifted eastward during the first 12 days until it became centered over the northeast Pacific (Figure 7a-d). This was also a region of strong northeastward propagation. To the west of this region, the propagation was predominantly eastward along the east Asian - North Pacific jet (e.g., Figure 7c). Over North America, the propagation described an arcing



pattern, with the energy directed southeastward over central Canada (e.g., Figure 7d).

The divergence of the flux vectors in Figure 8 indicates strong energy sources for the wave response over the subtropical North Pacific. Note, for example, the divergent vectors near Hawaii after eight days (Figure 7c), on the south flank of the basic state jet near the jet exit (see Figure 2a).

The strong zonal propagation along the jet over the North Pacific, and the strong meridional propagation in the midlatitude inter-jet regions over the North Pacific and North America, suggest that the jet acted as a wave guide (cf. Lau and Lim 1984). This is consistent with the restricted meridional propagation along the jets indicated by the basic state stationary wave numbers (Figure 2f). The strong wave energy source along the North Pacific jet flank suggests that the jet was an energy source for the response. The major energy source region in the subtropical North Pacific is collocated with the downstream end of the region of potential BTI in the basic state (Figure 2e). This suggests that BTI processes were involved in developing this wave energy source. Similar results were found by Woll (1993) and Springer (1994).

## **2. January Fixed Location-Variable Strength Runs**

The response patterns for the January fixed location-varied amplitude run (run PJ1A, Table 1) were qualitatively similar to those for the fixed forcing run (run PJ1, Table 1 and preceding section). The height response after 12 days (Figure 8) is similar to that in run PJ1 except that it is weaker and has a more zonal structure over the western

North Pacific (cf. Figure 5d). The Rossby wave sources are also similar for the two runs. The energy propagation and energy sources (not shown) are also similar to but more zonal than those for run PJ1 (Figure 7).

### **3. January Variable Location-Fixed Strength Runs**

Figure 9 shows the height response to the western North Pacific run with recurving, fixed amplitude forcing (run PJ1L, Table 1) after 12 days. This response, and the Rossby wave source and wave energy responses (not shown), were similar to but markedly stronger than those for runs PJ1 and PJ1A (see table 1 and the preceding sections of this chapter). This was especially true when the forcing approached the east Asian jet. There was also a significant energy source on the poleward flank of the east Asian - North Pacific jet (not shown) in the region of potential BTI in the basic state (Figure 2e). The movement of the perturbation forcing into the extratropics may explain the development of this midlatitude energy source which was not so apparent in the runs for which the forcing location was fixed. These differences in the runs suggest that the same basic mechanism was operating in all three cases and that interactions between the perturbation forcing and the jet (e.g., Rossby wave source processes) may be significant in producing the wave response.

### **4. January Recurving Cyclone Run**

The responses to the recurving, variable amplitude forcing (run PJ1R, Table 1) were similar to that for run PJ1L but with weaker responses (cf. Figures 9, 10 for the

height responses). This difference is consistent with a weaker average forcing in run PJ1R, especially when the forcing entered the extratropics. The energy propagation response showed strong wave guiding along the jet in the western North Pacific during days 1-10 (not shown). During days 12-18, there was a strong arcing energy propagation path out of the northeastern Pacific and across North America at 12 days (Figure 10). The major source region for this energy was the downstream end of the basic state region of potential BTI over the subtropical North Pacific (Figure 2a).

### **5. January Straight Running Cyclone Run**

The responses to the straight running, variable amplitude tropical forcing (run PJ1S, Table 1) were very similar to but weaker than those for the recurving variation of this run (run PJ1R), as shown by a comparison of Figures 10 and 11. These results are consistent with the previously discussed runs, and support the conclusion that the processes by which the response develops are relatively insensitive to the location of the forcing -- at least so long as the divergent outflow from the forcing reaches the east Asian - North Pacific jet.

### **6. July Fixed Forcing Runs**

The height response to the run using a fixed forcing in the western Pacific and a July basic state (run PJ2, Table 1) is shown in Figure 12. At 12 hours into the run there was a positive height response over the perturbation forcing (Figure 12a). By four days, this positive response had shifted about 1000 km to the west of the forcing, and a weak

zonal wave train had developed along approximately 40°N (Figure 12b). This wave train had a clear zonal wave number three component and a westward phase propagation of about 13 m/s. During the next eight days, this basic response pattern remained, with the midlatitude response growing in both the northern and southern hemispheres (Figure 12c,d). After the perturbation forcing was turned off after 11.5 days, the positive response near the forcing quickly disappeared, but the wave train at 40°N persisted and maintained its strength throughout most of the run. This was especially true over east Asia, where the waves amplified as they propagated westward through the region. Throughout the run, the northern hemisphere response was as strong or stronger than that in the southern hemisphere.

#### *a. Rossby Wave Source Analyses*

Figure 13 shows the early responses for some of the terms in the Rossby wave source equation, (15). The divergent wind response (Figure 13a) showed a distinct radial outflow from the perturbation forcing region, with strong flow crossing the jet over east Asia (Figure 3a). The ADVDIV component of the Rossby wave source response (Figure 13b) had a weak negative feature over the Sea of Japan that coincided with the position of a weak positive height response (Figure 12a). The stretching component of the Rossby wave source response (Figure 13c) had a strong negative feature over the perturbation forcing region which coincided with the positive height response there (Figure 12a). The stretching response also had distinct positive and negative features

over northeastern Asia, but these did not coincide with any significant height responses. The collocation over the Sea of Japan of the weak negative ADVDIV response and the weak positive height response at 12 hours suggests that the ADVDIV process may have made a small contribution to the initiation of the response in this region. However, the propagation of positive and negative height responses through this region suggests that the ADVDIV process was not so important in determining the response as was the case for the corresponding January run, PJ1. This difference was probably due to the weaker east Asian jet in the July basic state.

### ***b. Wave Energy Analyses***

The QG wave activity flux vectors corresponding to the height responses in Figure 12 are shown in Figure 14. During most of the first 12 days, there was energy propagation to the northeast, east, and/or southeast away from the forcing region (Figure 14a-d), indicating that the perturbation forcing was a significant source of wave energy. This is consistent with the strong stretching response seen in this area during the first 12 days (e.g., Figure 13c). During the remaining days, the major energy source was over the east Asian - northwest Pacific region at about 40-50°N. Figure 3e indicates that this region was potentially barotropically unstable, suggesting that the basic state flow may have contributed energy to the response in this region. From this region, the energy propagated eastward, opposite to the phase propagation indicated by the height responses (Figure 12). The zonal energy propagation during days 12-24 across east Asia and

the northwest Pacific at about 45°N is consistent with the zonal wave guide indicated by the stationary wave numbers in this area (Figure 3f).

The results from this run, PJ2, contrast sharply with those from the corresponding run which used a January basic, PJ1 (see Chapter III, section B1). These differences are due to the differences in the basic states, since those are the only differences between the runs (compare Figures 2 and 3). The weaker (stronger) northern (southern) hemisphere responses in PJ2 indicate that the strength of the ambient flow is a significant factor in allowing a large response to develop.

#### **7. July Fixed Location-Variable Strength Runs**

The July fixed location, variable amplitude run (PJ2A, Table 1) response (not shown) was qualitatively similar to that for run PJ2, but much weaker in the northern hemisphere. This suggests that a significant northern hemisphere response in the presence of a weak basic state flow requires a relatively sustained tropical forcing or, possibly, a forcing that travels closer to the extratropics.

#### **8. July Variable Location-Fixed Strength Runs**

The response after 12 and 16 days of the July run in which the forcing recurved into the extratropics with a fixed amplitude (run PJ2L, Table 1) is shown in Figure 15. The positive response over the Sea of Japan in Figure 15a was a feature that traveled northwestward with the forcing during the first 12 days. This feature dissipated within a few days of the forcing being turned off after 11.5 days. By day 16, the northern

hemisphere response resembled that seen in run PJ2 (Figure 12e). The phase propagation, Rossby wave source, and wave energy analyses (not shown) also indicate that these two runs were similar. The major differences between these runs seem to be the result of the northwestward shift of the positive height response over the forcing that occurred in PJ2L but not in PJ2.

#### **9. July Recurving Cyclone Run**

The response of the July run with recurving forcing with variable amplitude (run PJ2R, Table 1) was very similar to that for runs PJ2 and PJ2L. The height response after 12 and 16 days (Figure 16) is similar to the response at about 12-20 days seen in PJ2 and PJ2L (Figures 12 and 15). In particular, the response in the three runs had similar spatial and temporal scales, westward phase propagation, eastward group propagation, and amplification in areas of potential BTI in the east Asian - North Pacific region.

#### **10. July Straight Running Cyclone Run**

The response for run PJ2S (not shown) was very similar to that for run PJ2R. The Rossby wave source and wave energy analyses (not shown) that this similarity was due to the ability of the forcing in the two runs to generate a response in the area of potential BTI over east Asia at 40-50°N (Figure 3e).

### **C. BAY OF BENGAL RUN DESCRIPTIONS**

The runs for which the tropical perturbation forcing was located in the Bay of Bengal gave results that were similar in many ways to the corresponding runs with the

forcing in the tropical western North Pacific. In particular, the Rossby wave source and wave energy analyses showed that similar mechanisms were operating for both the Bay of Bengal and Pacific runs. Because of these similarities, only the key results from some of the Bay of Bengal runs are described here.

### **1. January Fixed Forcing Runs.**

Figure 17 shows the fixed forcing and height response for the most basic January Bay of Bengal run (run BJ1, Table 1). The response after 12 hours (Figure 17a) was a positive height response over the Tibetan Plateau north of the perturbation forcing location. A wave pattern developed rapidly across Asia and the North Pacific to the east of this early response. This wave pattern had a very slow westward drift during the first few days. However, by day four of the model run, the initial positive response became fixed over the southwest China (Figure 17b).

This fixed pattern continued to amplify eastward from the central Asian region along approximately  $35^{\circ}$  N. The pattern encircled the northern hemisphere by day eight with a clear zonal wavenumber four component (Figure 17c). During most of the middle and later periods of the run, the amplitude in the initial response region decreased as the amplitude increased progressively further to the east. This suggests an eastward group velocity for the wave response. The response persisted well after the perturbation forcing ceased (Figure 17b-g).



Throughout most of the run, the high and low height responses over the northeast Pacific had a pronounced northwest-southeast tilt and roughly resembled the PNA pattern.

These BJ1 responses were very similar to those for PJ1, the corresponding western Pacific run, except that the response over Asia was better developed in BJ1 and the overall responses were out of phase over most of the northern hemisphere. These results suggest that tropical disturbances in the Indian Ocean may be just as effective at producing anomalies in the North Pacific - North American region as those in the tropical Pacific.

#### *a. Rossby Wave Source Analyses*

A negative Rossby wave source response (not shown) developed early in the run at the location of the positive response over the Tibetan plateau. At this location, the dominant term for this response was the ADVDIV term (not shown). Thus, it appears that the ADVDIV response may have helped initiate the height response, as was the case for the corresponding western Pacific run (PJ1).

#### *b. Wave Energy Analyses*

The QG wave activity flux vectors corresponding to the height responses in Figure 17 are shown in Figure 18. There was a weak energy propagation away from the forcing region at 12 hours (Figure 18a). The region of strongest propagation shifted eastward during the first 12 days until it became centered over the northeast Pacific (Figure 18a-d). This was also a region of strong northeastward propagation. To the west

of this region, the propagation was predominantly eastward along the east Asian - North Pacific jet (e.g., Figure 18c). In the later part of the run, the propagation over North America described a rough arcing pattern, with the energy directed southeastward over eastern Canada (e.g., Figure 18e). The divergence of the flux vectors in Figure 18 indicates strong energy sources for the wave response over eastern Asia and the subtropical North Pacific. Note, for example, the divergent vectors near northeastern China and Hawaii after eight days (Figure 18c).

The strong zonal propagation along the jet over east Asia and the North Pacific, and the strong meridional propagation in the midlatitude inter-jet regions over the North Pacific and North America, suggest that the jet acted as a wave guide for the response. This is consistent with the restricted meridional propagation along the jets indicated by the basic state stationary wave numbers (Figure 2f). The strong wave energy sources along the east Asian - North Pacific jet flanks suggests that the jet was an energy source for the response. Both of the major energy sources were collocated with regions of potential BTI in the basic state (Figure 2e). This suggests that BTI processes were involved in developing these wave energy sources. Similar results were found for the corresponding January run, PJ1.

## **2. January Recurving Cyclone Run**

Figure 19 shows the height response to the recurving, variable amplitude forcing after 12 days (run BJ1R, Table 1). The similarity between this response and that for run

BJ1 (Figure 5d) occurred at other times and in the other model fields analyzed (not shown). In particular, the energy propagation response showed strong wave guiding along the jet in the east Asian - North Pacific during days 1-10 (not shown). During days 12-18, there was a strong arcing energy propagation path out of the northeastern Pacific and across North America at 12 days (Figure 20). The major source region for this energy was the downstream end of the basic state region of potential BTI over the subtropical North Pacific (Figure 2e).

### **3. July Recurving Cyclone Run**

The response of the July run with recurving forcing with variable amplitude (run BJ2R, Table 1) was qualitatively similar to that for the corresponding western Pacific runs PJ2R (compare, for example, Figures 21 and 16). The BJ2R and PJ2R responses had similar spatial and temporal scales, westward phase propagation, eastward group propagation, and amplification in areas of potential BTI in the east Asian - North Pacific region. The main differences between the two runs were due to longitudinal shifts in the response locations.

### **D. NORTH ATLANTIC RUN DESCRIPTIONS**

The runs for which the tropical perturbation forcing was located in the North Atlantic gave results that had some clear similarities and differences when compared with the results from the corresponding tropical western North Pacific or Bay of Bengal runs (see Table 1).

The key results from some of the North Atlantic runs are described here to highlight these similarities and differences.

### **1. January Fixed Forcing Runs**

Figure 22 shows the fixed forcing and height response for the most basic January North Atlantic run (run AJ1, Table 1). The response after 12 hours (Figure 22a) was a positive height response approximately collocated with the perturbation forcing northeast of Colombia (Figure 22a). A wave pattern developed rapidly from North America eastward across the North Atlantic and into Asia and the North Pacific to the east of this early response (Figure 22a-d). This wave pattern had a very slow westward drift during the first few days. However, by day eight of the model run, the positive and negative centers of the response were approximately fixed in place (Figure 22c).

This fixed pattern amplified eastward from the North Atlantic region along approximately 30-50°N. This suggests an eastward group velocity for the wave response. The pattern encircled the northern hemisphere by day eight with a clear zonal wavenumber four component (Figure 22c). Throughout the run, the strongest responses were in the North Atlantic - European region. The response persisted well after the perturbation forcing ceased (Figure 22e-g). Throughout most of the run, the high and low height responses over the North Atlantic - European region had a pronounced northwest-southeast tilt.

This tilt was also seen during the middle part of the run in the North Pacific - North American region where a pattern roughly similar to the PNA pattern developed (Figure 22d-e).

The overall AJ1 height responses over Asia and the North Pacific were roughly similar to those for PJ1 and BJ1 (Figures 5 and 17). However, over the North Atlantic - European region, the AJ1 responses were stronger, more persistent, more tilted. These results suggest that tropical disturbances in the North Atlantic region may affect the circulation throughout the northern hemisphere, but have their greatest impact in the North Atlantic - European area.

*a. Rossby Wave Source Analyses*

After 12 hours of the AJ1 run, a weak negative ADVDIV response (Figure 23b) had developed in association with the divergent wind response (Figure 23a) across the North Atlantic jet (Figure 2a). However, the development of the early height response was mainly associated with a strong negative stretching term in the Rossby wave source response (Figure 23c). This is in contrast to the corresponding Pacific and Bay of Bengal results (runs PJ1 and BJ1) in which the ADVDIV term was better correlated with the height anomalies. This difference is probably due to the North Atlantic jet being considerably weaker than the Asian - North Pacific jet.

### ***b. Wave Energy Analyses***

The QG wave activity flux vectors corresponding to the height responses in Figure 23 are shown in Figure 24. There was a weak eastward and northeastward energy propagation away from the forcing region at 12 hours which grew stronger during the first 10 days (Figure 24a-c). The region of strongest propagation shifted eastward during the first 16 days until it became centered over the northeast Pacific (Figure 24a-e). This was also a region of northeastward propagation. To the west of this region, the propagation was predominantly eastward along the north African - south Asian - North Pacific jet (compare Figures 24d and 2a). In the later part of the run, the propagation over the North Pacific - North American region described a weak arcing pattern, with the energy directed southeastward over the central U.S. (e.g., Figure 24f). The divergence of the flux vectors in Figure 24 indicates strong energy sources for the wave response over the western North Atlantic - Iberian - Mediterranean region and the subtropical North Pacific. Note, for example, the divergent vectors near the western Mediterranean and west of Hawaii after twelve days (Figure 24d).

The strong propagation along the jets over the North Atlantic, north Africa, southern Asia, and the North Pacific, plus the strong meridional propagation in the midlatitude inter-jet regions over the North Pacific, North America, and North Atlantic, suggest that the jets acted as a wave guide for the response. As an example, note the northeastward propagation at 8 and 12 days between the North Atlantic jet and

the north African jet (Figure 24c-d). The basic state stationary wave number analysis (Figure 2f) indicates that this is a region of relatively unrestricted meridional propagation, or a propagation duct, between the barriers posed by the two jets.

In addition, the strong wave energy sources along the flanks of the North Atlantic jet and the north African - south Asian - North Pacific jet suggests that these jets were energy sources for the response. The major energy sources along the jets were collocated with regions of potential BTI in the basic state (Figure 2e). This suggests that BTI processes were involved in developing these wave energy sources. Similar results were found for the corresponding January run in the Pacific, PJ1, and Bay of Bengal, BJ1.

## **2. January Recurring Cyclone Run**

Figure 25 shows the height response to the recurving, variable amplitude forcing after 12 days (run AJ1R, Table 1). The similarity between this response and that for run AJ1 (Figure 22d) occurred at other times and in the other model fields analyzed (not shown). In particular, there was a strong energy source in the North Atlantic - Iberian - Mediterranean region (e.g., Figure 26) associated with the basic state region of potential BTI between the North Atlantic and north African jets (Figure 2e). During the middle parts of the AJ1R run, the responses were stronger than for AJ1, probably because during this period the forcing was stronger and located closer to the areas of potential BTI.

### **3. July Recurving Cyclone Run**

The response of the July run with recurving forcing with variable amplitude (run AJ2R, Table 1) was similar to that for the other North Atlantic July runs. After 4 days, the height response for run AJ2R (Figure 27b) had a positive response over and to the northwest of the forcing and a negative response to the northeast. This pattern persisted until the forcing was turned off after 11.5 days (Figure 27b-d). During days 10-20, an arcing wave train occurred over the North American - North Atlantic - European area which drifted westward after the forcing was turned off (Figure 27d-f). The response over most of Asia was noticeably weaker and less persistent than in the Pacific and Bay of Bengal July runs.

#### ***a. Rossby Wave Source Analyses***

After 12 hours of the AJ2R run, a weak negative ADVDIV response (not shown) had developed in association with the divergent wind response (not shown) across the subtropical North Atlantic jet (Figure 3a). However, the development of the early height response was mainly associated with a strong negative stretching term in the Rossby wave source response (not shown). This was similar to the corresponding January runs, AJ1 and AJ1R.

#### ***b. Wave Energy Analyses***

The QG wave activity flux vectors corresponding to the height responses at 4, 8, 12, and 16 days (Figure 27) are shown in Figure 28. There was a weak eastward



and northeastward energy propagation away from the forcing region at 4 days. At 8 days, when the forcing was near its maximum amplitude and located over Florida, there was very strong and divergent southeastward and eastward propagation from the forcing region. This energy source was located at the upstream end of an area of potential BTI between the North American jet and the subtropical North Atlantic jet (Figure 3a). By 12 days, this energy source was gone. During days 14-20, there was moderate to weak propagation on an arcing path across North America. The upstream end of this path was collocated with the downstream end of an area of potential BTI on the southern flank of the North Pacific jet (Figure 3e). At this time near 12 hours which grew stronger during the first 10 days (Figure 24a-c).

## **E. SUMMARY**

The model results showed a number of patterns which are summarized in the following sections.

### **1. Height Responses**

All the runs showed clear teleconnection responses to the tropical perturbation forcing. These responses were most clear in the height responses, in which distinct wave trains tended to develop. The runs with relatively simple representations of a tropical perturbation forcing gave responses that were qualitatively similar to those found in the corresponding runs with more realistically varying forcing. This indicates that this model is relatively insensitive to many of the specifics of the perturbation forcing. The height

response patterns in the July and January runs were distinctly different. In particular, the northern hemisphere response in January tended to be stronger and more stationary than in July. For the July runs, the response had a clear westward phase propagation and the southern hemisphere response was generally as strong as the northern hemisphere response, even when the forcing was located well north of the equator. This tendency for a strong winter hemisphere response has been found in other studies (e.g., Opsteegh and Van den Dool, 1980).

There was a tendency for the height responses to start with a positive response somewhere to the north of the forcing (most of the January runs) or approximately over the forcing (the July and North Atlantic runs). The response then developed by eastward energy propagation away from the initial positive response. This eastward propagation of the response tended to be most rapid for the North Atlantic runs and least rapid for the Bay of Bengal runs. The poleward propagation was also most rapid for the North Atlantic runs and least rapid for forcing in the Bay of Bengal. This is consistent with the southwest to northeast tilt of the jets and the propagation ducts in the northeast Atlantic region (Figures 2a,f and 3a,f). The responses downwind of the forcing longitude tended to be zonally shorter than those on upwind side. This is consistent with the dispersion relationship for Rossby waves (Holton, 1992). The response patterns tended to shift longitudinally as the forcing was shifted between the tropical basins.

The January runs generally had northeastward energy propagation over the northeast Pacific and the northeast Atlantic. This is consistent with the low wind speed regions between the jets and the propagation ducts over the northeast Pacific - North American region and over the northeast Atlantic region (Figures 2a,f and 3a,f). The January runs also had response patterns that persisted well after the forcing was turned off, with the shorter waves decaying more rapidly after the forcing was turned off.

The July runs had response patterns that generally drifted to the west, with the response to North Atlantic forcing drifting least rapidly. The responses tended to amplify as they passed through the region of potential BTI over east Asian near northern Japan.

The runs with forcing in the Bay of Bengal or western North Pacific had similar responses, although they tended to be out of phase with each other. The runs with North Atlantic forcing had distinctly different response patterns. However, for all of these runs, there tended to be a clear response in the northeast Pacific - North American region, with the positive and negative height response centers describing a poleward and eastward arcing pattern.

## **2. Teleconnection Dynamics**

### ***a. Rossby Wave Source Analyses***

The initial positive height responses were associated with a Rossby wave source process. For the January runs with forcing in the Bay of Bengal or in the western North Pacific, this process depended on the advection of absolute vorticity as the

forcing's divergent outflow crossed a nearby subtropical jet. For the January runs with North Atlantic forcing, this process depended on vortex stretching within the forcing. For the July runs, the process depended mainly on vortex stretching. These differences in the Rossby wave initiation were due to longitudinal and seasonal variations in the position and strength of the jet poleward of the forcing, with the jet being: (1) stronger and closer to the forcing in the January Bay of Bengal and western North Pacific cases; and (2) weaker and further from the equator in the North Atlantic and July cases.

### ***b. Wave Energy Analyses***

The wave activity fluxes confirmed the predominantly eastward energy propagation indicated by the development of height responses. These fluxes also showed regions of strong poleward and equatorward energy propagation in the weak flow areas between the jets. The basic state stationary wave number calculations indicated that these areas were also potential propagation ducts.

The divergence of the wave activity fluxes showed that the major sources of energy for the response were: (1) the perturbation forcing during the initial development of the response; (2) areas of potential barotropic instability in the basic state. The unstable area on the southern flank of the North Pacific jet was collocated with relatively large energy sources in many of the responses, especially for the January runs. This may explain why the northeast Pacific - North American region tended to have large and persistent responses.

## IV. CONCLUSIONS

### A. SUMMARY

We used a global shallow water model to investigate the dynamics of teleconnections initiated by relatively small scale, short term tropical perturbations (e.g., tropical cyclones). Our emphasis was on the northern hemisphere response to perturbations in the northern tropics. Our study is a companion to those by Woll (1993), Springer (1994), and Jakus (1995) who used a global data assimilation system and numerical weather prediction (NWP) model to investigate the response to individual tropical cyclones in the western Pacific. The model for our study was much easier to modify and more economical to run than a NWP model. This allowed us to conduct many runs and investigate the importance of many variables (e.g., variations in the path, amplitude, and longitude of the perturbation forcing; the seasonal variations of the basic state).

The major hypotheses tested in this study, and in those by Woll (1993), Springer (1994), and Jakus (1995), are given below.

- Tropical cyclones can produce strong teleconnections.
- The development of teleconnections is strongly influenced by wave guiding and amplification effects associated with the mid-latitude westerly jet.

- The absolute vorticity flux associated with the divergent outflow from the tropical cyclone crossing the jet may initiate the wave response to the storm.
- Barotropic instability (BTI) processes play a major role in the amplification process.
- The basic teleconnection process varies with season and the forcing location due to temporal and spatial variations in the ambient flow, especially the westerly jets.
- The results of the simplified general circulation model and the results of the NWP model are qualitatively similar because: (1) the ambient upper tropospheric flow plays a dominant role in the development of the teleconnection response; and (2) the ambient flow is similar in the two models.

The results of this study confirm all of these hypotheses. In particular, they indicate that the simplified global model used in this study may yield results that are at least qualitatively consistent with those from a much more sophisticated NWP model.

## **B. IMPLICATIONS FOR EXTENDED-RANGE FORECASTING**

The upper tropospheric height responses seen in this and previous studies (e.g., Woll 1993, Springer 1994, Jakus 1995, and Harr and Elsberry 1995) indicate that

relatively small scale and short term tropical disturbances, such as tropical cyclones, may have significant global impacts on time scales of one to three weeks. The mechanism results from this study suggest that these impacts are more likely at certain times and locations. For example, strong and persistent impacts are more likely when the tropical disturbance is able to interact with a strong jet. Thus, when the disturbance travels well away from the equator, or when the jet shifts toward the equator, significant teleconnections are more likely. Thus, in the development of extended range forecast models, close attention should be paid to accurately simulating such tropical disturbances and their potential interactions with the jets. In addition, special attention should be paid to locations and times when such interactions are more likely (e.g., in the tropical western North Pacific during northern hemisphere winter when recurving cyclones may readily approach the subtropical east Asian-North Pacific jet).

### **C. RECOMMENDATIONS FOR FUTURE RESEARCH**

We recommend additional studies with the global shallow water model because of the similarity of its results to those from more sophisticated models and its convenience and low cost. We would, however, recommend using a considerably higher resolution version of the model (e.g., R 80). This would help in producing tropical forcings with more realistic areal extents and tracks, and basic state fields with more realistic waveguides and instability features. This increased realism would help in assessing the relative importance of variations in the forcing and interactions of the forcing with the

basic state. In addition to more studies with the simple global model, we also recommend additional NWP modeling studies, combined with diagnostic studies of observed teleconnections.

Some of the key cases we recommend for these studies are:

1. Studies in which the basic state is more realistic (e.g., a basic state calculated as the mean of the analyzed conditions during a particular two week period; a time varying basic state) .
2. Studies using more realistic tropical disturbances (e.g., multiple simultaneous typhoons in the same and/or different basins and possible interference effects; multiple sequential disturbances and their cumulative impacts) .
3. NWP studies using straight running tropical cyclones and tropical cyclones in the Indian and Atlantic basins.
4. Studies in which the analytic tools applied to the model results are applied to observed anomalies (e.g., the anomalies used by Harr and Elsberry 1995).
5. Studies in which the energy tendencies and conversions involved in the development of short term teleconnections are examined further.
6. Studies investigating the impacts of short term teleconnection periods on the midlatitude atmosphere and ocean (e.g., on the circulation of the northeast Pacific ocean).



Such studies should increase our understanding of short term teleconnections and the improvement of extended-range forecasting techniques. The dynamical links between short term and long term teleconnections indicates that the above studies may also help improve our understanding seasonal and longer period teleconnections and the dynamics of global climate change.



	FIXED LOCATION, FIXED AMPLITUDE	FIXED LOCATION, VARIABLE AMPLITUDE	VARIABLE LOCATION, FIXED AMPLITUDE	VARIABLE LOCATION VARIABLE AMPLITUDE	
				Recurving	Straight running
WESTERN NORTH PACIFIC					
JANUARY	PJ1	PJ1A	PJ1L	PJ1R	PJ1S
JULY	PJ2	PJ2A	PJ2L	PJ2R	PJ2S
BAY OF BENGAL					
JANUARY	BJ1	BJ1A	BJ1L	BJ1R	BJ1S
JULY	BJ2	BJ2A	BJ2L	BJ2R	BJ2S
NORTH ATLANTIC					
JANUARY	AJ1	AJ1A	AJ1L	AJ1R	AJ1S
JULY	AJ2	AJ2A	AJ2L	AJ2R	AJ2S

Table 1. Summary of model runs. The runs are categorized by: (a) the tropical ocean basin in which the perturbation forcing was located (western North Pacific, Bay of Bengal, or North Atlantic); (b) the basic state conditions (January or July); and (c) the location and amplitude of the perturbation forcing (fixed or variable). The run names are indicated by the three- or four-character names shown in the cells of the table. The first character indicates the basin (e.g., P for Pacific); the second two indicate the basic state month (e.g., J1 for January); and the fourth indicates the variable factor in the perturbation forcing (e.g., A for amplitude, R for recurving location).



## **APPENDIX A - FIGURES**

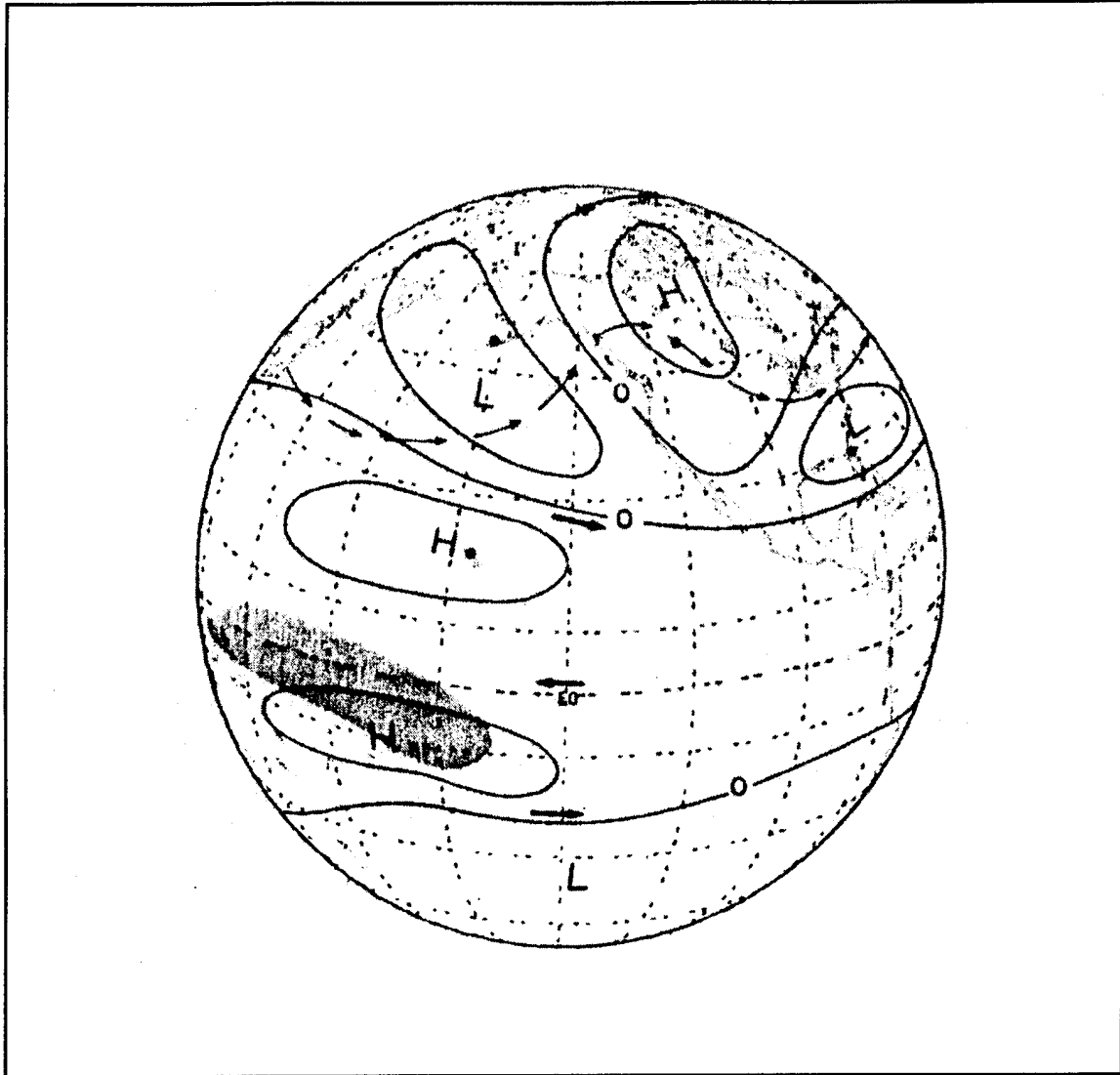
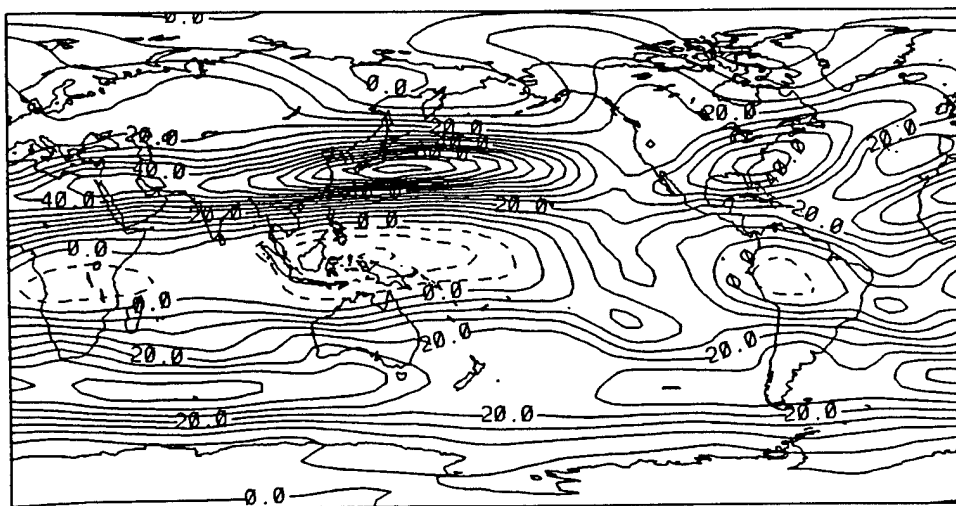
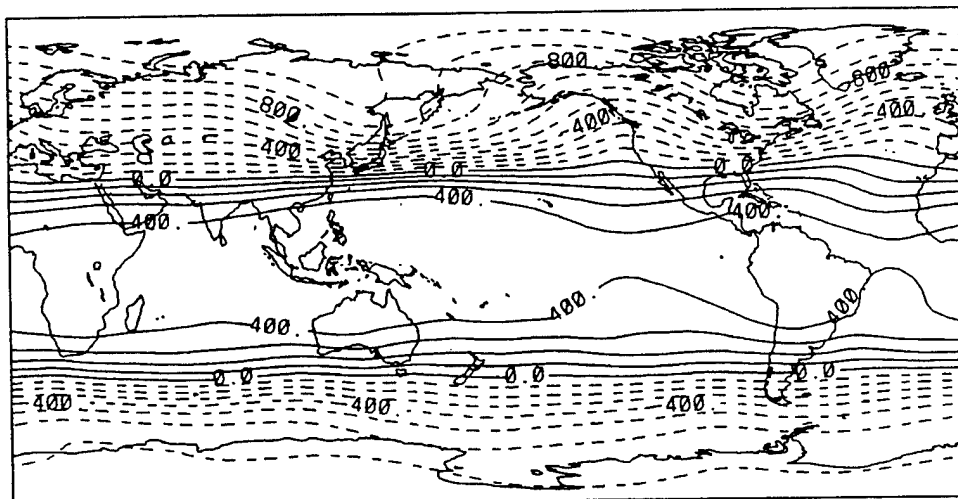


Figure 1. The Pacific-North American (PNA) teleconnection pattern. The hypothesized global pattern of tropospheric height anomalies (solid lines) during a northern hemisphere winter which coincides with an episode of anomalously warm sea surface temperatures in the central and eastern equatorial Pacific. The bold arrows in dark type represent strengthened subtropical jets. The light arrows depict streamline distortions caused by the height anomaly pattern of troughing over the central Pacific and ridging over western Canada. The shaded area represents enhanced cloudiness and rainfall. (From Horel and Wallace 1981)

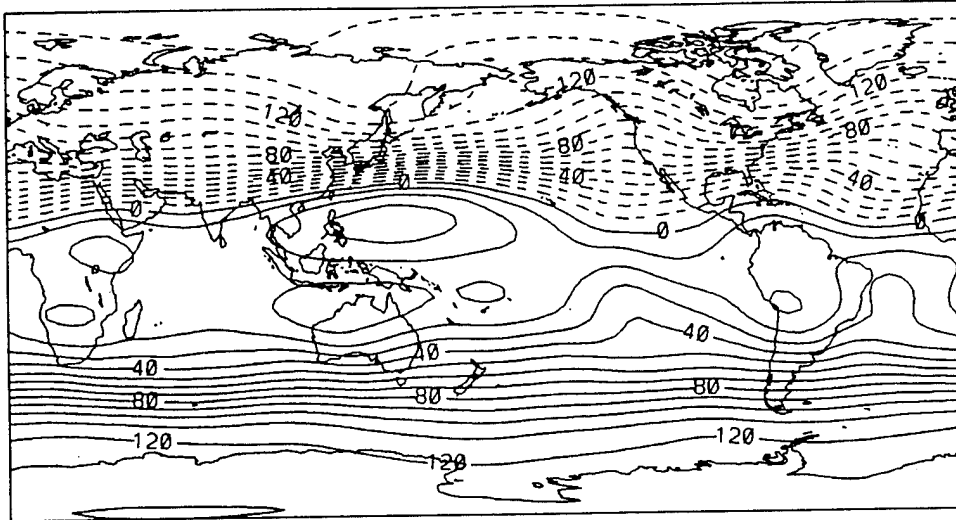


a.  $u_{200}$

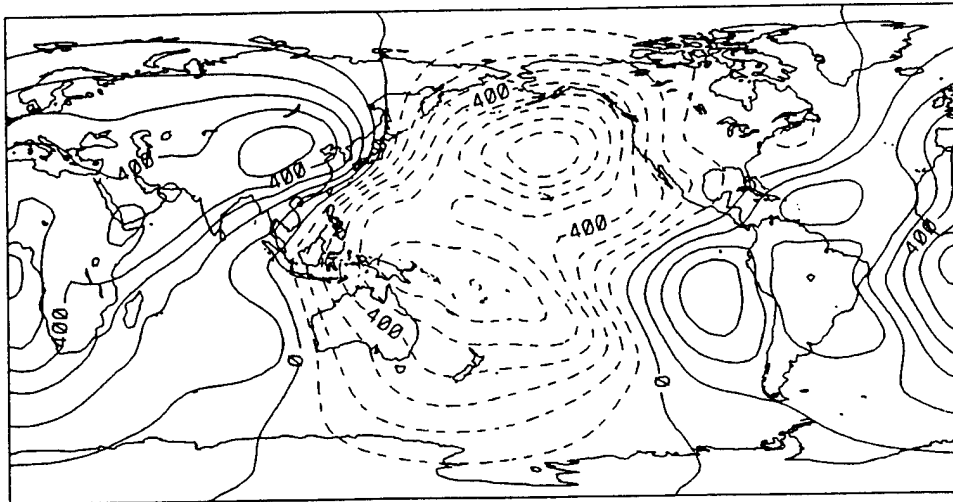


b. Geopotential height

Figure 2. 200 mb January basic state fields. Solid (dashed) contours indicate positive (negative) values. (a) Zonal wind component, contour interval is 5 m/s. (b) Geopotential heights after subtracting a global mean value of 11,784 gpm, contour interval is 100 gpm. (c) Streamfunction, contour interval is  $1 \times 10^9 \text{ m}^2/\text{s}$ . (d) Velocity potential, contour interval is  $1 \times 10^8 \text{ m}^2/\text{s}$ .



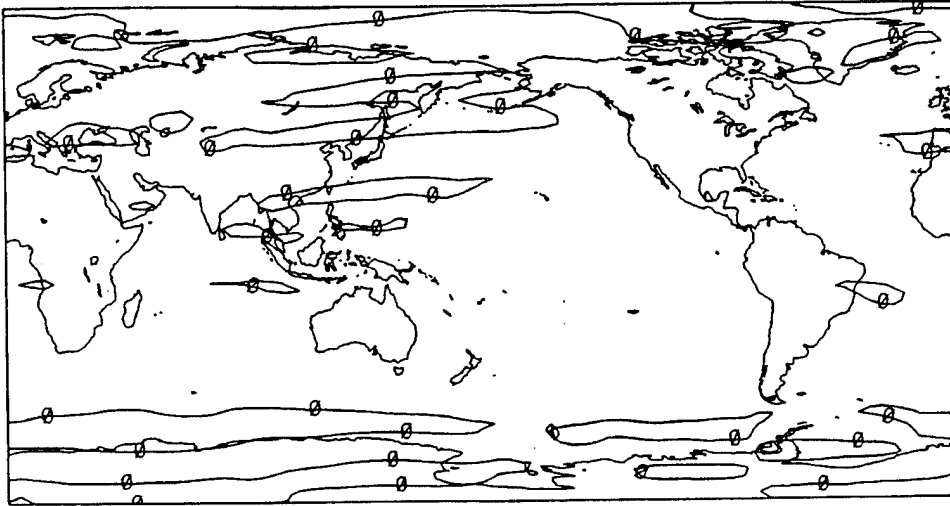
c. Streamfunction



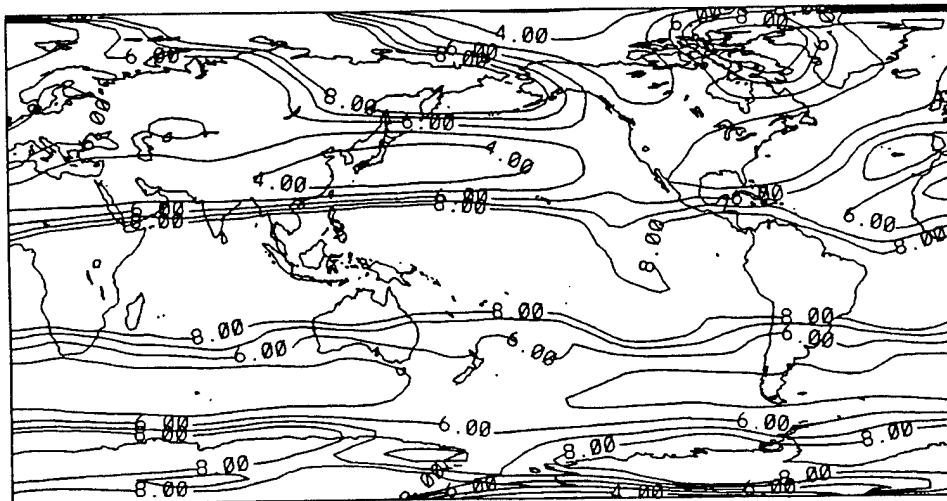
d. Velocity potential

Figure 2. (Continued) (e) Indications of potential for barotropic instability. Zero contour indicates regions where  $\beta - u_{yy} = 0$ . (f) Stationary wavenumber with each contour indicating the limit of meridional propagation for low frequency quasi-geostrophic waves with zonal wavenumber less than or equal to the number on the contour, for wave numbers  $\leq 8$ .



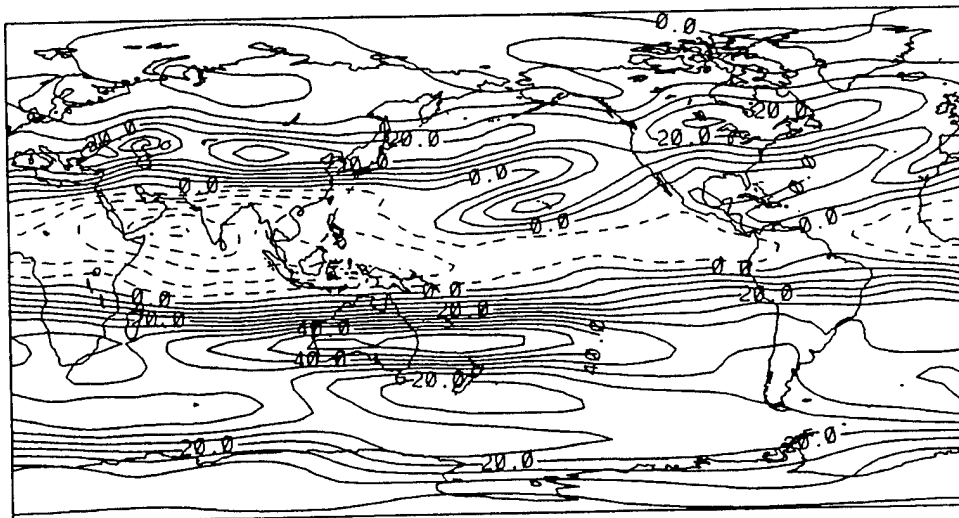


e. Barotropic instability

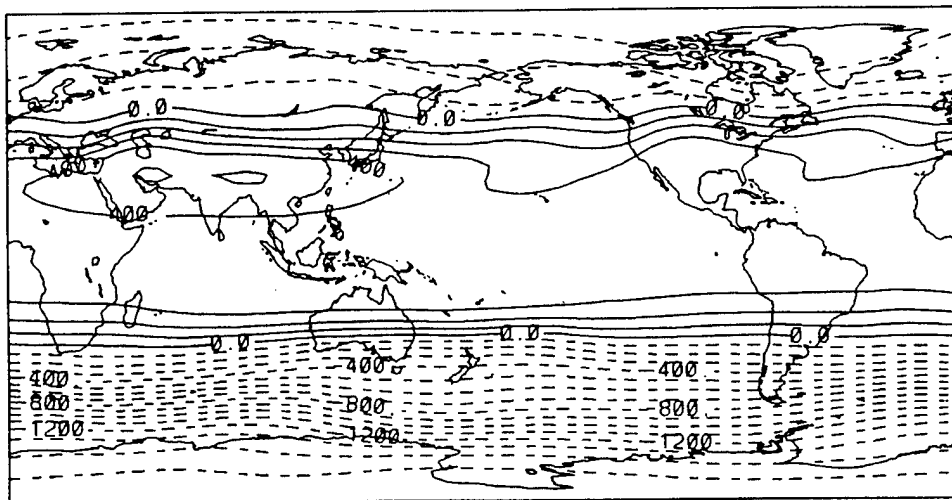


f. Stationary wavenumber

Figure 2. (Continued)

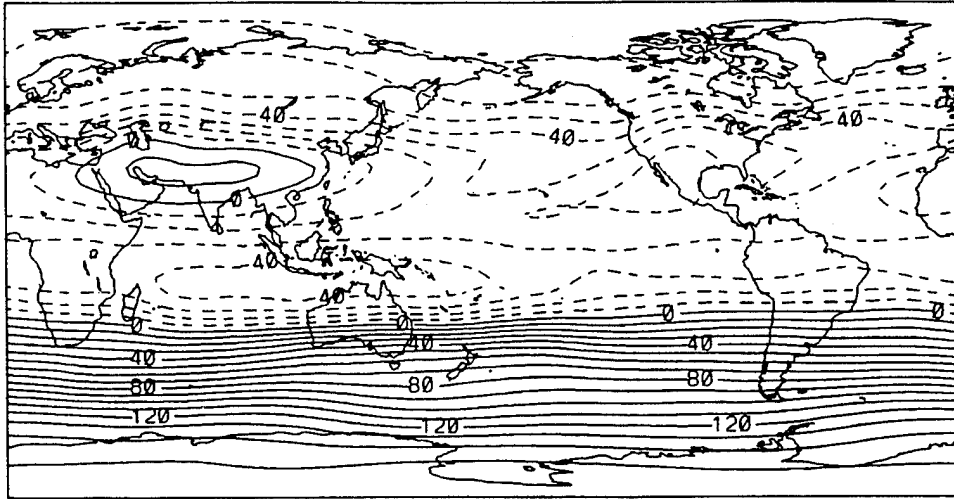


a.  $u_{200}$

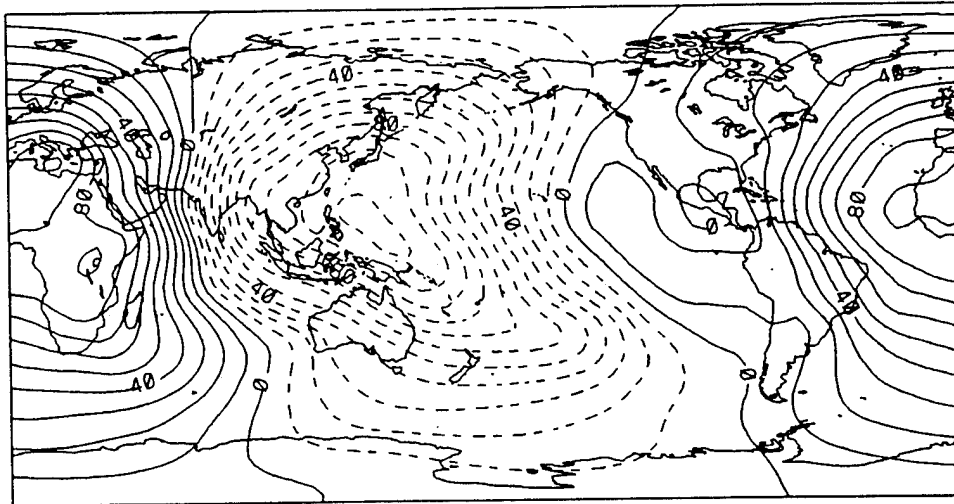


b. Geopotential height

Figure 3. 200 mb July basic state fields. Solid (dashed) contours indicate positive (negative) values. (a) Zonal wind component, contour interval is 5 m/s. (b) Geopotential heights after subtracting a global mean value of 11,784 gpm, contour interval is 100 gpm. (c) Streamfunction, contour interval is  $1 \times 10^9 \text{ m}^2/\text{s}$ . (d) Velocity potential, contour interval is  $1 \times 10^8 \text{ m}^2/\text{s}$ .

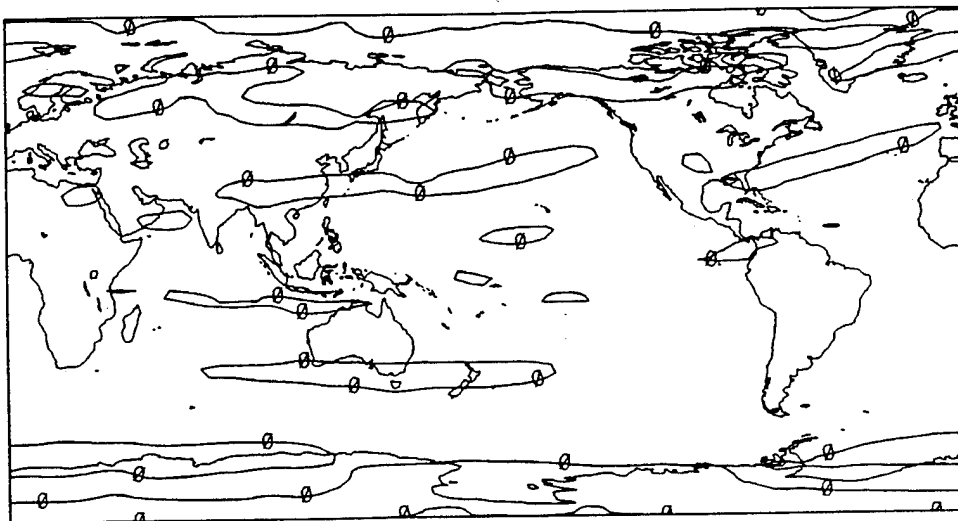


c. Streamfunction

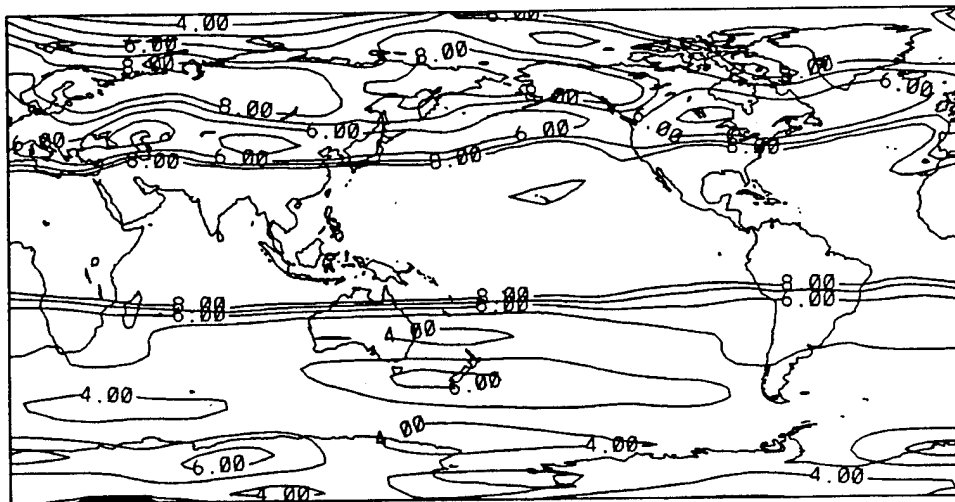


d. Velocity potential

Figure 3. (Continued) (e) Indications of potential for barotropic instability. Zero contour indicates regions where  $\beta - u_{yy} = 0$ . (f) Stationary wavenumber with each contour indicating the limit of meridional propagation for low frequency quasi-geostrophic waves with zonal wavenumber less than or equal to the number on the contour, for wave numbers  $\leq 8$ .



e. Barotropic instability



f. Stationary wavenumber

Figure 3. (Continued)

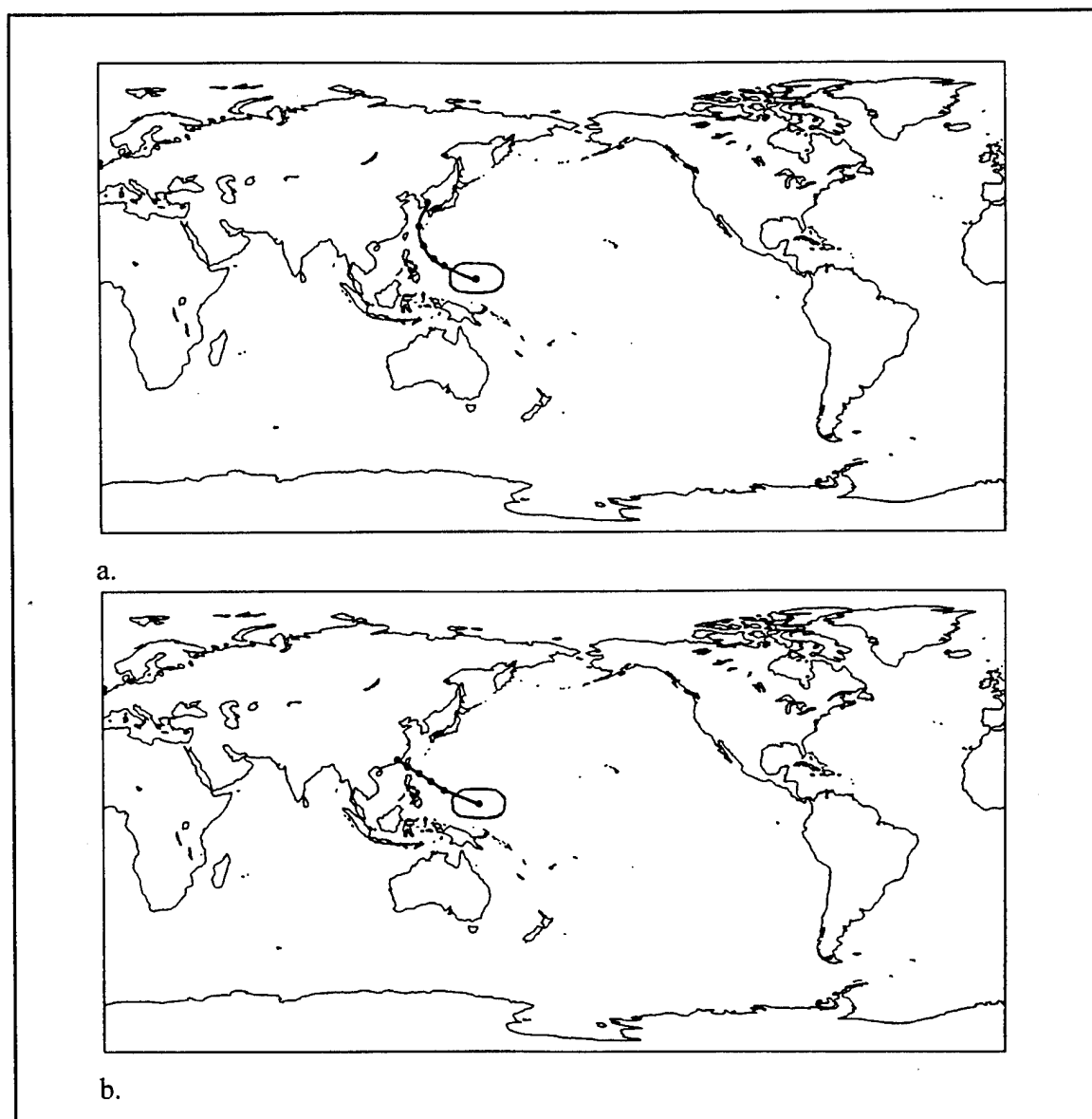
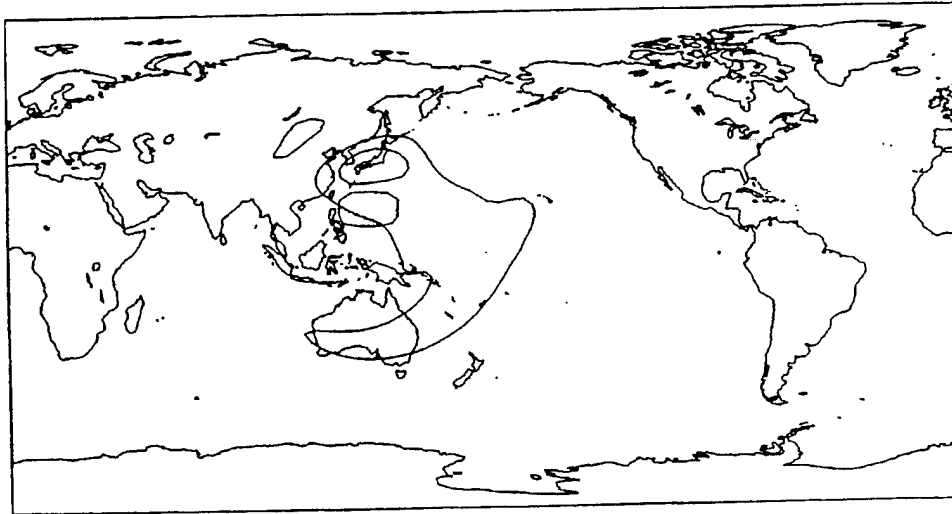
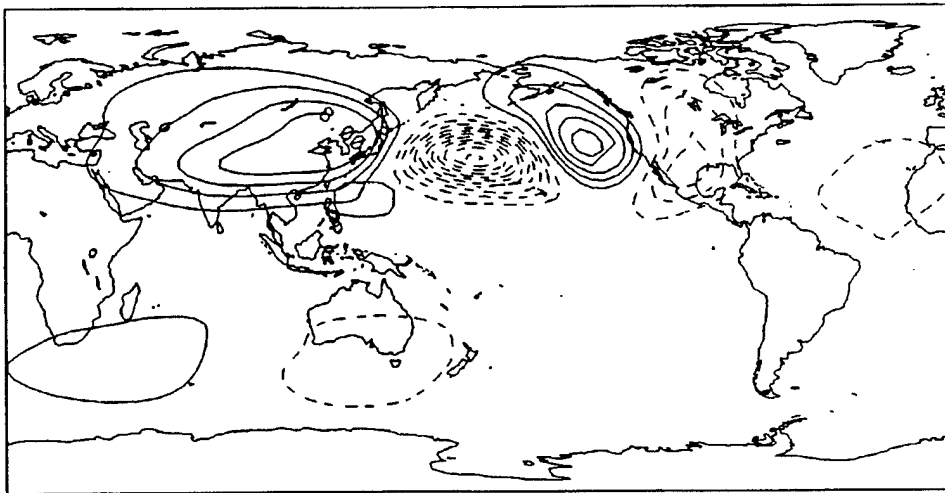


Figure 4. The model's tropical perturbation forcing for two western North Pacific examples. The small oval surrounds the region in which the forcing is equivalent to heating of  $\geq 1\text{K/day}$ . The oval is located at the initial position, while the line leading northwestward from the center of the oval shows the forcing's successive positions in: (a) the recurving case and (b) the straight running case. The dots along the path indicate the forcing's central positions at 48 hour intervals. The most poleward dot shows the position at 11.5 days, after which the forcing was turned off. For the Bay of Bengal and North Atlantic runs, the forcing was simply shifted to the west or east, with no other changes. For a summary of all the runs and their different forcing conditions, see Table 1.

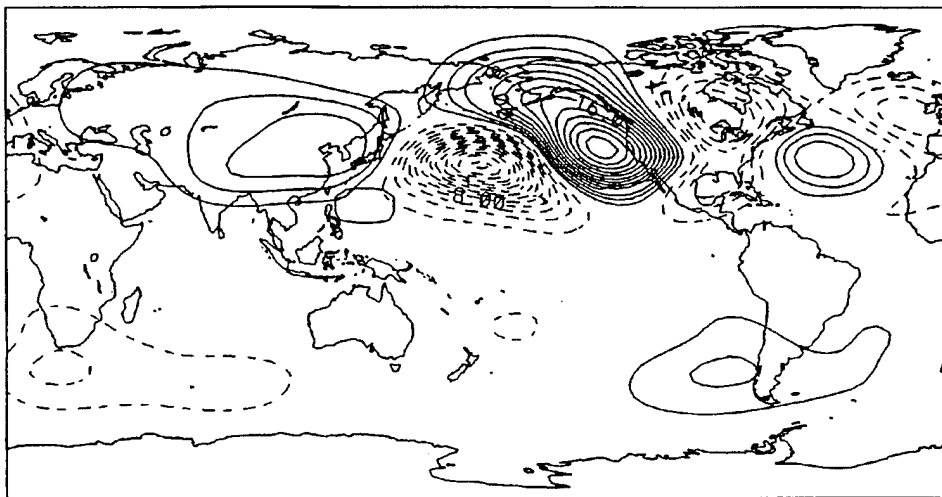


a. 12 hours

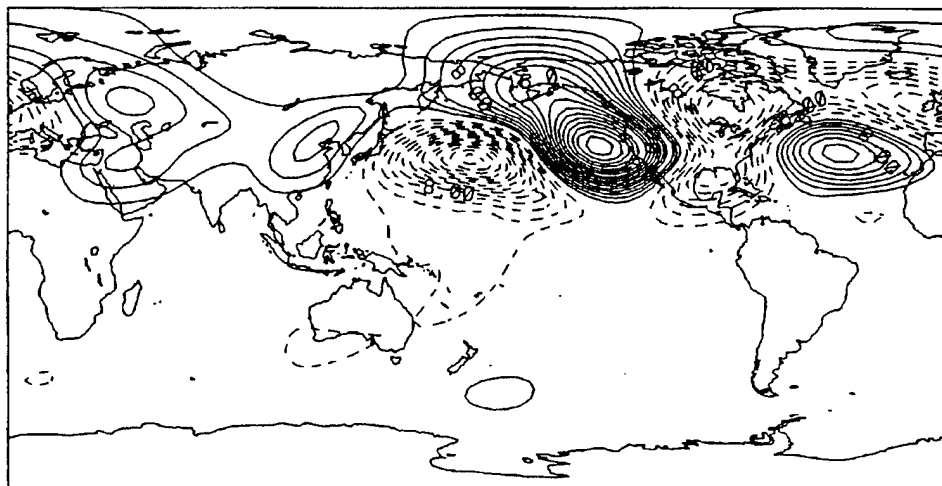


b. 4 days

Figure 5. Height response for run PJ1 which used: (1) a January basic state; and (2) a fixed location, fixed amplitude tropical perturbation forcing in the western North Pacific. For each panel, the elapsed model time is indicated. The small oval contour in the tropical western North Pacific surrounds the region in which the forcing was equivalent to heating  $\geq 1$  K/day. Positive (negative) responses are indicated by the solid (dashed) contours. Contour interval is 2 gpm. Zero contour omitted.



c. 8 days



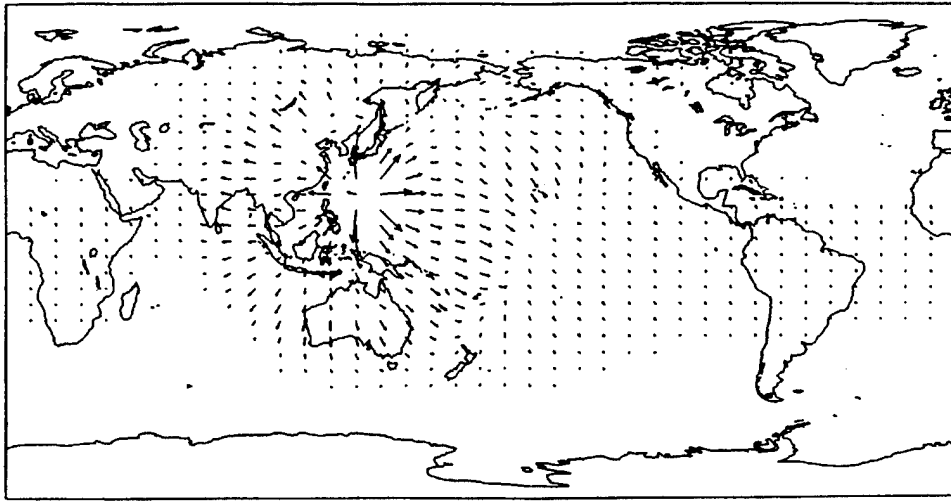
d. 12 days

Figure 5. (Continued)





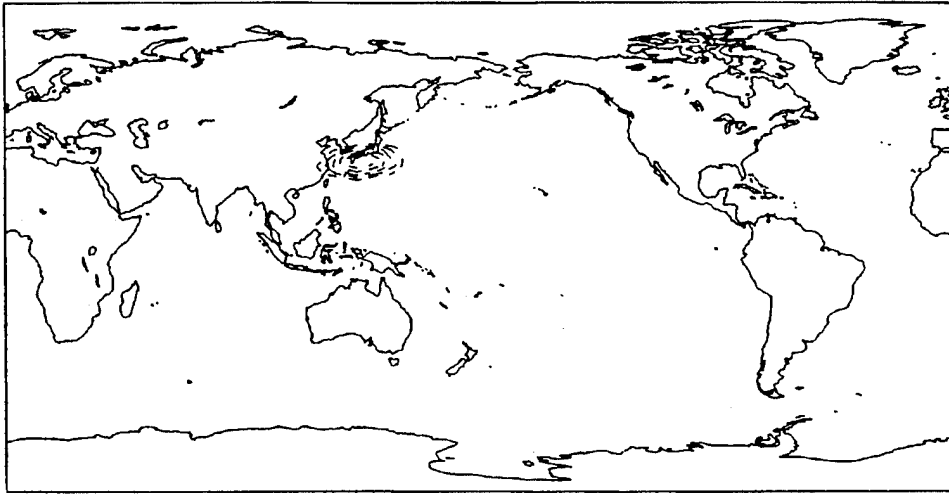




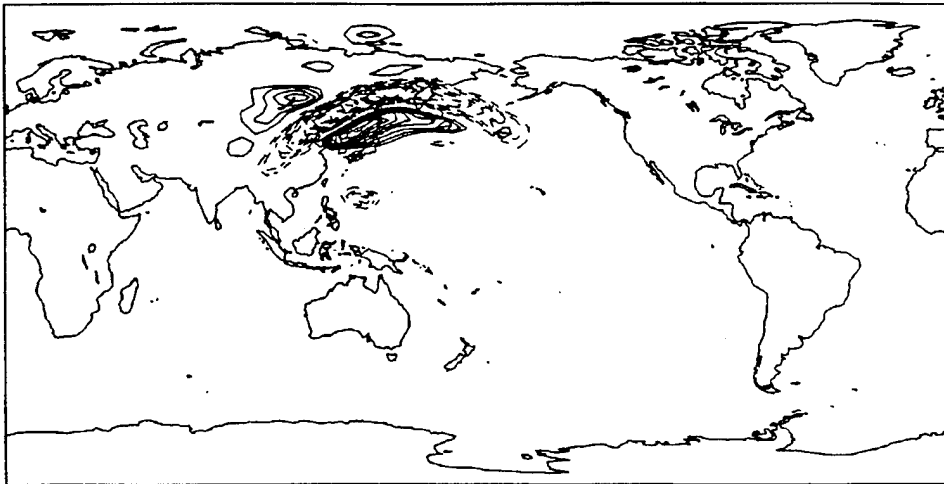
a.  $\vec{V}_x$

Figure 6. 200 mb Rossby wave source response terms for run PJ1 after 12 hours of the model run. (a) Divergent wind response, with vector scale, in  $\text{ms}^{-1}$ , as shown below. (b) Advection by divergent wind (ADVDIV) response. (c) vortex stretching response. Positive (negative) responses are indicated by the solid (dashed) contours. Contour interval is  $0.5 \times 10^{-11} \text{ s}^{-2}$ . Zero contour omitted.

0.150E+01  
MAXIMUM VECTOR

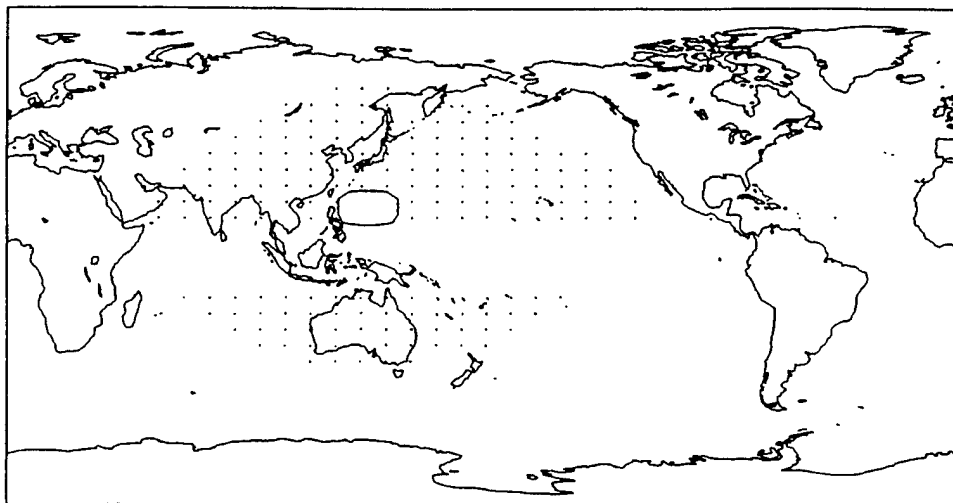


b. Advection by divergent wind

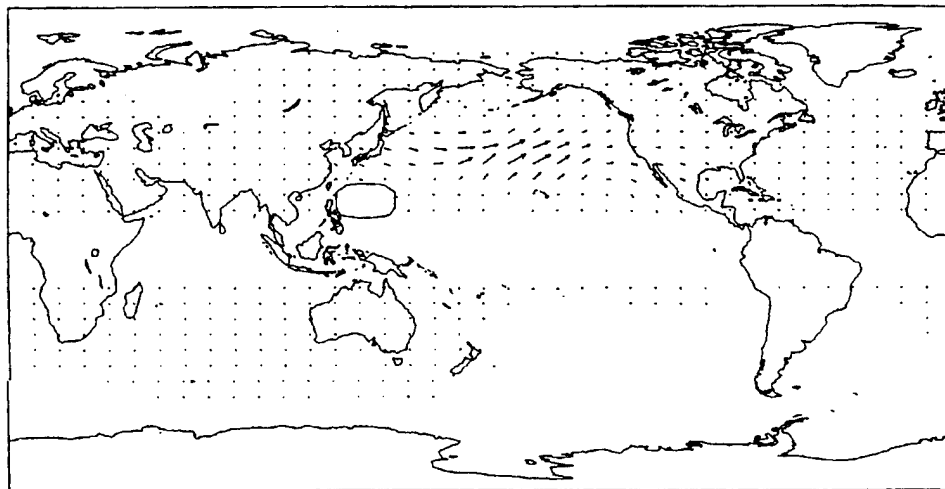


c. Vortex stretching

Figure 6. (Continued)



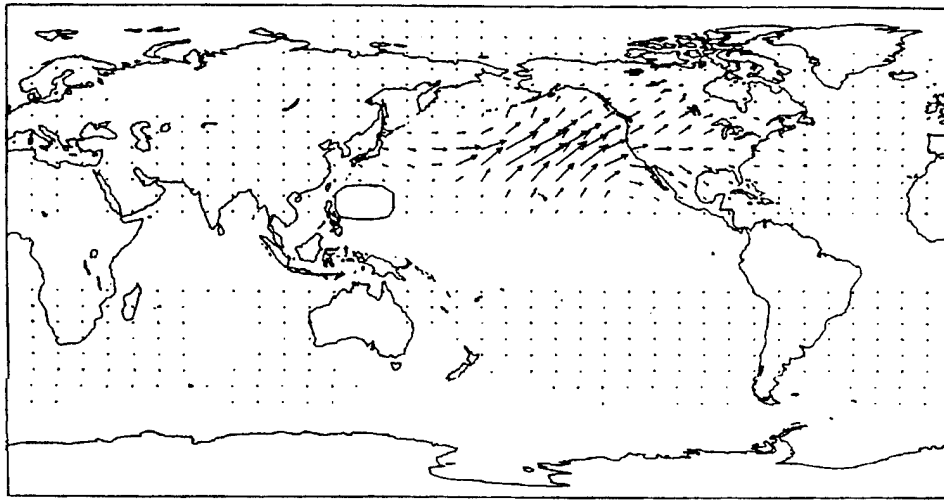
a. 12 hours



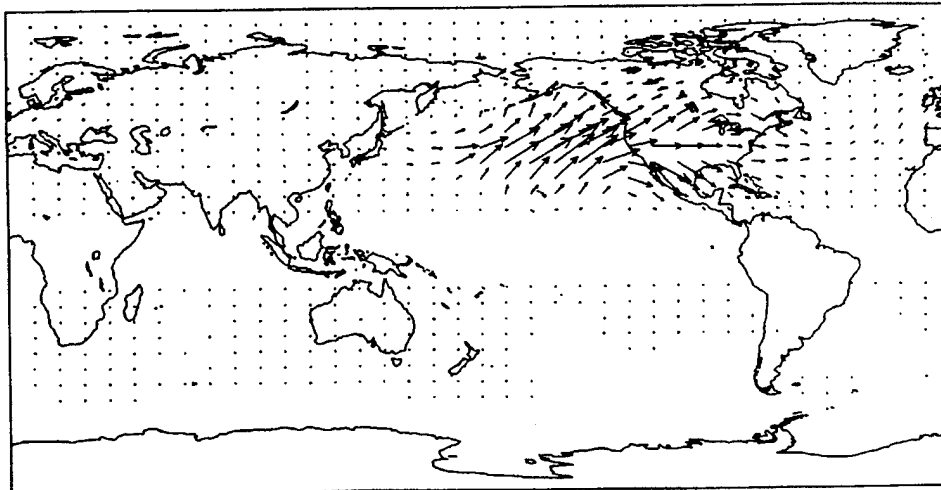
b. 4 days

Figure 7. Quasi-geostrophic wave activity flux response for run PJ1. For each panel, the elapsed model time is indicated. Tropical western North Pacific perturbation forcing of  $\geq 1$  K/day is indicated by the small oval region. Vector scale, in  $\text{m}^2/\text{s}^2$  as shown.

0.100E+06  
MAXIMUM VECTOR

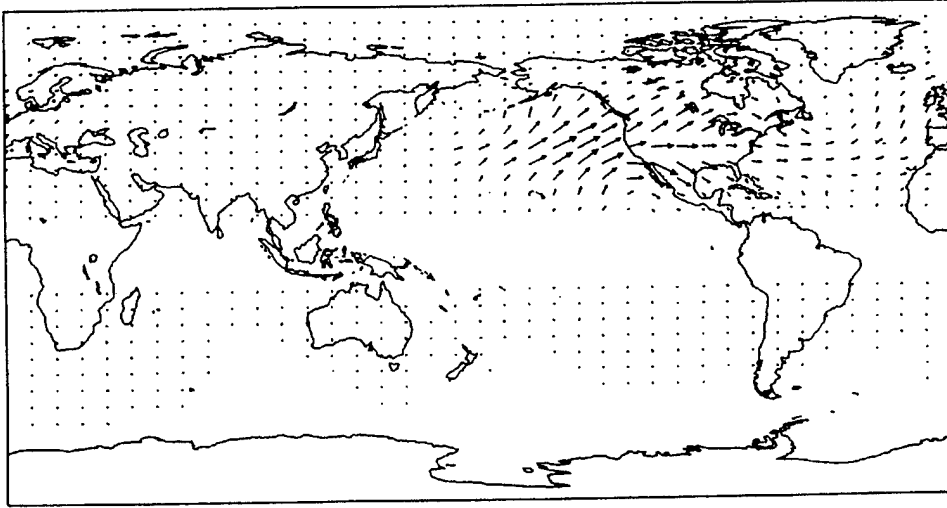


c. 8 days

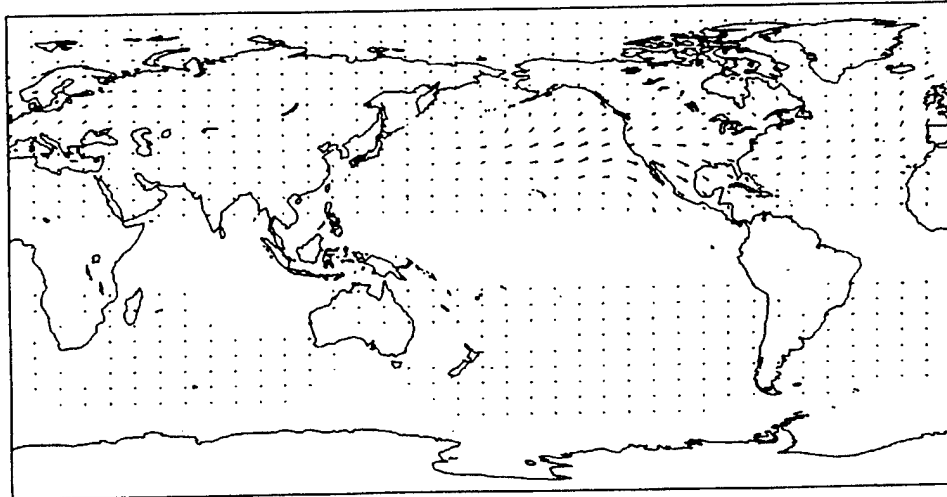


d. 12 days

Figure 7. (Continued)

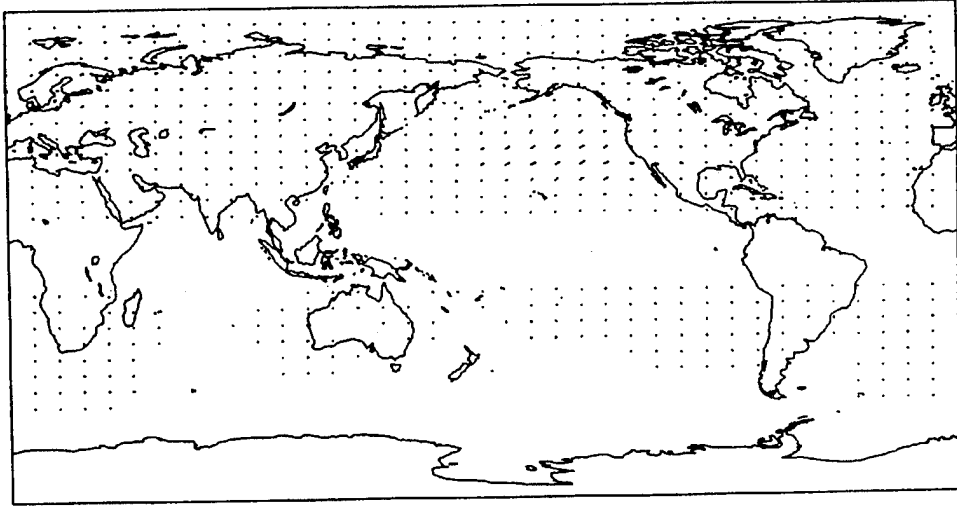


e. 16 days



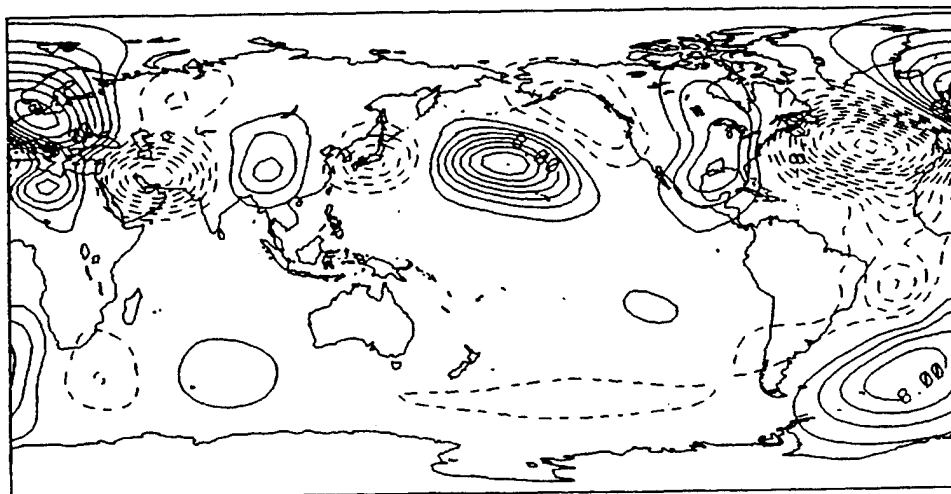
f. 20 days

Figure 7. (Continued)



g. 24 days

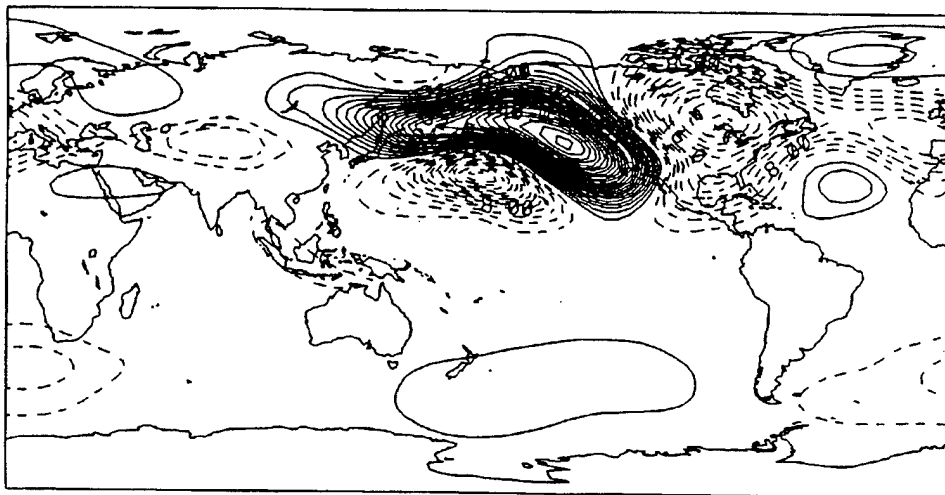
Figure 7. (Continued)



12 days

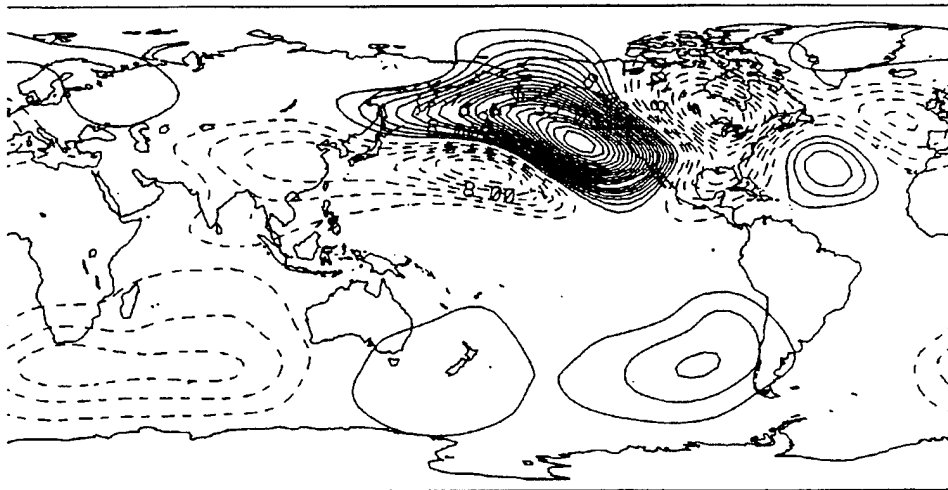
Figure 8. Height response for run PJ1A which used: (1) a January basic state; and (2) a fixed location, variable amplitude tropical perturbation forcing in the western North Pacific. The elapsed model time is indicated. Positive (negative) responses are indicated by the solid (dashed) contours. Contour interval is 2 gpm. Zero contour omitted.





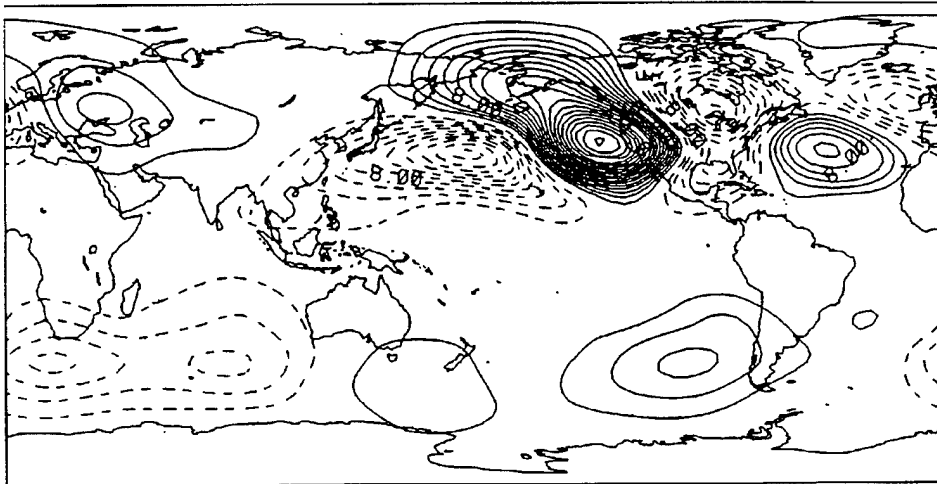
12 days

Figure 9. Height response for run PJ1L which used: (1) a January basic state; (2) a recurving path; and (3) fixed amplitude tropical perturbation forcing in the western North Pacific. The elapsed model time is indicated. Positive (negative) responses are indicated by the solid (dashed) contours. Contour interval is 2 gpm. Zero contour omitted.



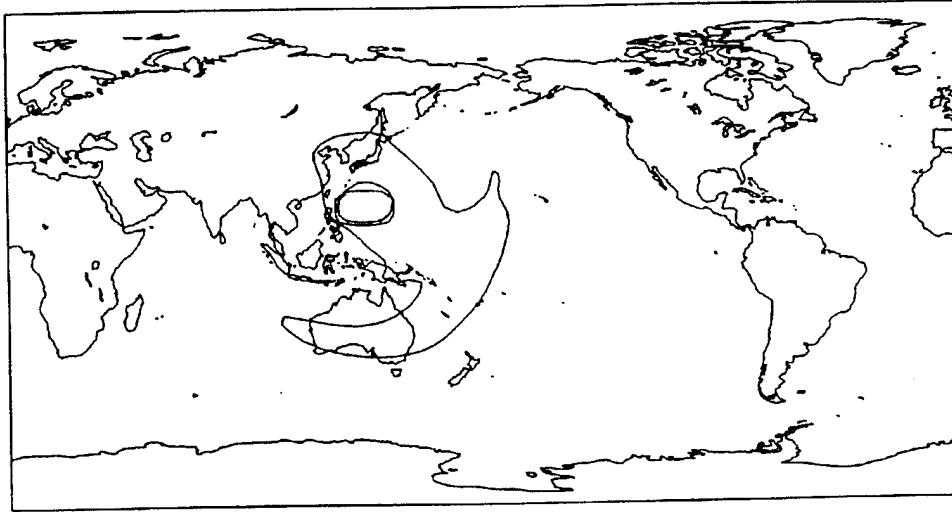
12 days

Figure 10. Height response for run PJ1R which used: (1) a January basic state; (2) a recurving path; and (3) variable amplitude tropical perturbation forcing in the western North Pacific. The elapsed model time is indicated. Positive (negative) responses are indicated by the solid (dashed) contours. Contour interval is 2 gpm. Zero contour omitted.

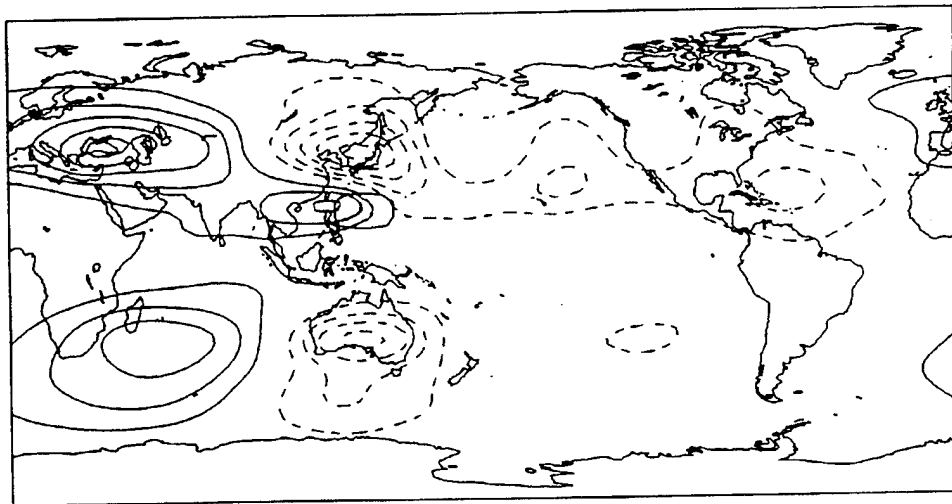


12 days

Figure 11. Height response for run PJ1S which used: (1) a January basic state; (2) a straight running path; and (3) variable amplitude tropical perturbation forcing in the western North Pacific. The elapsed model time is indicated. Positive (negative) responses are indicated by the solid (dashed) contours. Contour interval is 2 gpm. Zero contour omitted.

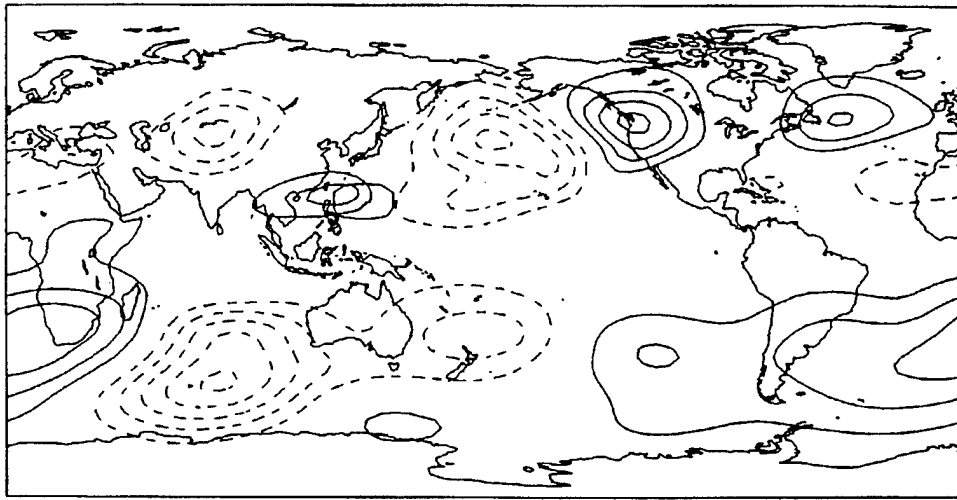


a. 12 hours

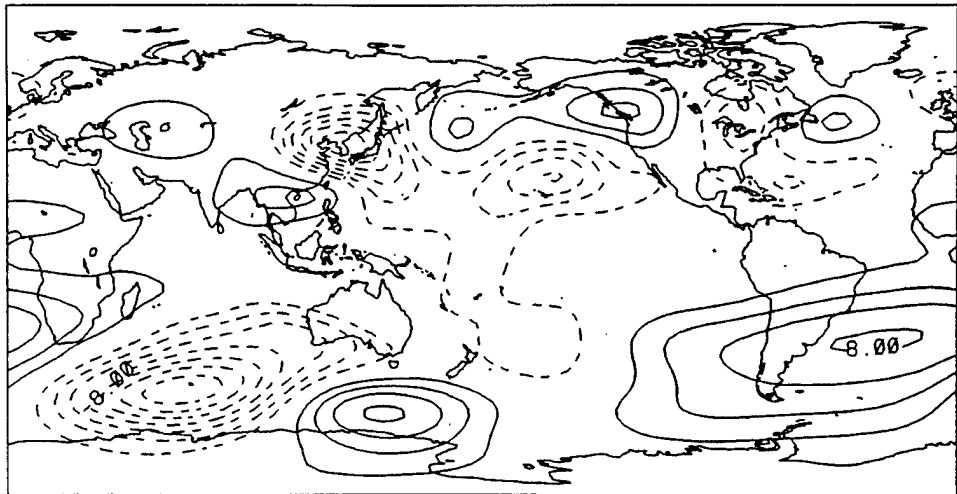


b. 4 days

Figure 12. 200 mb height response for run PJ2 which used: (1) a July basic state; and (2) a fixed location, fixed amplitude tropical perturbation forcing in the western North Pacific. For each panel, the elapsed model time is indicated. The small oval contour in the tropical western North Pacific surrounds the region in which the forcing was equivalent to heating  $\geq 1$  K/day. Positive (negative) responses are indicated by the solid (dashed) contours. Contour interval is 2 gpm. Zero contour omitted.

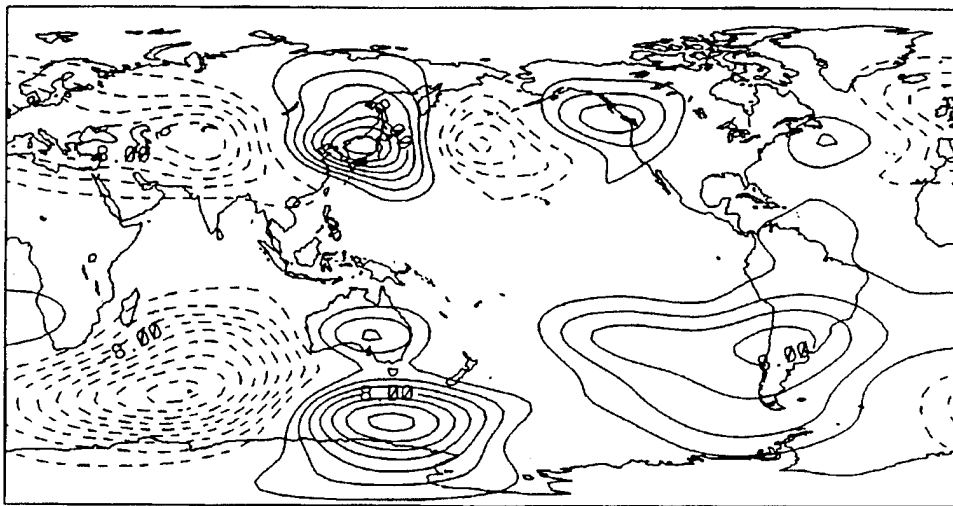


c. 8 days

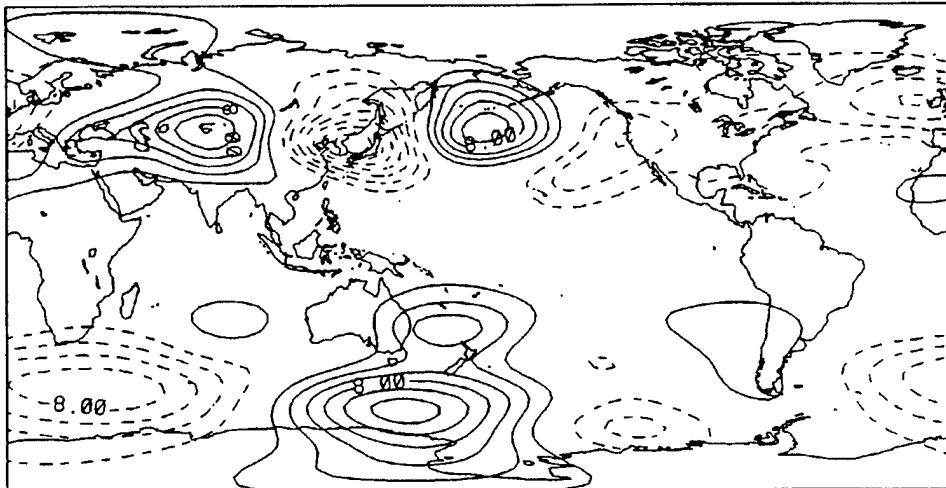


d. 12 days

Figure 12. (Continued)

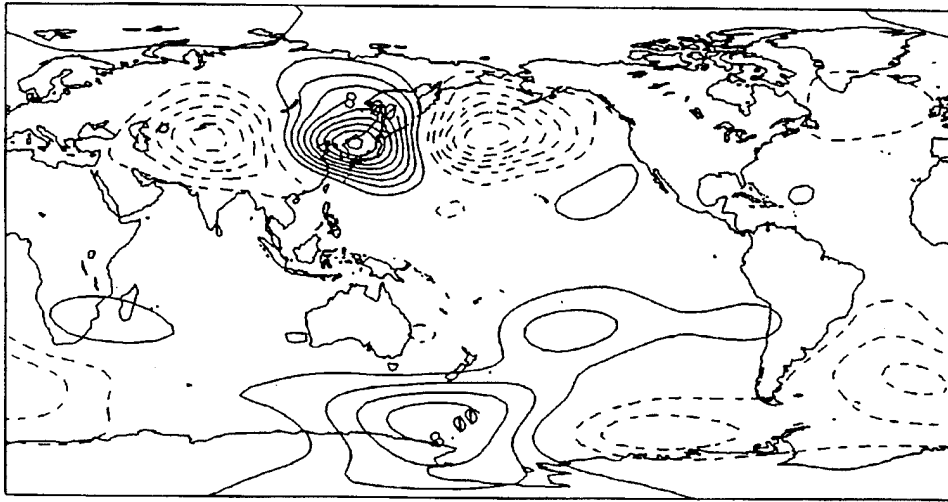


e. 16 days



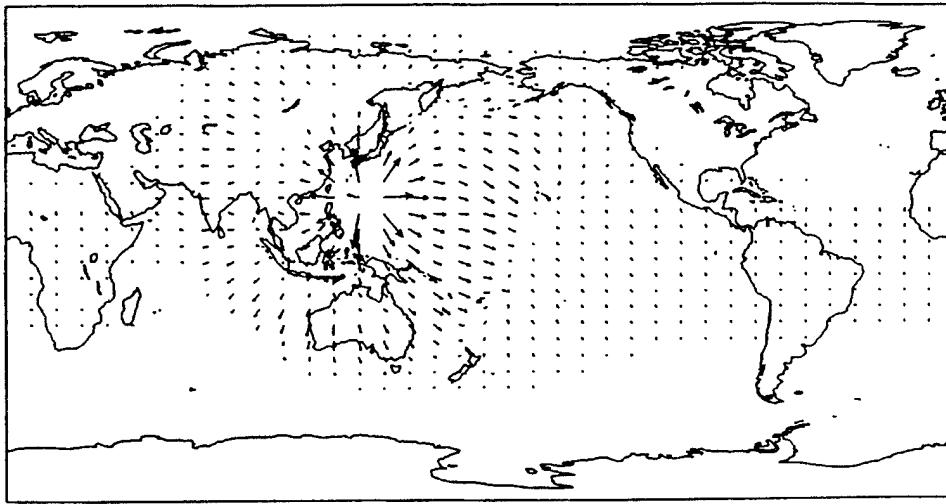
f. 20 days

Figure 12. (Continued)



g. 24 days

Figure 12. (Continued)

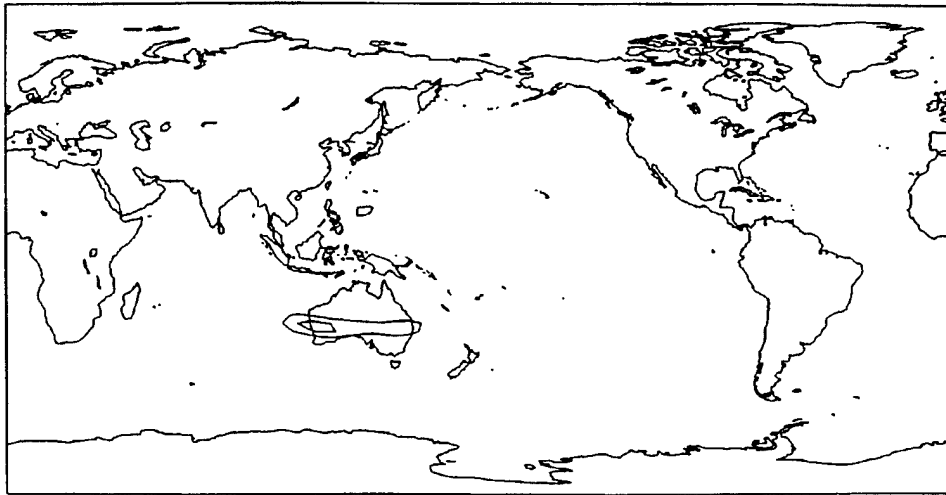


a.  $\vec{V}_x$

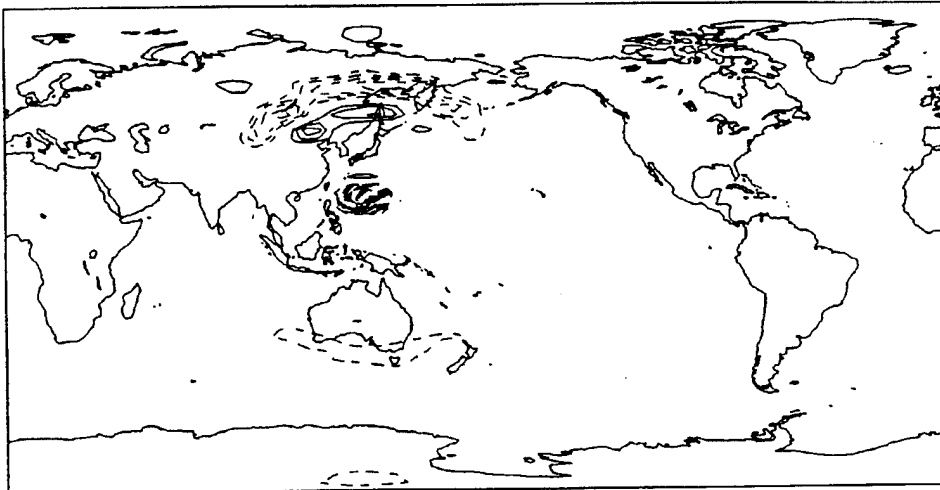
Figure 13. 200 mb Rossby wave source response terms for run PJ2 after 12 hours of the model run. (a) Divergent wind response, with vector scale, in  $\text{ms}^{-1}$ , as shown below. (b) Advection by divergent wind (ADVDIV) response. (c) vortex stretching response. Positive (negative) responses are indicated by the solid (dashed) contours. Contour interval is  $0.5 \times 10^{-11} \text{ s}^{-2}$ . Zero contour omitted.

0 150E+01  
MAXIMUM VECTOR



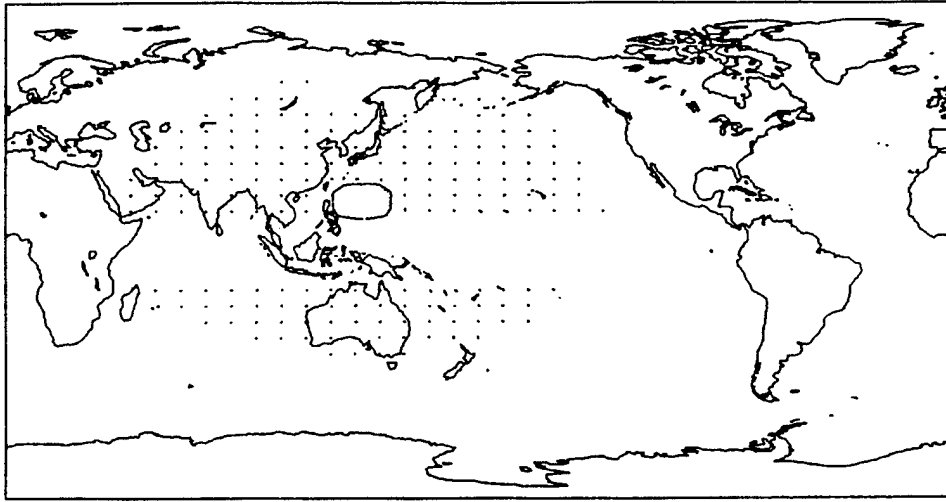


b. Advection by divergent wind

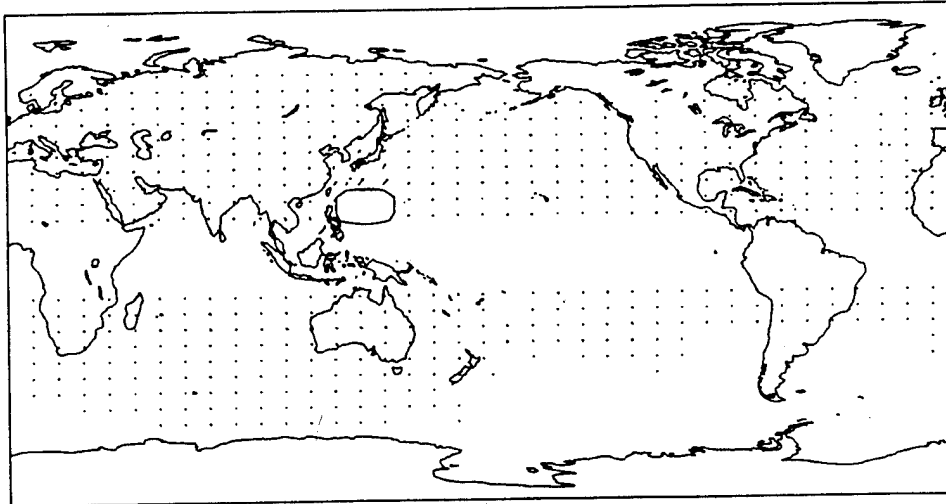


c. Vortex stretching

Figure 13. (Continued)



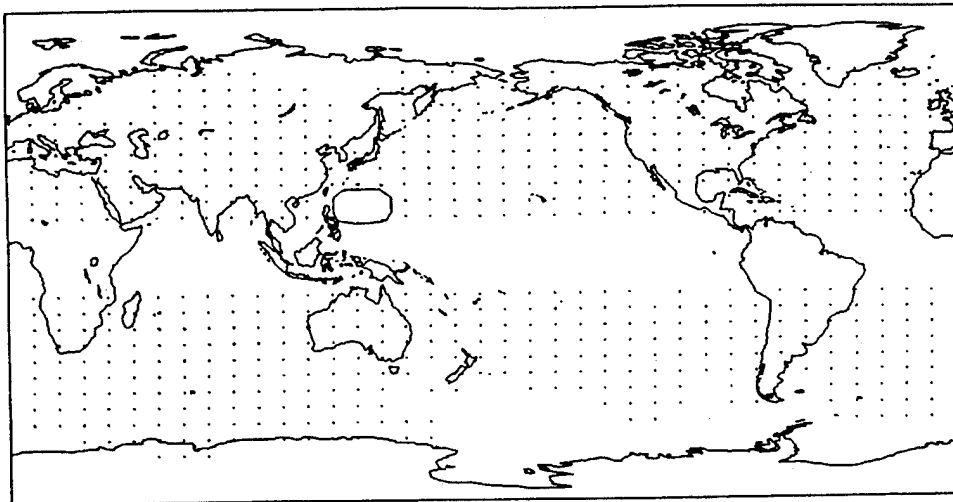
a. 12 hours



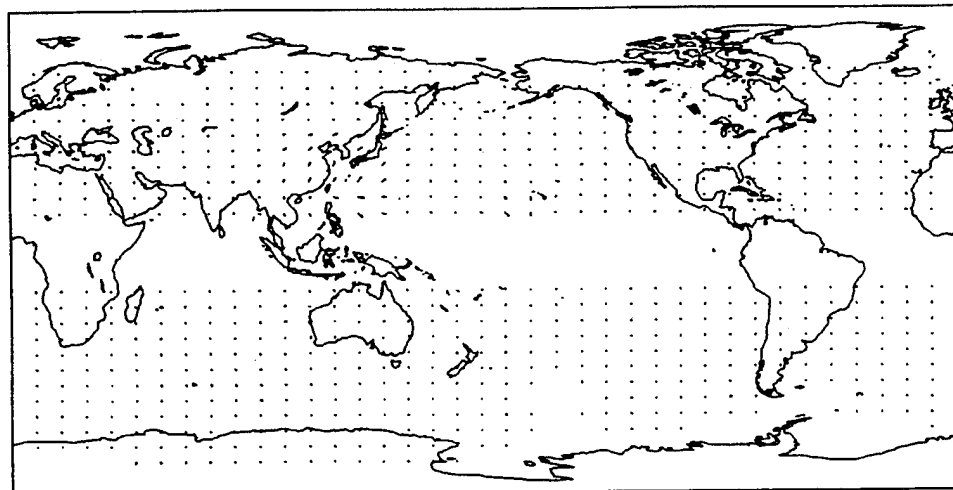
b. 4 days

Figure 14. Quasi-geostrophic wave activity flux response for run PJ2. For each panel, the elapsed model time is indicated. Tropical perturbation forcing of  $\geq 1$  K/day is indicated by the small oval region. Vector scale, in  $\text{m}^2/\text{s}^2$  as shown.

$0.100\text{E}+06$   
MAXIMUM VECTOR

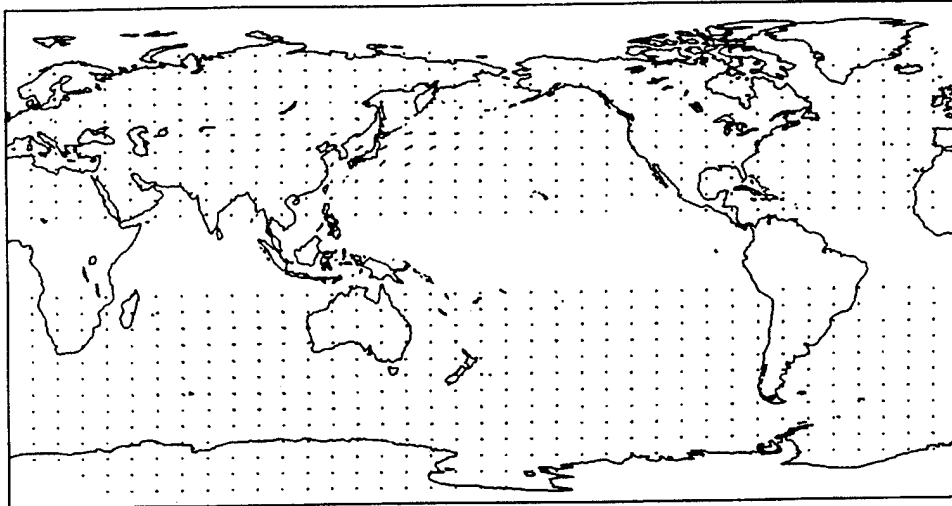


c. 8 days

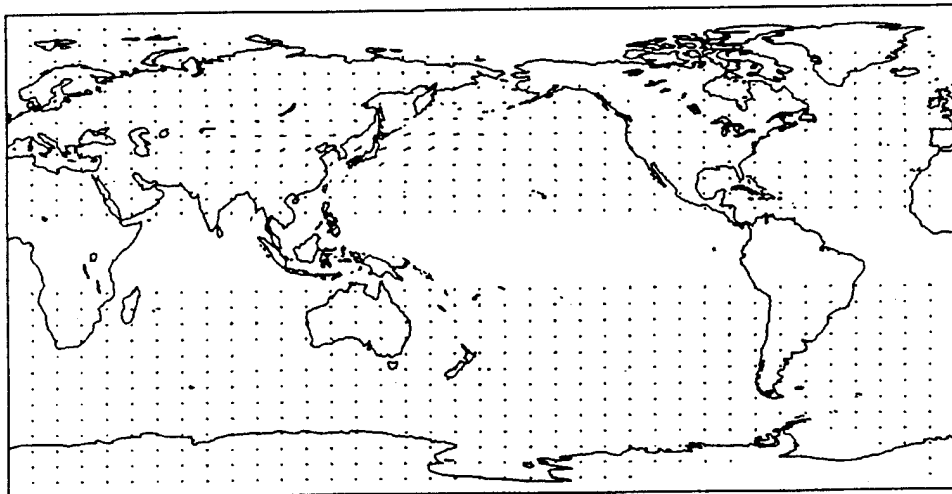


d. 12 days

Figure 14. (Continued)

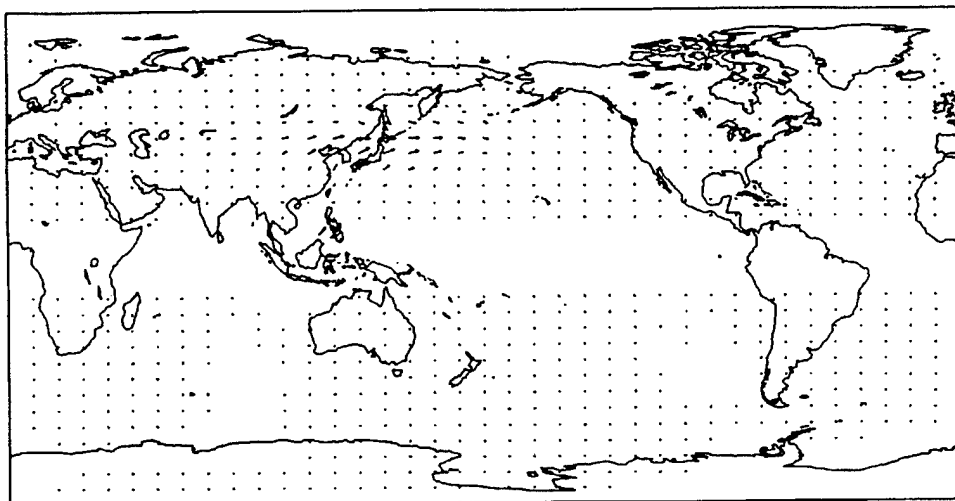


e. 16 days



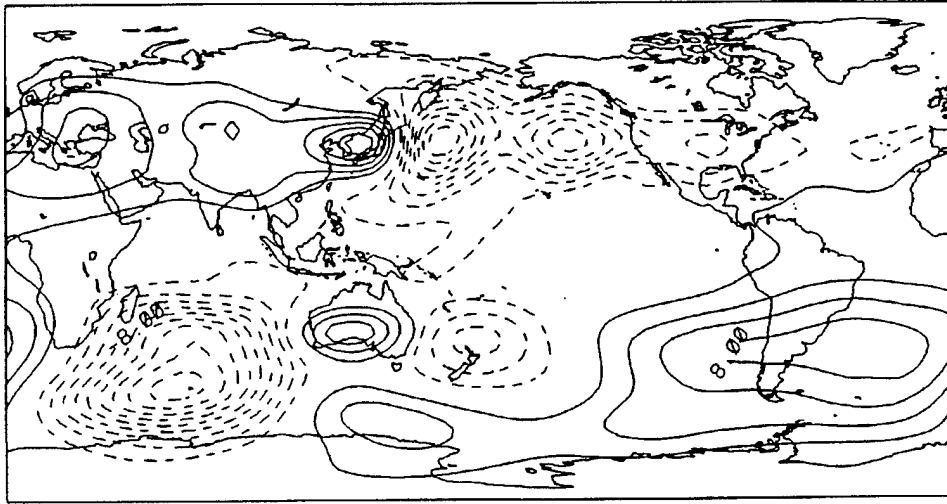
f. 20 days

Figure 14 (Continued)

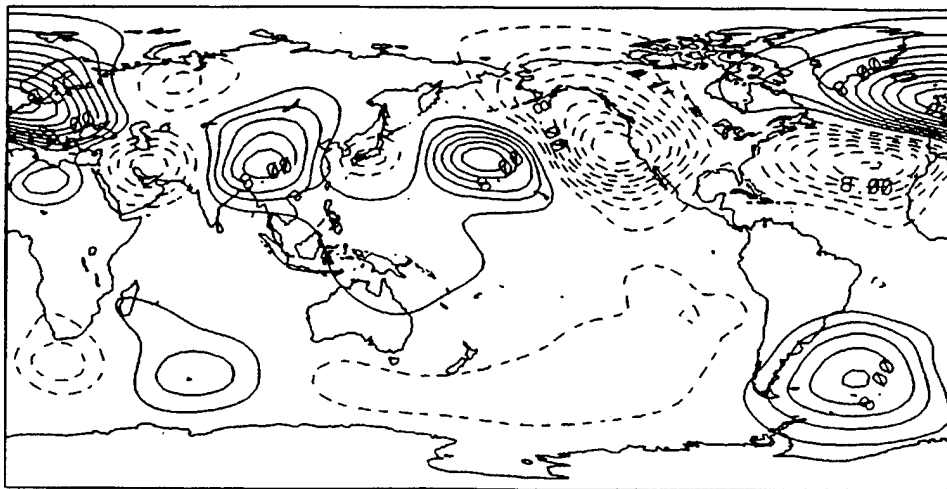


g. 24 days

Figure 14 (Continued)

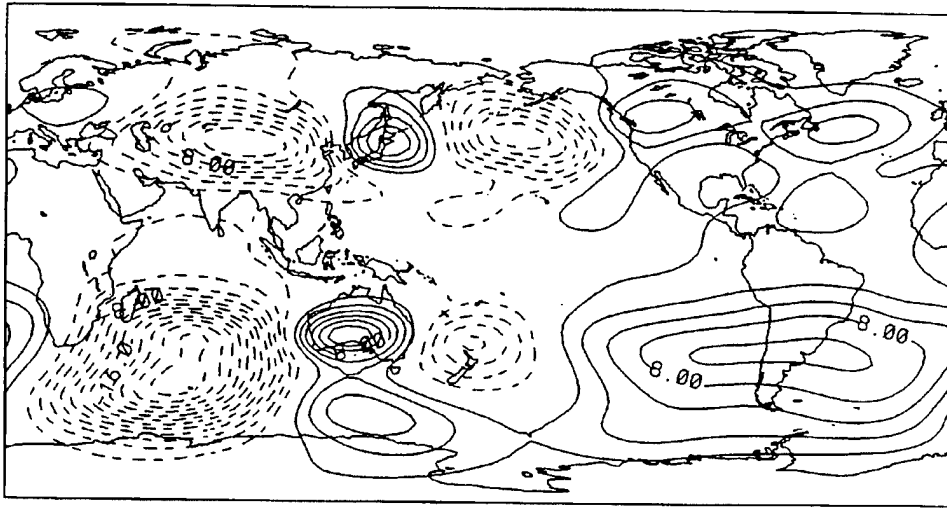


a. 12 days

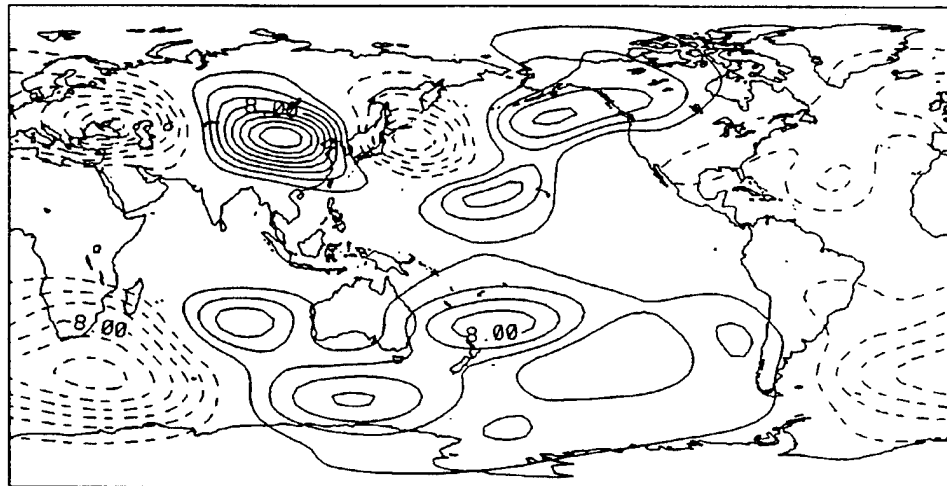


b. 16 days

Figure 15. Height response for run PJ2L which used: (1) a July basic state; (2) a recurving path; and (3) fixed amplitude tropical perturbation forcing in the western North Pacific. The elapsed model time is indicated. Positive (negative) responses are indicated by the solid (dashed) contours. Contour interval is 2 gpm. Zero contour is omitted.

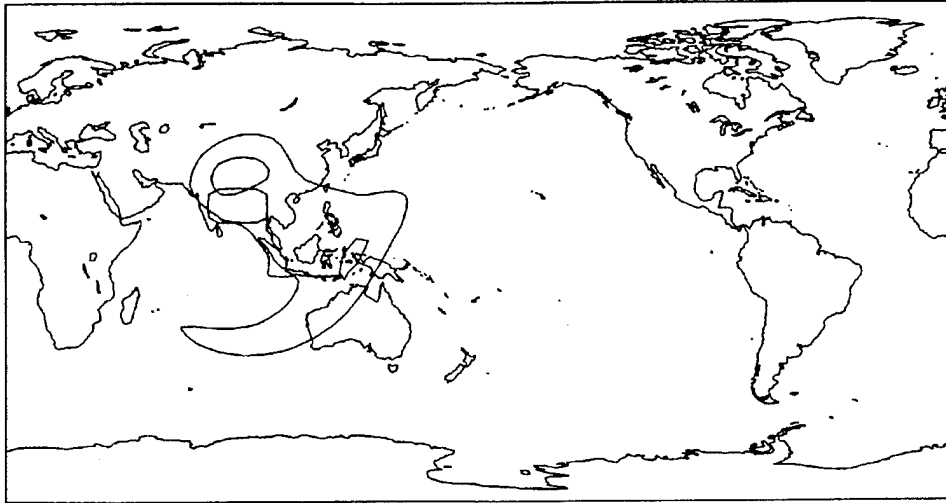


a. 12 days

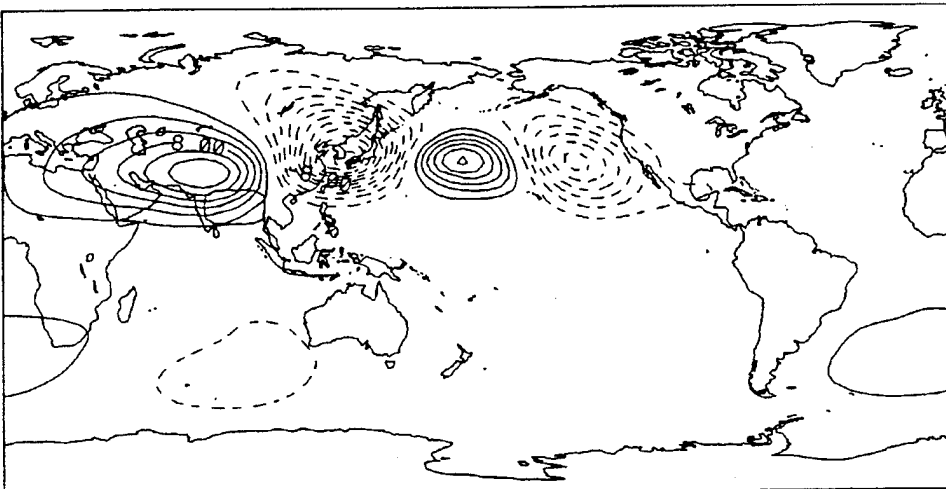


b. 16 days

Figure 16. Height response for run PJ2R which used: (1) a July basic state; (2) a recurring path; and (3) variable amplitude tropical perturbation forcing in the western North Pacific. The elapsed model time is indicated. Positive (negative) responses are indicated by the solid (dashed) contours. Contour interval is 2 gpm. Zero contour is omitted.



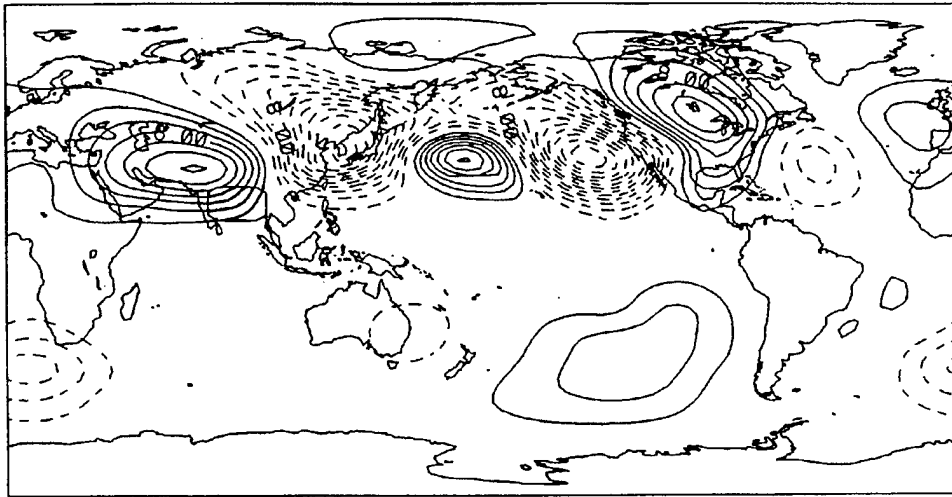
a. 12 hours



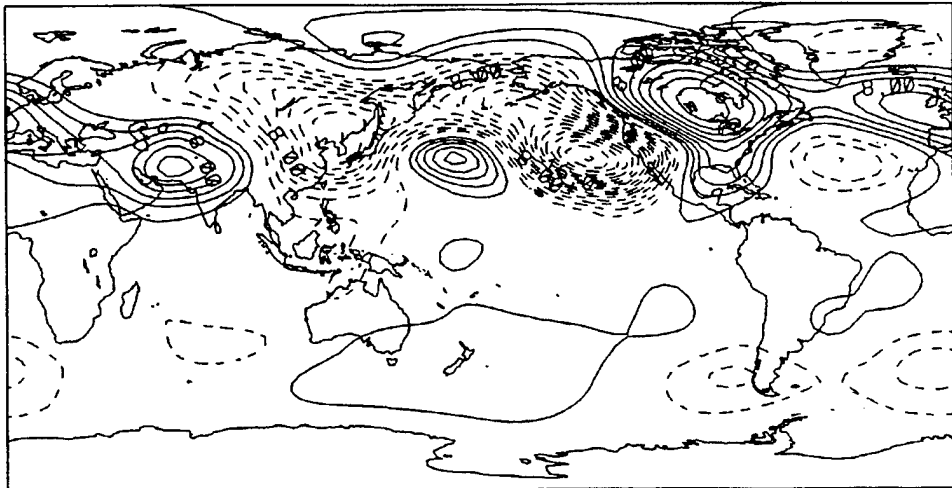
b. 4 days

Figure 17. Height response for run BJ1 which used: (1) a January basic state; (2) a fixed location; and (3) fixed amplitude tropical perturbation forcing in the Bay of Bengal. The elapsed model time is indicated. Positive (negative) responses are indicated by the solid (dashed) contours. Contour interval is 2 gpm. Zero contour is omitted.



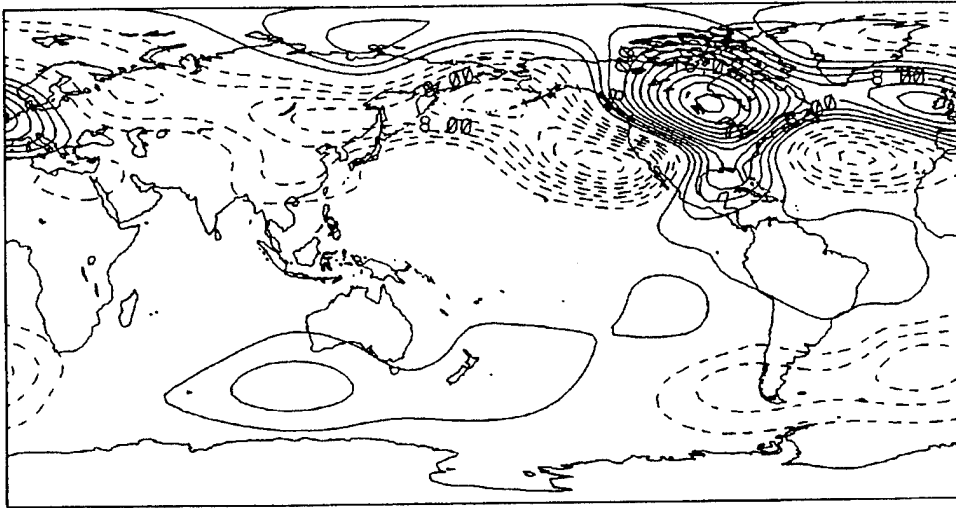


c. 8 days

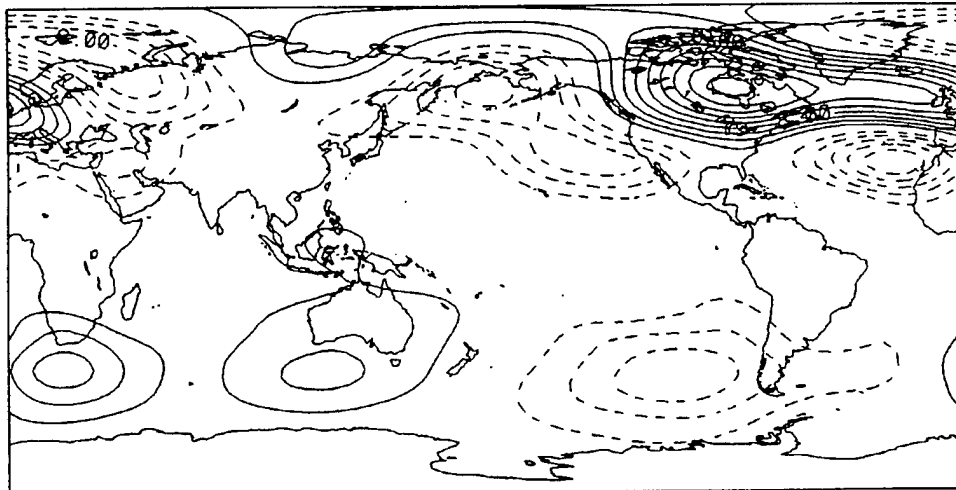


d. 12 days

Figure 17. (Continued)

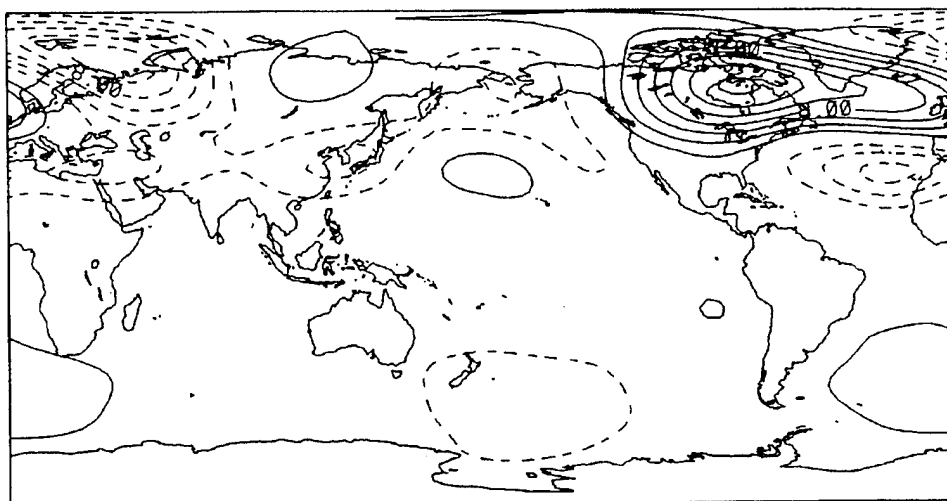


e. 16 days



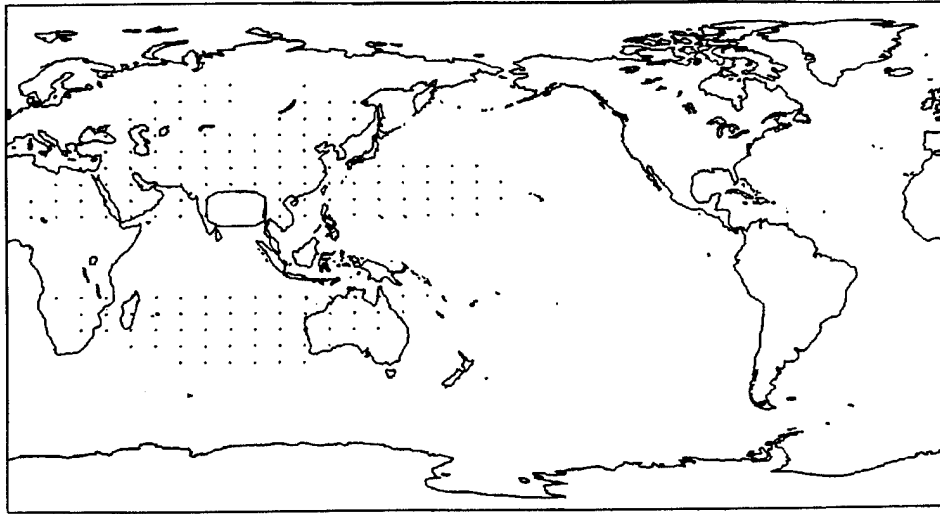
f. 20 days

Figure 17. (Continued)

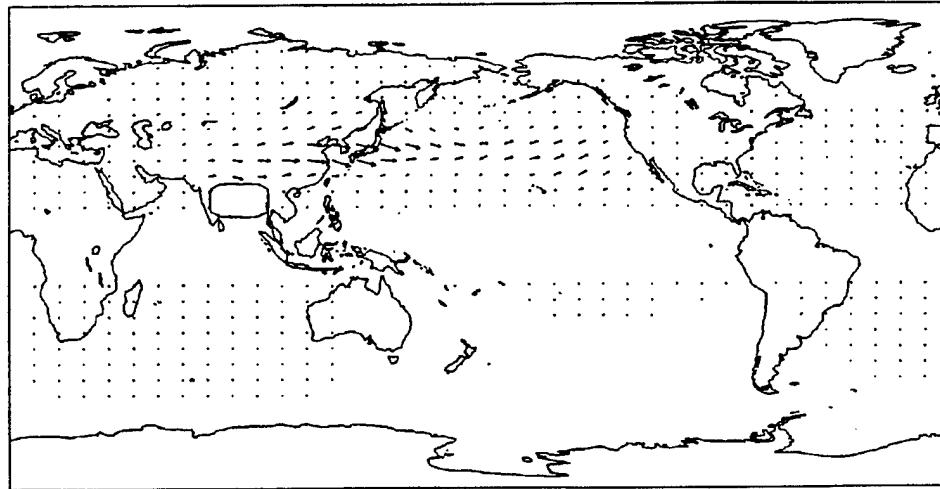


g. 24 days

Figure 17. (Continued)



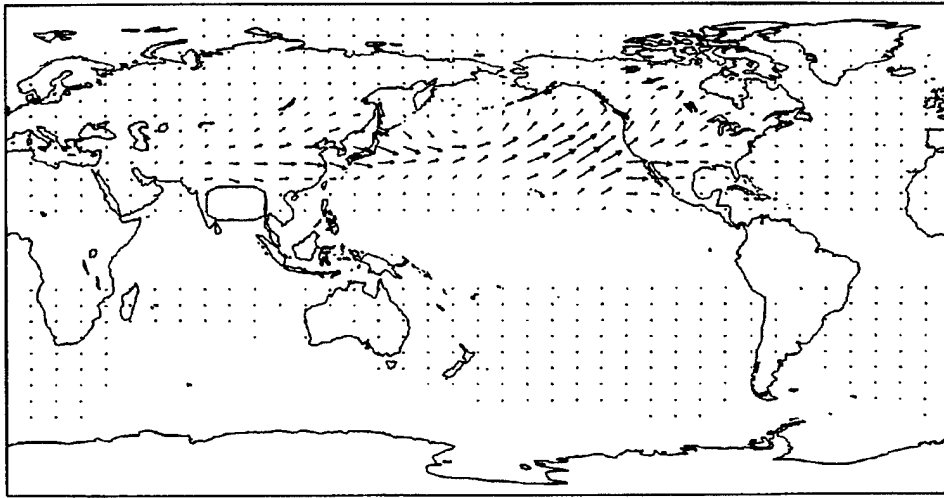
a. 12 hours



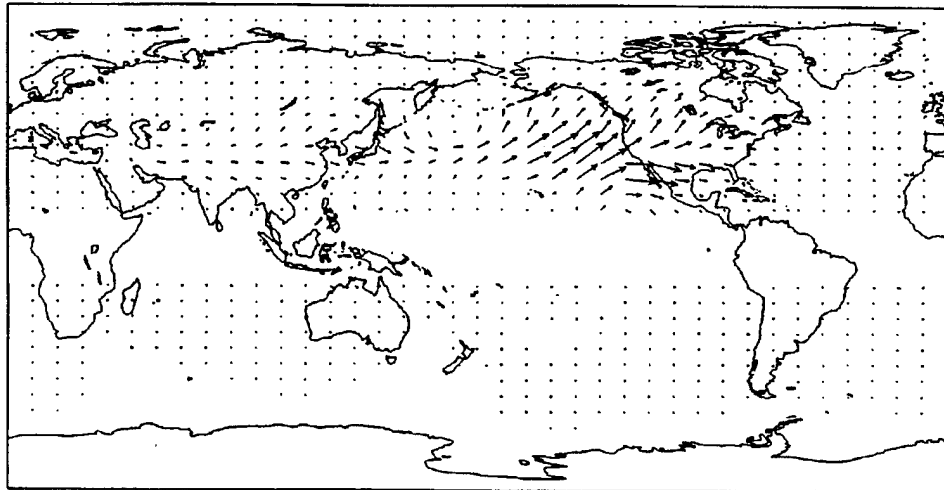
b. 4 days

Figure 18. Quasi-geostrophic wave activity flux response for run BJ1. For each panel, the elapsed model time is indicated. Tropical Bay of Bengal perturbation forcing of  $\geq 1$  K/day is indicated by the small oval region. Vector scale, in  $\text{m}^2/\text{s}^2$  as shown.

0.100E+06  
MAXIMUM VECTOR

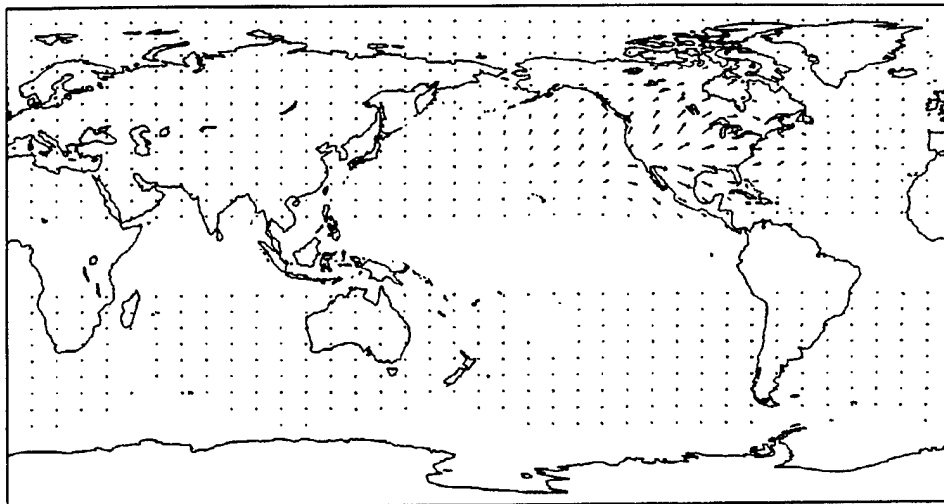


c. 8 days

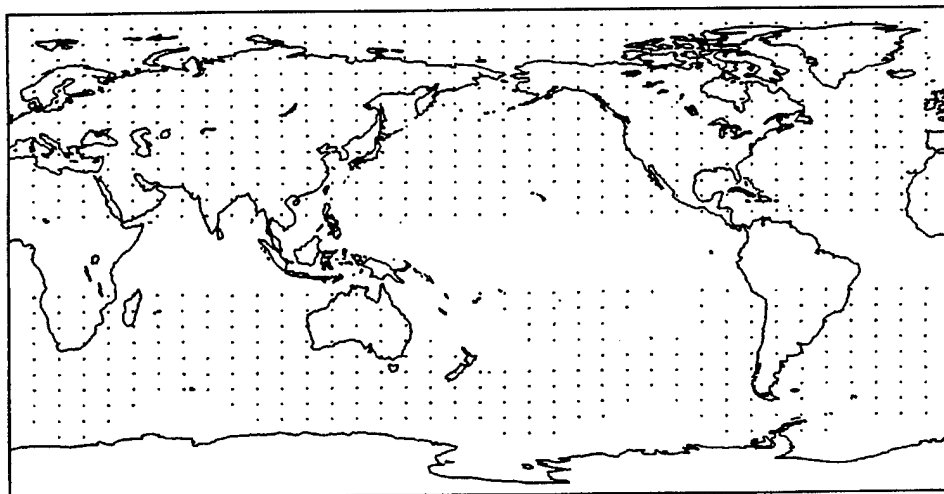


d. 12 days

Figure 18. (Continued)

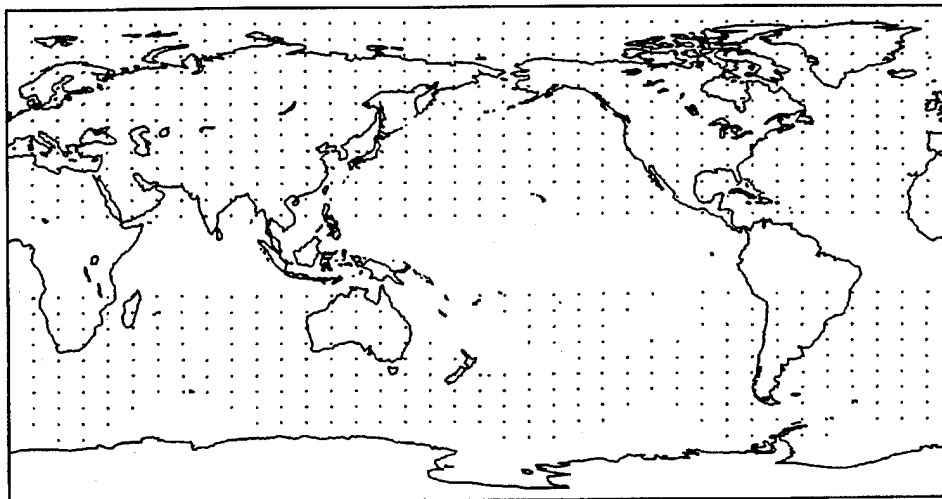


e. 16 days



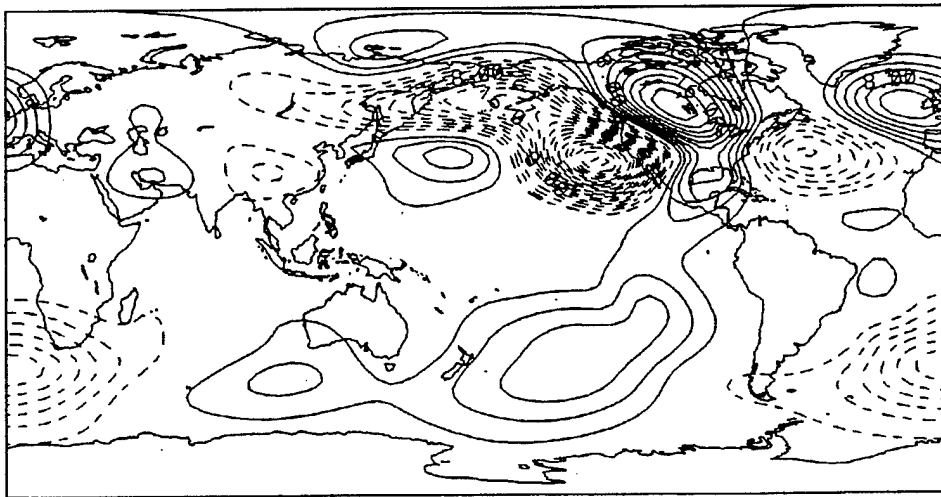
f. 20 days

Figure 18. (Continued)



g. 24 days

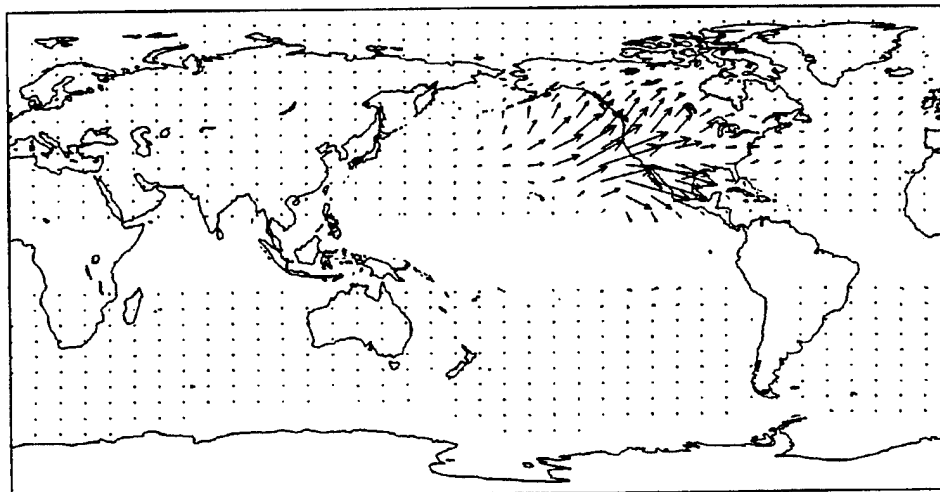
Figure 18. (Continued)



a. 12 days

Figure 19. Height response for run BJ1R which used: (1) a January basic state; (2) a recurving path; and (3) variable amplitude tropical perturbation forcing in the Bay of Bengal. The elapsed model time is indicated. Positive (negative) responses are indicated by the solid (dashed) contours. Contour interval is 2 gpm. Zero contour is omitted.

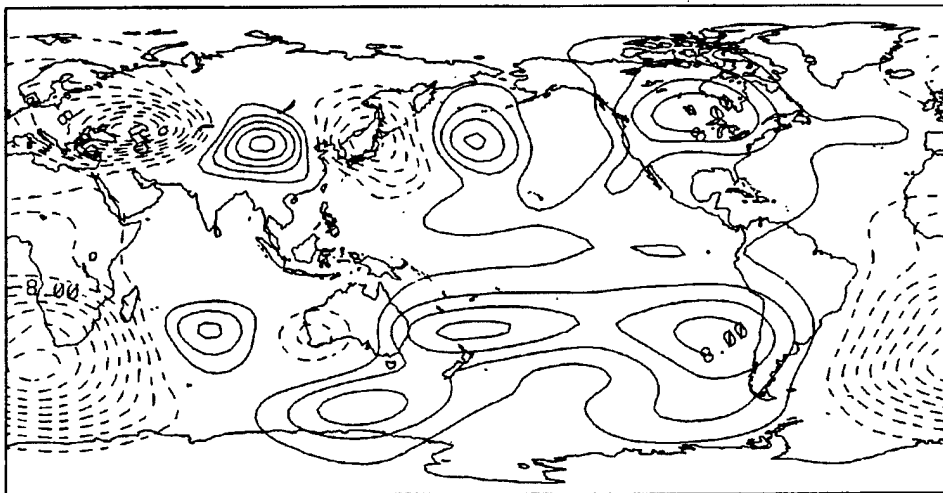




a. 12 days

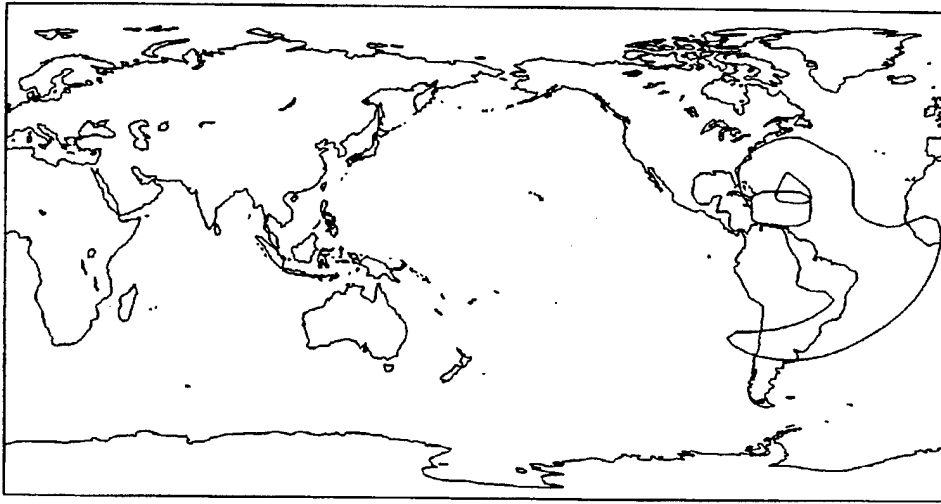
Figure 20. Quasi-geostrophic wave activity flux response for run BJ1R. For each panel, the elapsed model time is indicated. Tropical perturbation forcing of  $\geq 1$  K/day is indicated by the small oval region. Vector scale, in  $\text{m}^2/\text{s}^2$  as shown.

0.100E+06  
MAXIMUM VECTOR

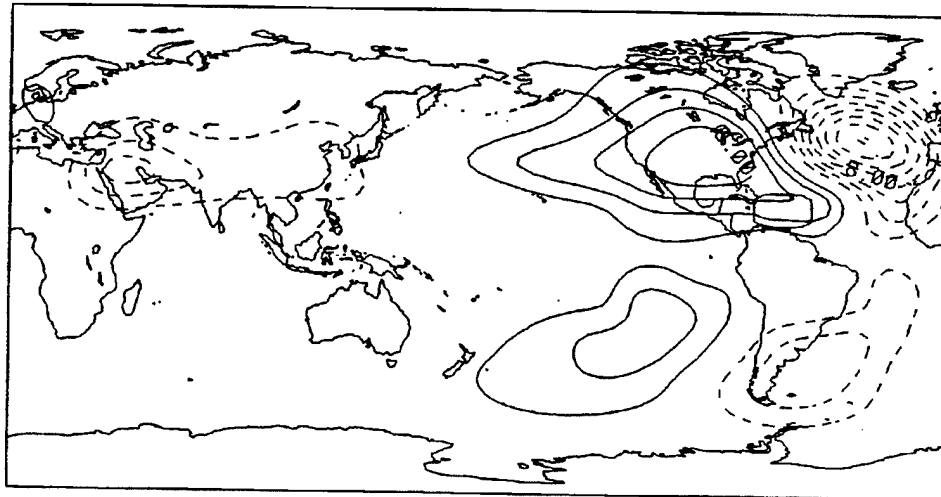


a. 12 days

Figure 21. Height response for run BJ2R which used: (1) a July basic state; (2) a recurving path; and (3) variable amplitude tropical perturbation forcing in the Bay of Bengal. The elapsed model time is indicated. Positive (negative) responses are indicated by the solid (dashed) contours. Contour interval is 2 gpm. Zero contour is omitted.

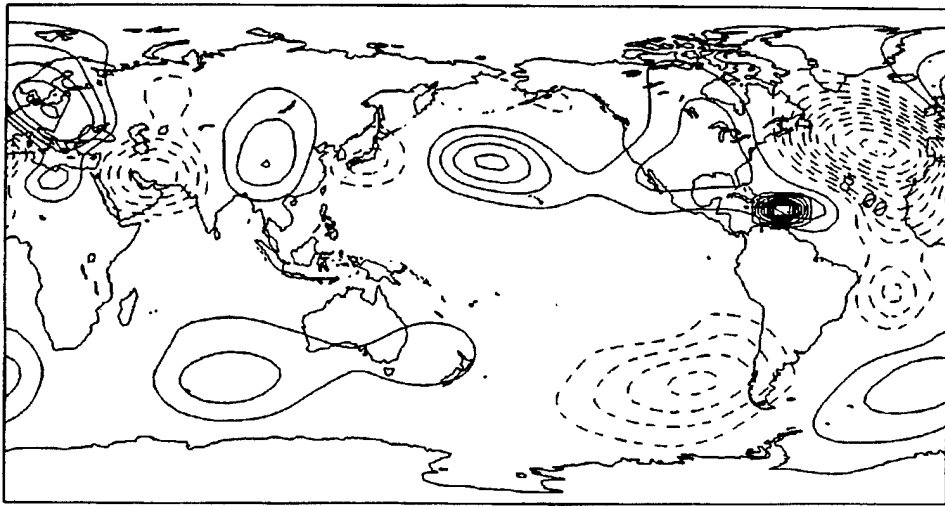


a. 12 hours

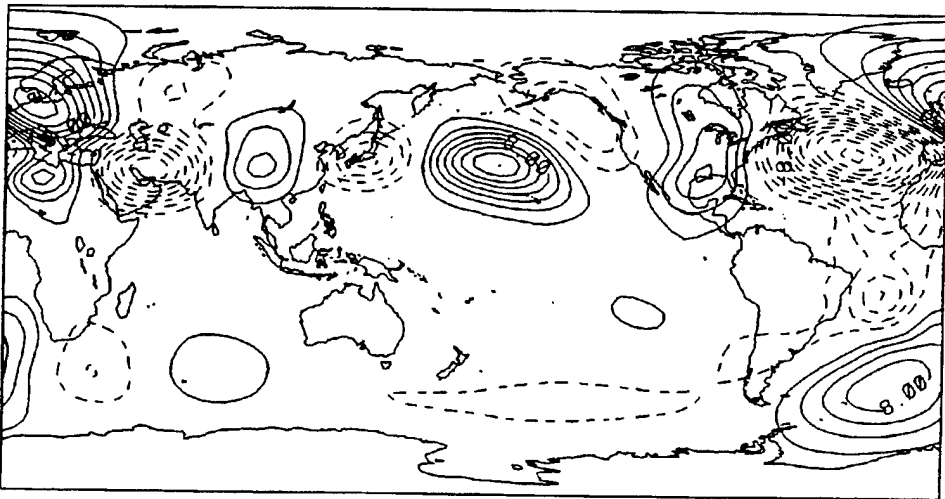


b. 4 days

Figure 22. Height response for run AJ1 which used: (1) a January basic state; (2) a fixed location; and (3) fixed amplitude tropical perturbation forcing in the North Atlantic. The elapsed model time is indicated. Positive (negative) responses are indicated by the solid (dashed) contours. Contour interval is 2 gpm. Zero contour is omitted.

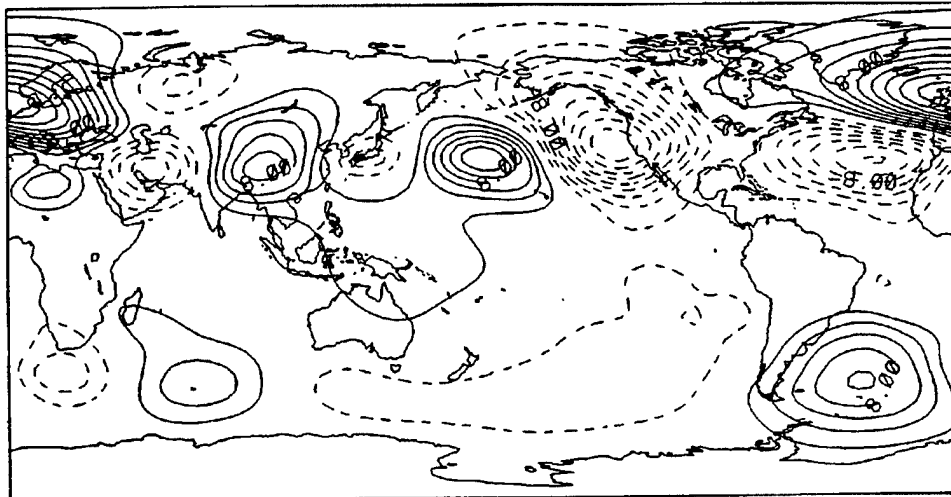


c. 8 days

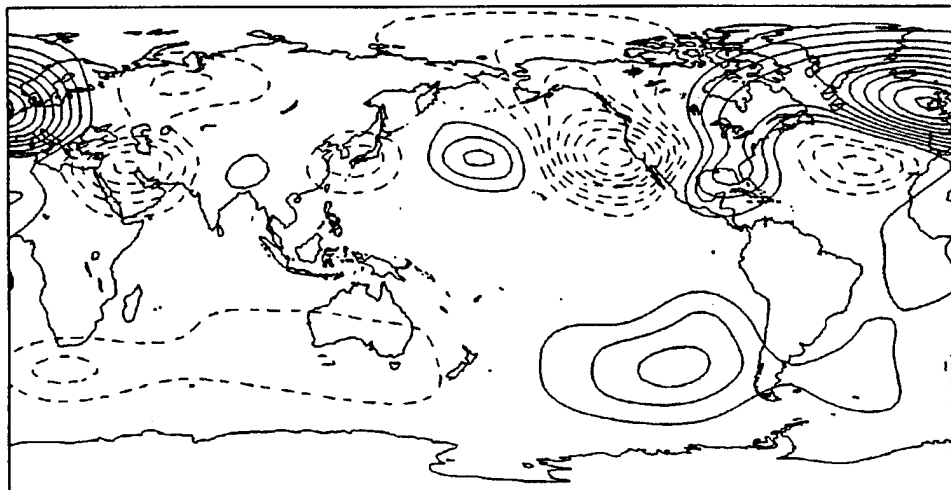


d. 12 days

Figure 22 (Continued)

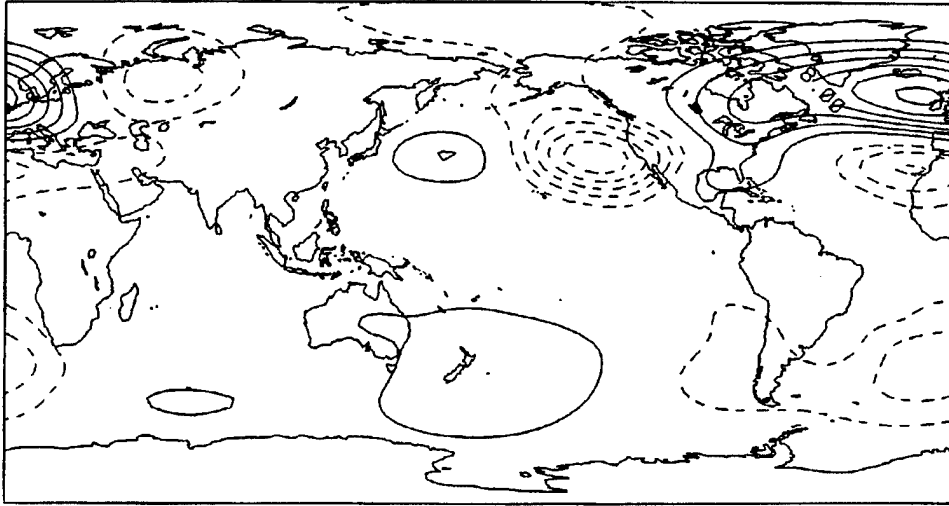


e. 16 days



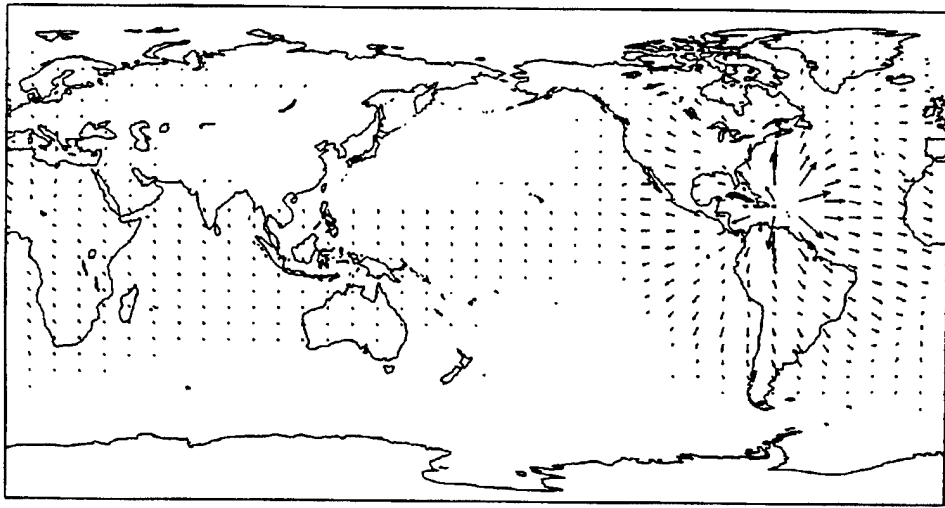
f. 20 days

Figure 22. (Continued)



g. 24 days

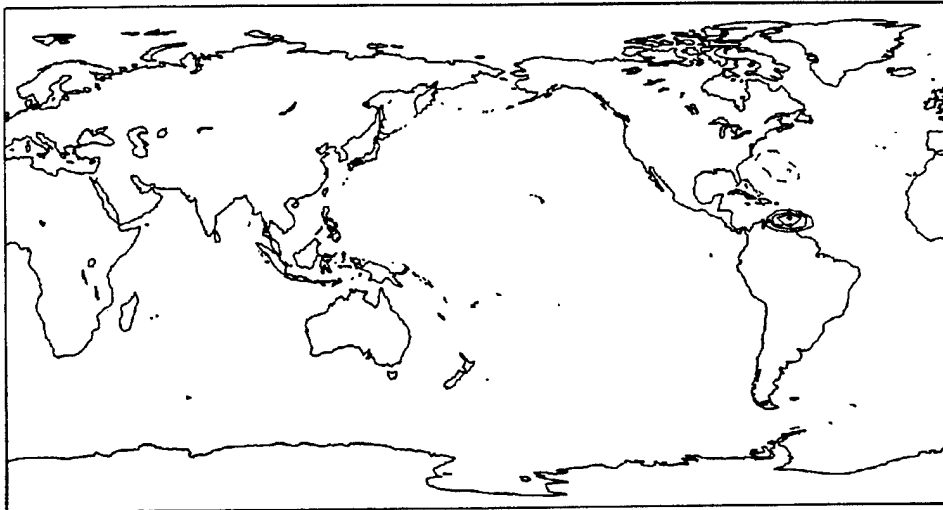
Figure 22. (Continued)



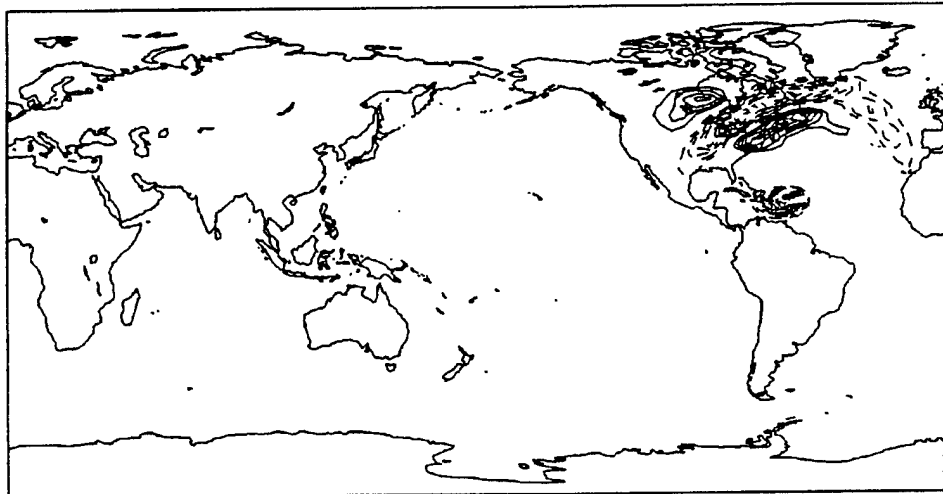
a.  $\vec{V}_\chi$

Figure 23. 200 mb Rossby wave source response terms for run AJ1 after 12 hours of the model run. (a) Divergent wind response, with vector scale, in  $\text{ms}^{-1}$ , as shown below. (b) Advection by divergent wind (ADVDIV) response. (c) vortex stretching response. Positive (negative) responses are indicated by the solid (dashed) contours. Contour interval is  $0.5 \times 10^{-11} \text{ s}^{-2}$ . Zero contour omitted.

$0.150\text{E}+01$   
MAXIMUM VECTOR



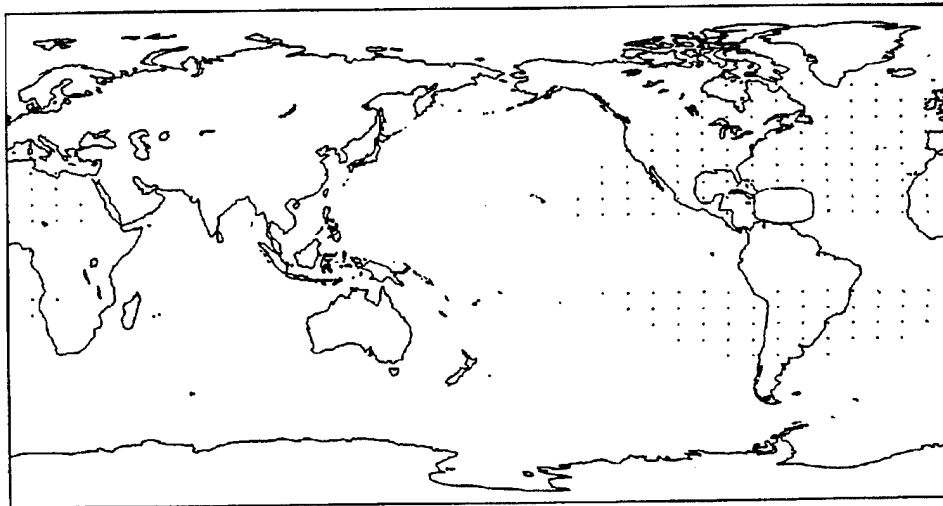
b. Advection by divergent wind



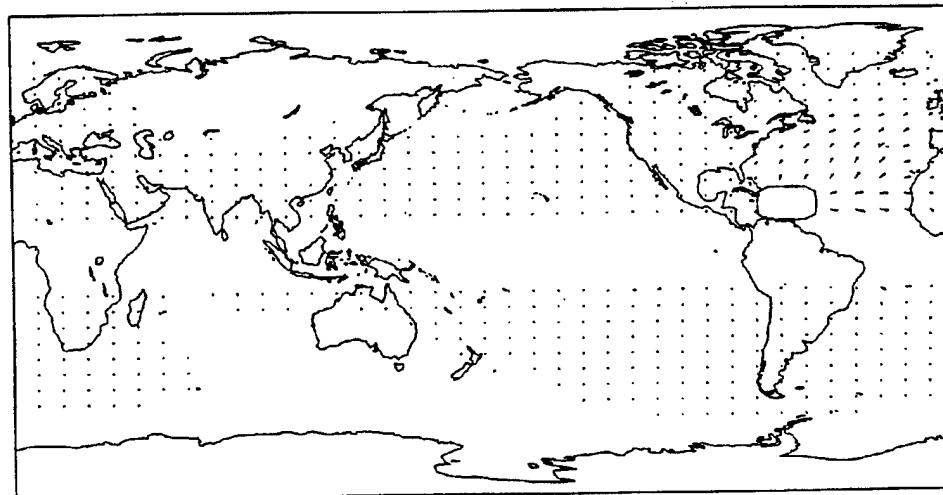
c. Vortex stretching

Figure 23 (Continued)





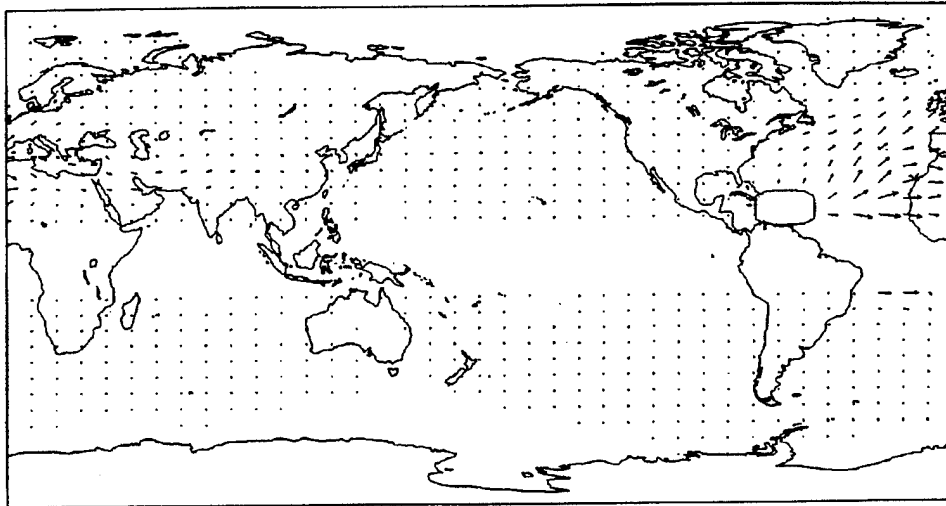
a. 12 hours



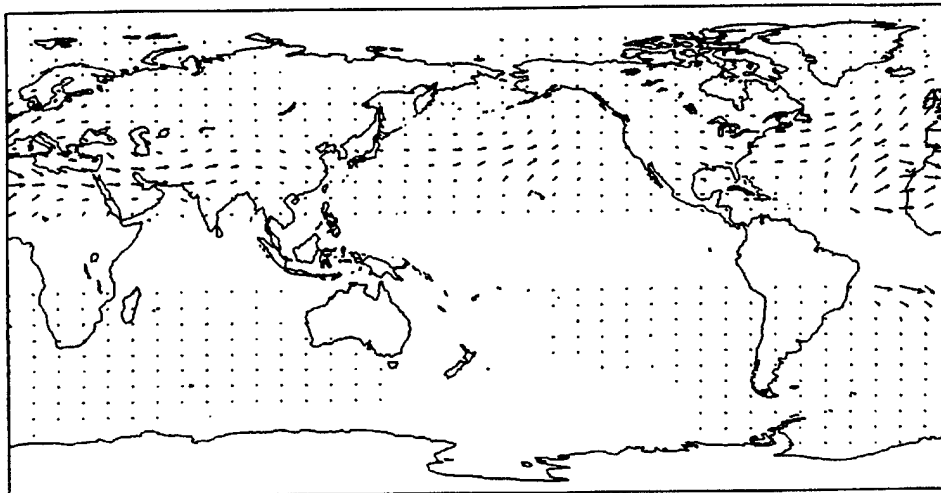
b. 4 days

Figure 24. Quasi-geostrophic wave activity flux response for run AJ1. For each panel, the elapsed model time is indicated. Tropical western North Pacific perturbation forcing of  $\geq 1$  K/day is indicated by the small oval region. Vector scale, in  $\text{m}^2/\text{s}^2$  as shown.

0.100E+06  
MAXIMUM VECTOR

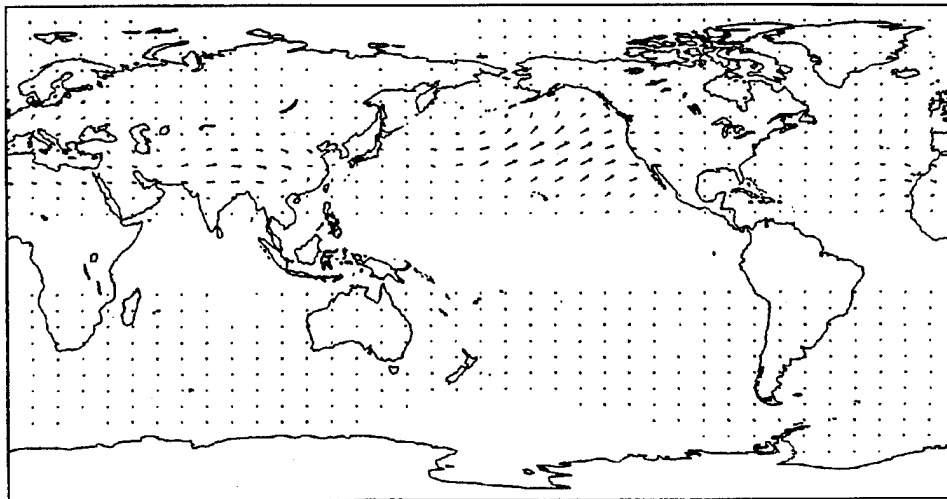


c. 8 days

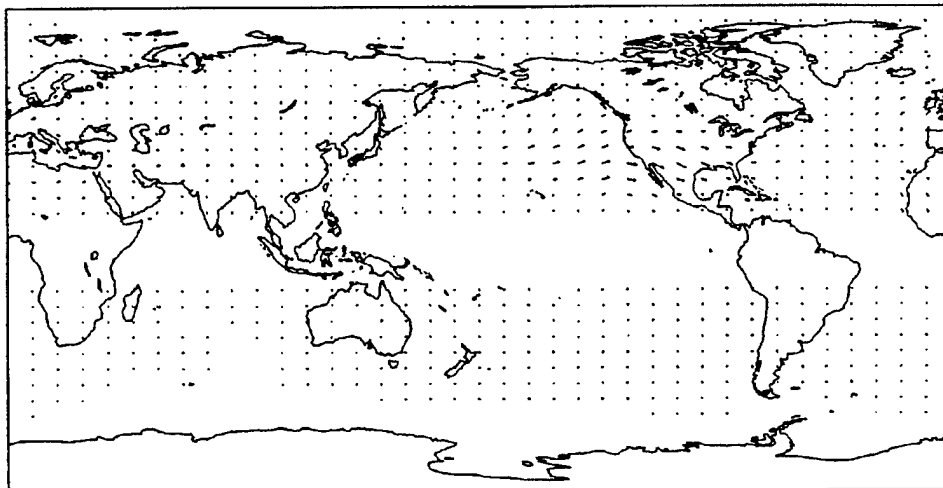


d. 12 days

Figure 24. (Continued)

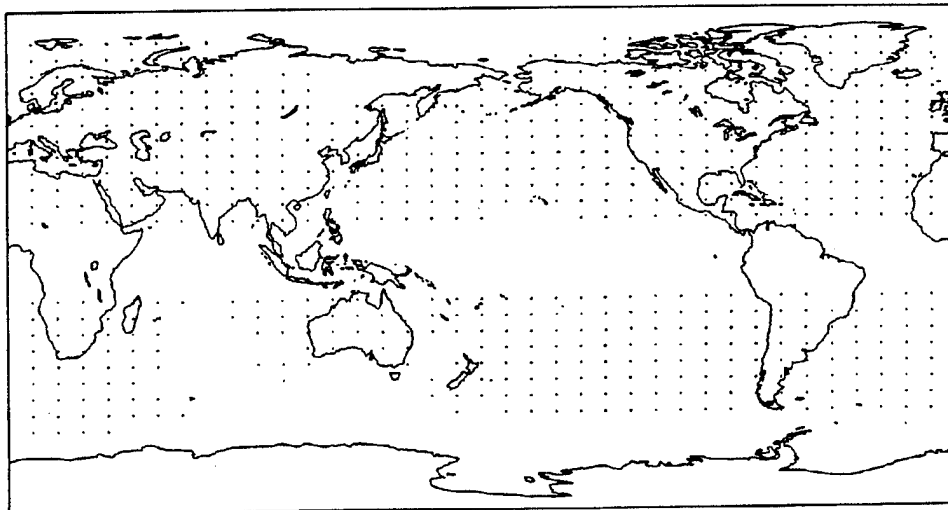


e. 16 days



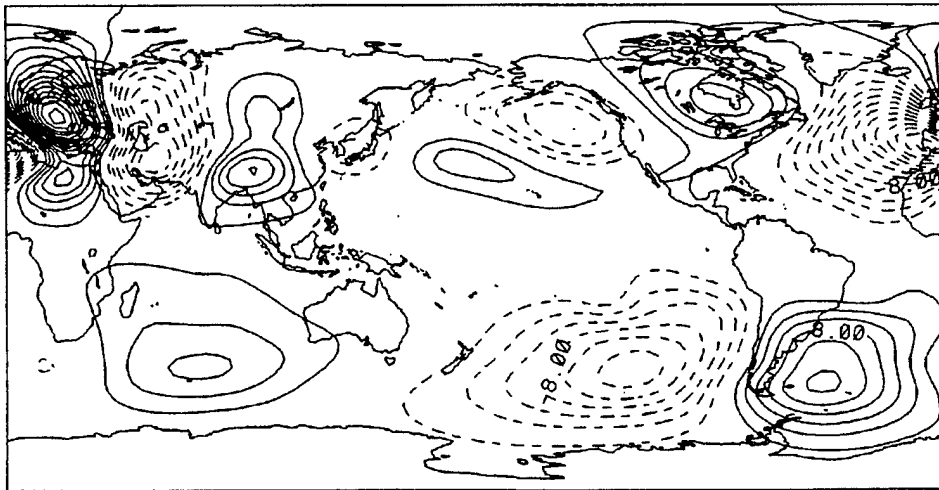
f. 20 days

Figure 24. (Continued)



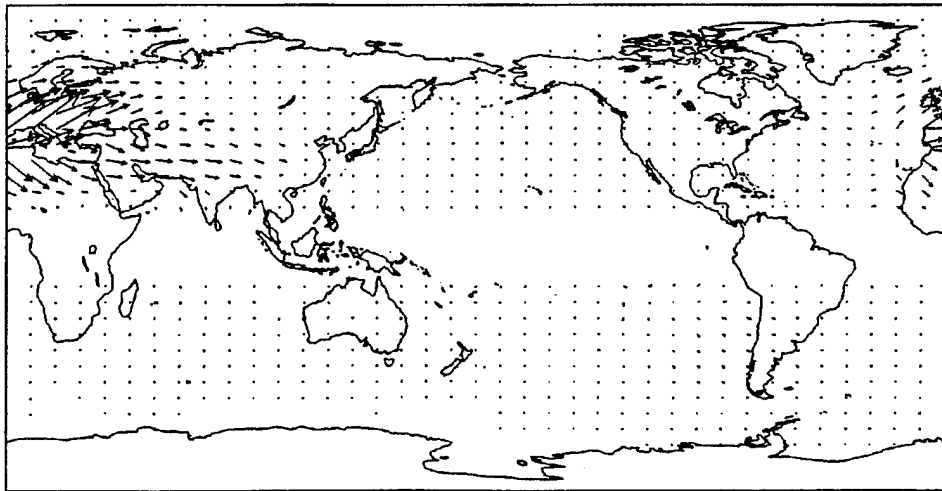
g. 24 days

Figure 24. (Continued)



a. 12 days

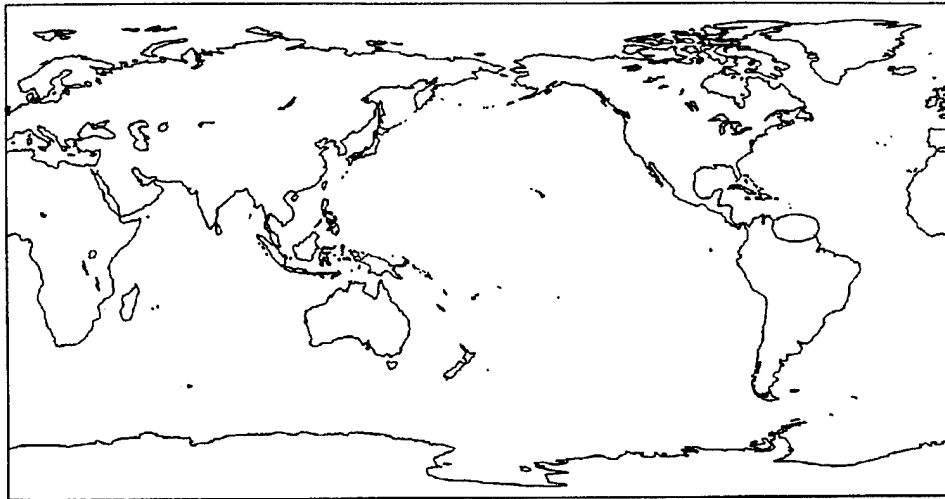
Figure 25. Height response for run AJ1R which used: (1) a July basic state; (2) a recurving path; and (3) variable amplitude tropical perturbation forcing in the North Atlantic. The elapsed model time is indicated. Positive (negative) responses are indicated by the solid (dashed) contours. Contour interval is 2 gpm. Zero contour is omitted.



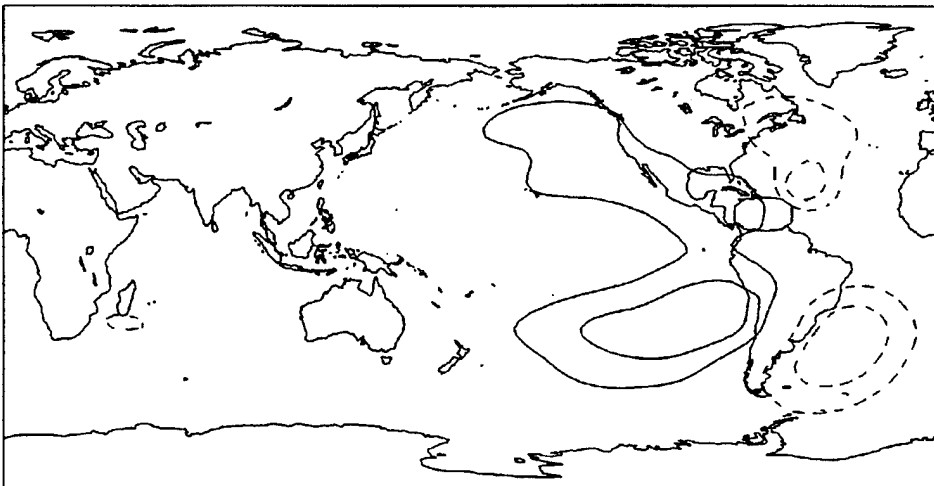
a. 12 days

Figure 26. Quasi-geostrophic wave activity flux response for run AJ1R. For each panel, the elapsed model time is indicated. Tropical perturbation forcing of  $\geq 1$  K/day is indicated by the small oval region. Vector scale, in  $\text{m}^2/\text{s}^2$  as shown.

0.100E+06  
MAXIMUM VECTOR

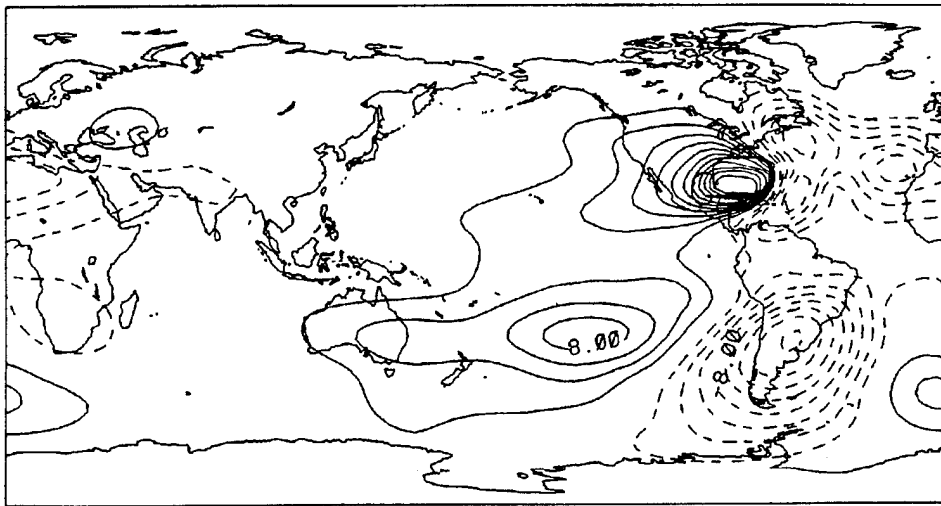


a. 12 hours

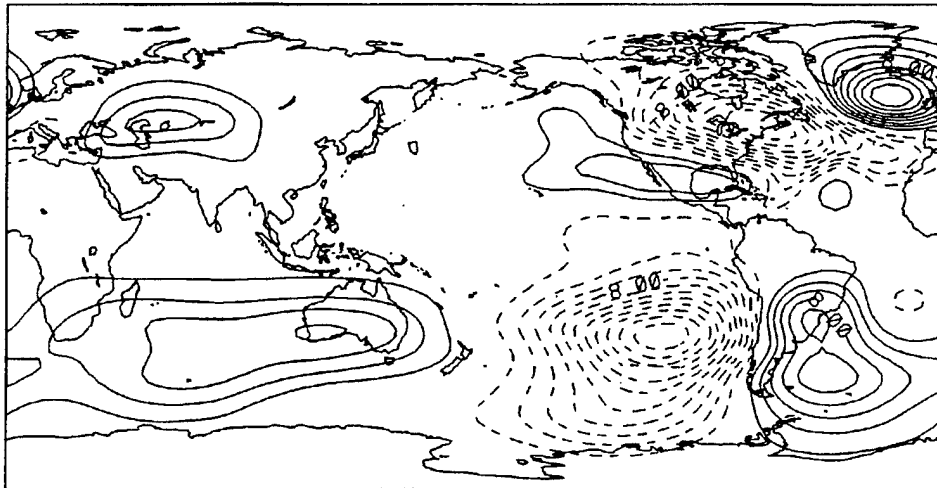


b. 4 days

Figure 27. Height response for run AJ2R which used: (1) a July basic state; (2) a recurving path; and (3) variable amplitude tropical perturbation forcing in the North Atlantic. The elapsed model time is indicated. Positive (negative) responses are indicated by the solid (dashed) contours. Contour interval is 2 gpm. Zero contour is omitted.



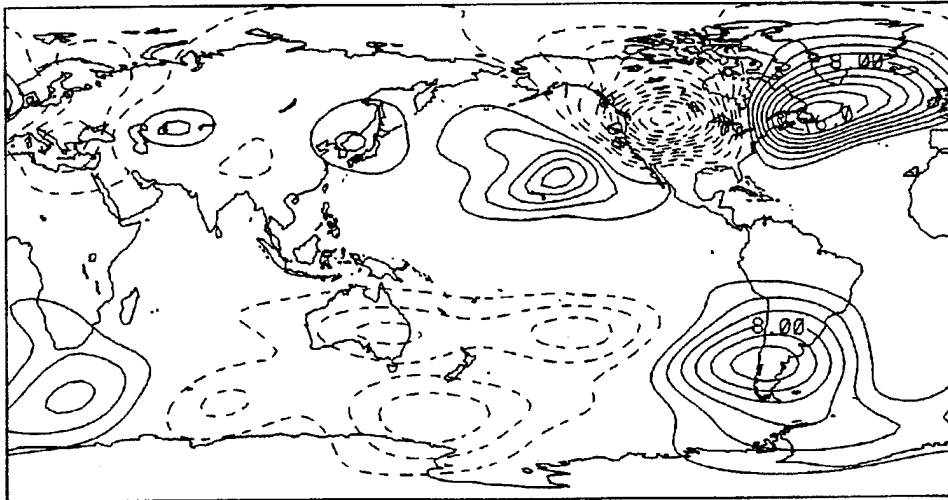
c. 8 days



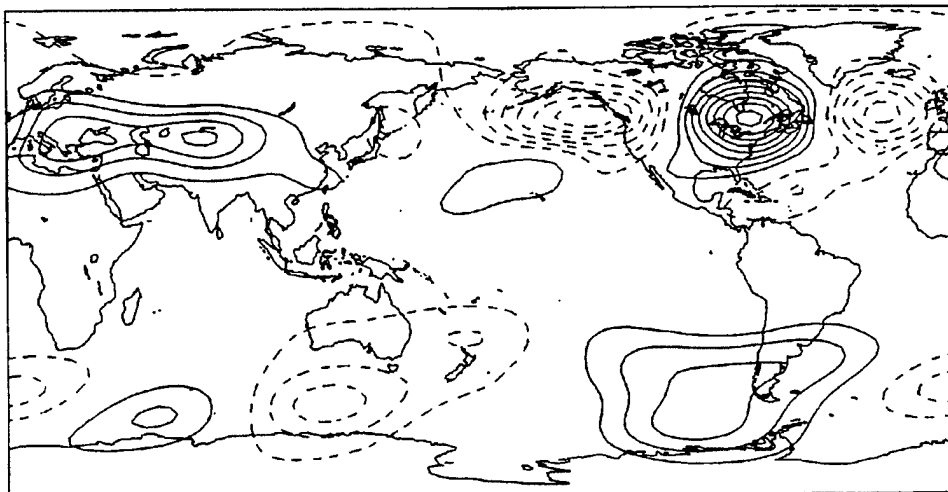
d. 12 days

Figure 27. (Continued)



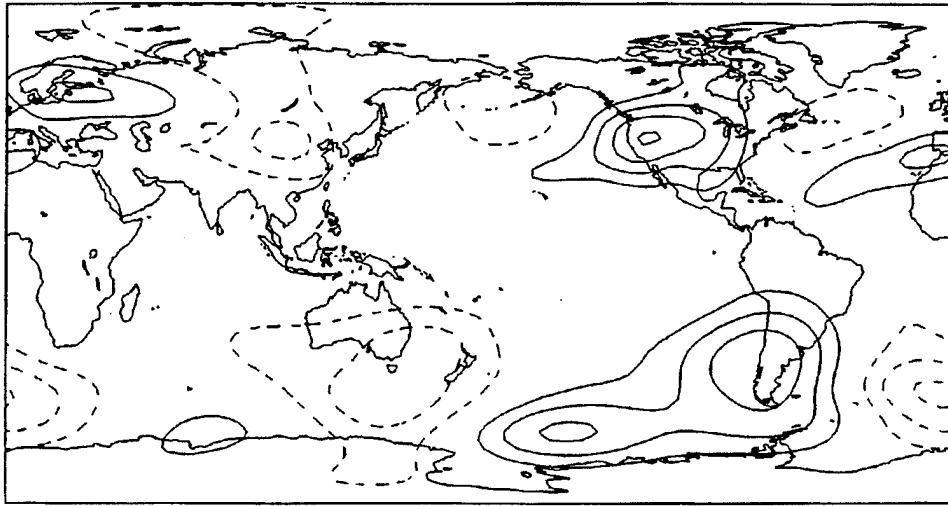


e. 16 days



f. 20 days

Figure 27. (Continued)



g. 24 days

Figure 27. (Continued)

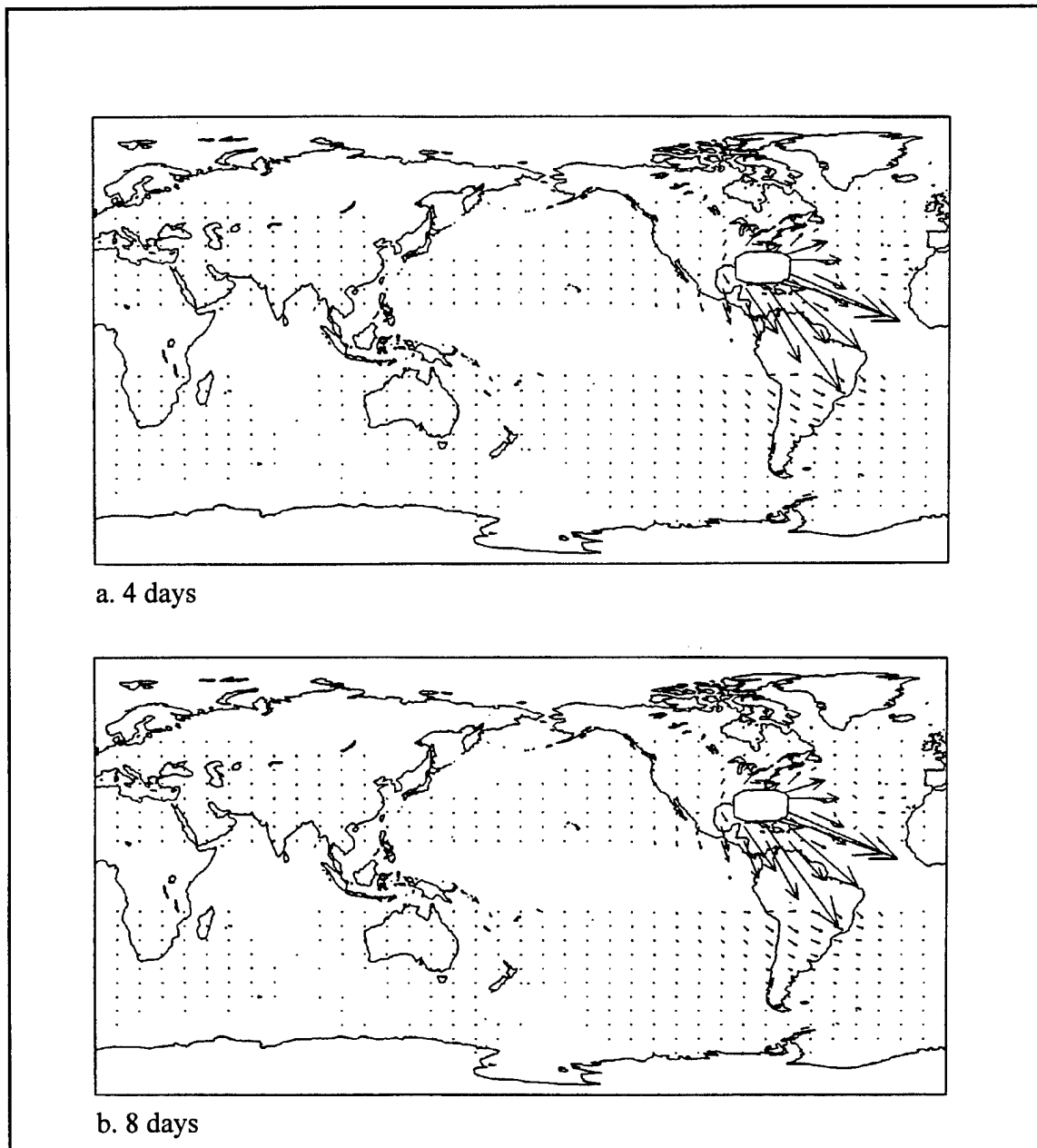
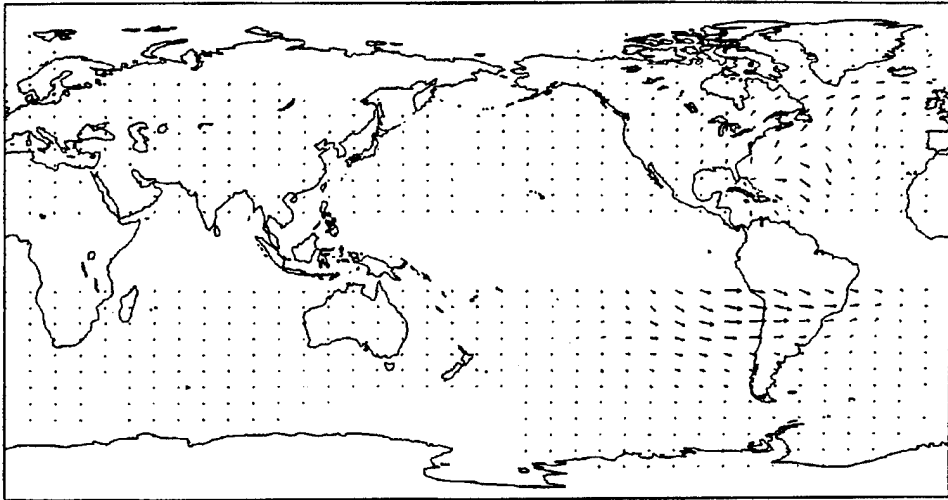
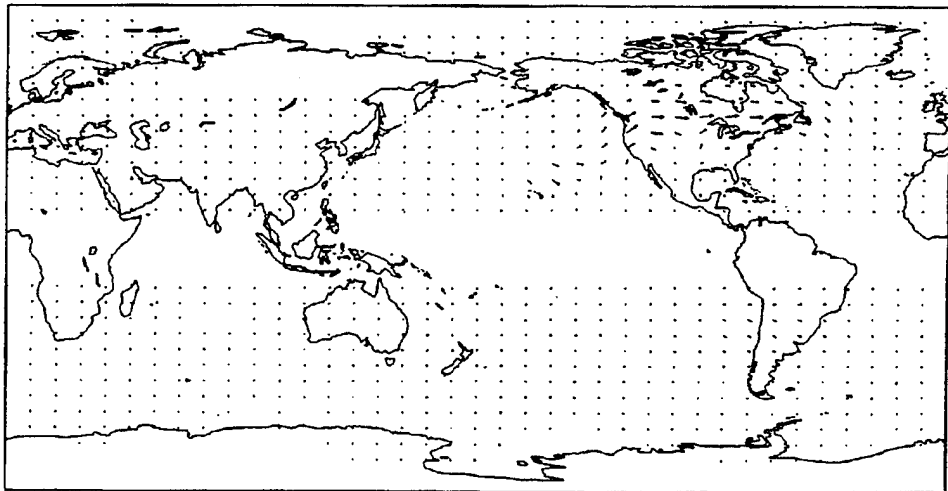


Figure 28. Quasi-geostrophic wave activity flux response for run AJ2R. For each panel, the elapsed model time is indicated. Tropical perturbation forcing of  $\geq 1$  K/day is indicated by the small oval region. Vector scale, in  $\text{m}^2/\text{s}^2$  as shown.



c. 12 days



d. 16 days

Figure 28 (Continued)

## LIST OF REFERENCES

- Bjerknes, J., 1966: A possible response of the atmospheric Hadley circulation to equatorial anomalies of ocean temperature. *Tellus*, **18**, 820-829.
- , 1969: Atmospheric teleconnections from the equatorial Pacific. *Mon. Wea. Rev.*, **97**, 163-172.
- , 1972: Large-scale atmospheric response to the 1964-65 Pacific equatorial warming. *J. Phys. Oceanogr.*, **2**, 212-217.
- Bourke, W., 1972: An efficient, one-level, primitive equation spectral model. *Mon. Wea. Rev.*, **100**, 683-689.
- Bradley, R., H. Diaz, G. Kiladis, and J. Eischeid, 1987: ENSO signal in continental temperature and precipitation records. *Nature*, **327**, 497.
- Branstator, G., 1983: Horizontal energy propagation in a barotropic atmosphere with meridional and zonal structure. *J. Atmos. Sci.*, **40**, 1689-1708.
- Chang, C.-P., and K. Lum, 1985: Tropical-midlatitude interactions over Asia and the western Pacific Ocean during the 1983/84 northern winter. *Mon. Wea. Rev.*, **113**, 1345-1358.
- Egger, J., 1977: On the linear theory of the atmospheric response to sea surface temperature anomalies. *J. Atmos. Sci.*, **34**, 603-614.
- Elsberry, R. L. ed., 1985: *A Global View of Tropical Cyclones*. Office of Naval Research. 185 pp.
- Gill, A. E., 1980: Some simple solutions for heat induced tropical circulation. *Quarterly Journal of the Royal Meteorological Society*, **106**, 447-462.
- Haltiner, G.J., and R.T. Williams, 1980: *Numerical Prediction and Dynamical Meteorology* (2nd ed.). Wiley and Sons. 477pp.

- Harr, P.A., and R. L. Elsberry, 1995a: Large-scale circulation variability over the tropical western North Pacific. Part I: Spatial patterns and tropical cyclone characteristics. *Mon. Wea. Rev.*, **123**, 1225-1246.
- , and -----, 1995b: Large-scale circulation variability over the tropical western North Pacific. Part II: Persistence and transition characteristics. *Mon. Wea. Rev.*, **123**, 1247-1268.
- Hogan, T., and T. Rosmond, 1991: The description of the Navy Operational Global Atmospheric Prediction Systems's Spectral Forecast Model. *Mon. Wea. Rev.*, **119**, 1786-1815.
- Holton, J. R., 1992: *An Introduction to Dynamic Meteorology* (3rd ed.). Academic Press. 511 pp.
- Horel, J. D. and J. M. Wallace, 1981: Planetary-scale atmospheric phenomena associated with the Southern Oscillation. *Mon. Wea. Rev.*, **109**, 813-829.
- Hoskins, B., and D. Karoly, 1981: The steady linear response of a spherical atmosphere to thermal and orographic forcing. *J. Atmos. Sci.*, **38**, 1179-1196.
- Hurrell, J., and D. Vincent, 1991: On the maintenance of short term subtropical wind maxima in the Southern Hemisphere during SOP-1, FGGE. *J. Climate*, **4**, 1009-10021.
- Jakus, C. E., 1995: *The Remote Impacts of a Western Pacific Tropical Cyclone*. Master's Thesis, Naval Postgraduate School, Monterey, California, September 1995.
- Karoly, D. J., 1978: Rossby wave ray paths and horizontal wave propagation. *The General Circulation: Theory, Modeling, and Observations. Notes from the NCAR Colloquium*. [ Available from the National Center for Atmospheric Research Information Services, Boulder, CO, 80307-3000.]
- Kuo, H. L., 1949: Dynamic instability of two-dimensional nondivergent flow in a barotropic atmosphere. *J. Meteor.*, **6**, 105-122.
- Lau, N.-C., and H. Lim, 1984: On the dynamics of equatorial forcing of climate teleconnections. *J. Atmos. Sci.*, **41**, 161-176.

- Matsuno, T., 1966: Quasi-geostrophic motions in the equatorial area. *J. Meteor. Soc. Japan*, **44**, 25-43.
- Nitta, T., 1987: Convective activities in the tropical western Pacific and their impact on the northern hemisphere summer circulation. *J. Meteor. Soc. Japan*, **65**, 373-390.
- Opsteegh, J. D., and H.M. Van den Dool, 1980: Seasonal differences in the stationary response of a linearized primitive equation model: Prospects for long range weather forecasting? *J. Atmos. Sci.*, **37**, 2169-2185.
- Plumb, R., 1985: On the three dimensional propagation of stationary waves *J. Atmos. Sci.*, **42**, 217-229.
- Rasmusson, E. M. and T. H. Carpenter, 1982: Variations in tropical sea surface temperature and surface wind fields associated with the Southern Oscillation/El Niño. *Mon. Wea. Rev.*, **109**, 1827-1835.
- Sardeshmukh, P., and B. Hoskins, 1988: The generation of global rotational flow by idealized tropical divergence. *J. Atmos. Sci.*, **45**, 1228-1251.
- Sawyer, J. S., 1970: Observational characteristics of atmospheric oscillations with a time scale of a month. *Quarterly Journal of the Royal Meteorological Society*, **96**, 610-625.
- Simmons, A. J., J. M. Wallace, and G. Branstator, 1983: Barotropic propagation and instability, and atmospheric teleconnection patterns. *J. Atmos. Sci.*, **40**, 1363-1392.
- Springer, Cory A., 1994: *Short Term Teleconnections Associated with Western Pacific Tropical Cyclones*. Master's Thesis, Naval Postgraduate School, Monterey, California, June 1994.
- Wallace, J. M., 1987: Low-frequency dynamics -- Observations. *Dynamics of Low-Frequency Phenomena in the Atmosphere, Volume I. Notes from an NCAR Summer Colloquium*. [Available from National Center for Atmospheric Research Information Services, Boulder, CO, 80307-3000.]
- Wallace, J. M., and D. S. Gutzler, 1981: Teleconnections in the geopotential height field during the northern hemisphere winter. *Mon. Wea. Rev.*, **109**, 784-812.

Walker, G., 1924: Correlation in seasonal variations of weather IX: A further study of world weather. *Memoirs of the Royal Meteorological Society*, 24, 275-322.

-----, and E. Bliss, 1932: World Weather V. *Memoirs of the Royal Meteorological Society*, 4, 53-84.

Webster, P. J., 1981: Mechanisms determining the atmospheric response to sea surface temperature anomalies. *J. Atmos. Sci.*, **38**, 554-571.

Woll, S., 1993: *Short Term Teleconnections Associated with an Individual Tropical Cyclone*. Master's Thesis, Naval Postgraduate School, Monterey, California, December 1993.



## DISTRIBUTION LIST

	No. Copies
1. Defense Technical Information Center .....	2
Cameron Station	
Alexandria, VA 22304-6145	
2. Librarian, Code 52 .....	2
Naval Postgraduate School	
411 Dyer Road Room 104	
Monterey, CA 93943-5101	
3. Oceanography Department .....	1
Code OC/CO	
Naval Postgraduate School	
833 Dyer Road Room 331	
Monterey, CA 93943-5122	
4. Meteorology Department .....	1
Code MR/HY	
Naval Postgraduate School	
589 Dyer Road Room 252	
Monterey, CA 93943-5114	
5. Dr. Tom Murphree .....	6
Code MR/ME	
Naval Postgraduate School	
589 Dyer Road Room 231	
Monterey, CA 93943-5114	
6. LCDR Mark D. Malsick, USN .....	1
205 Robin Hood Road	
Chesapeake, VA 23320	

7. Director Naval Meteorology and Oceanography Division ..... 1  
Naval Observatory  
34th and Massachusetts Avenue NW  
Washington, DC 20390
8. Commander ..... 1  
Naval Meteorology and Oceanography Command  
Stennis Space Center  
MS 39529-5000
9. Commanding Officer ..... 1  
Naval Oceanographic Office  
Stennis Space Center  
MS 39529-5001
10. Commanding Officer ..... 1  
Fleet Numerical Meteorology and Oceanography Center  
7 Grace Hopper Avenue Stop 4  
Monterey, CA 93943-0001-0120
11. Dr. Carolyn Reynolds ..... 1  
Naval Research Laboratory  
7 Grace Hopper Way Stop 2  
Monterey, CA 93943-5502